

A Non-alternant Aromatic Belt: Methylene-bridged [6]Cycloparaphenylene Synthesized from Pillar[6]arene

Yuanming Li, Yasutomo Segawa, Akiko Yagi, Kenichiro Itami

Submitted date: 03/06/2020 • Posted date: 04/06/2020

Licence: CC BY-NC-ND 4.0

Citation information: Li, Yuanming; Segawa, Yasutomo; Yagi, Akiko; Itami, Kenichiro (2020): A Non-alternant Aromatic Belt: Methylene-bridged [6]Cycloparaphenylene Synthesized from Pillar[6]arene. ChemRxiv.

Preprint. <https://doi.org/10.26434/chemrxiv.12415166.v1>

The synthesis, structure, and properties of methylene-bridged [6]cycloparaphenylene ([6]CPP), a non-alternant aromatic belt, are described. This belt-shaped methylene-bridged [6]CPP, in which each phenylene unit is tethered to its neighbors by methylene bridges, was constructed through six-fold intramolecular nickel-mediated aryl-aryl coupling of triflate-functionalized pillar[6]arene in 15% isolated yield. Compared with the analogous [6]CPP, the methylene bridges co-planarize neighboring paraphenylene units and enhance the degree of p-conjugation, resulting in a significant decrease in energy gap. Moreover, the incorporation of small molecules in the defined pocket of methylene-bridged [6]CPP makes it an attractive supramolecular architecture. Methylene-bridged [6]CPP is characterized by high internal strain energy reaching $110.2 \text{ kcal}\cdot\text{mol}^{-1}$, attributed to its restricted structure. This work not only exhibits an efficient strategy to construct a new family of aromatic belt, but also showcases their properties, which combine the merits of CPPs and pillararenes.

File list (4)

NonAlternantBelt_20200603.pdf (1.17 MiB)	view on ChemRxiv • download file
SI_NonAlternantBelt_20200603.pdf (5.93 MiB)	view on ChemRxiv • download file
TOC.png (268.26 KiB)	view on ChemRxiv • download file
4.cif (622.82 KiB)	view on ChemRxiv • download file

A Non-alternant Aromatic Belt: Methylene-bridged [6]Cycloparaphenylene Synthesized from Pillar[6]arene

Yuanming Li,[†] Yasutomo Segawa,^{‡,§,§} Akiko Yagi,[‡] and Kenichiro Itami^{*,†,‡,§}

[†]Institute of Transformative Bio-Molecules (WPI-ITbM), Nagoya University, Chikusa, Nagoya 464-8602, Japan

[‡]Graduate School of Science, Nagoya University, Chikusa, Nagoya 464-8602, Japan

[§]JST-ERATO, Itami Molecular Nanocarbon Project, Nagoya University, Chikusa, Nagoya 464-8602, Japan

[§]Institute for Molecular Science, Myodaiji, Okazaki, 444-8787, Japan

^{*}Department of Structural Molecular Science, SOKENDAI (The Graduate University for Advanced Studies), Myodaiji, Okazaki, 444-8787, Japan.

ABSTRACT: The synthesis, structure, and properties of methylene-bridged [6]cycloparaphenylene ([6]CPP), a non-alternant aromatic belt, are described. This belt-shaped methylene-bridged [6]CPP, in which each phenylene unit is tethered to its neighbors by methylene bridges, was constructed through six-fold intramolecular nickel-mediated aryl–aryl coupling of triflate-functionalized pillar[6]arene in 15% isolated yield. Compared with the analogous [6]CPP, the methylene bridges coplanarize neighboring paraphenylene units and enhance the degree of π -conjugation, resulting in a significant decrease in energy gap. Moreover, the incorporation of small molecules in the defined pocket of methylene-bridged [6]CPP makes it an attractive supramolecular architecture. Methylene-bridged [6]CPP is characterized by high internal strain energy reaching 110.2 kcal·mol^{−1}, attributed to its restricted structure. This work not only exhibits an efficient strategy to construct a new family of aromatic belt, but also showcases their properties, which combine the merits of CPPs and pillararenes.

Introduction

The development of novel curved π -conjugated nanocarbon structures is of particular interest and is critical in discovering new organic materials.¹ Belt-shaped aromatic compounds are one of the most important classes of radial π -conjugated nanocarbon molecules,² and have been the subject of extensive research ranging from synthetic methodologies to materials science.³ Compared to single-stranded paraphenylenes, ladder-type paraphenylenes (LPPs) (Figure 1A)⁴ have a ribbon-like geometry and favorable properties such as enhanced π -conjugation, high photoluminescent efficiency, and remarkable hole mobility.⁵ These characteristics make LPPs attractive materials for potential use in organic electronic devices. This encouraged us to pursue the synthesis of methylene-bridged cycloparaphenylene (CPP) as a new type of non-alternant aromatic belt (Figure 1B), in which the cyclic paraphenylene chain is ladderized by methylene bridges. Due to the intrinsic flexibility of CPPs, particularly their free rotation of phenylene units around the phenylene-phenylene linkage,⁶ CPPs possess torsion angles of ca. 27–35° between phenylene units.⁷ Therefore, the structure of methylene-bridged CPPs possessing enhanced π -conjugation and well-defined conformations would be of great interest, in addition to presenting a fascinating synthetic challenge.

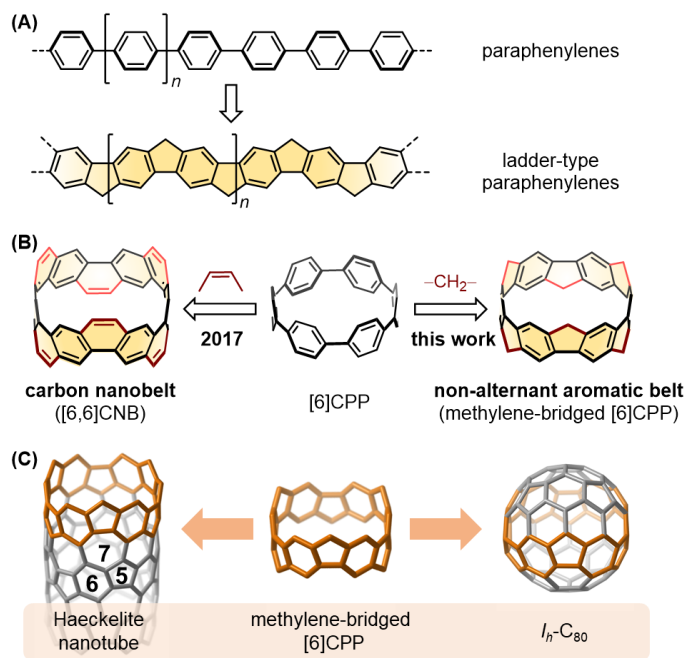


Figure 1. (A) Structures of paraphenylenes and ladder-type paraphenylenes. (B) Aromatic belts having [6]CPP skeleton. (C) The segment of nanotube and fullerenes.

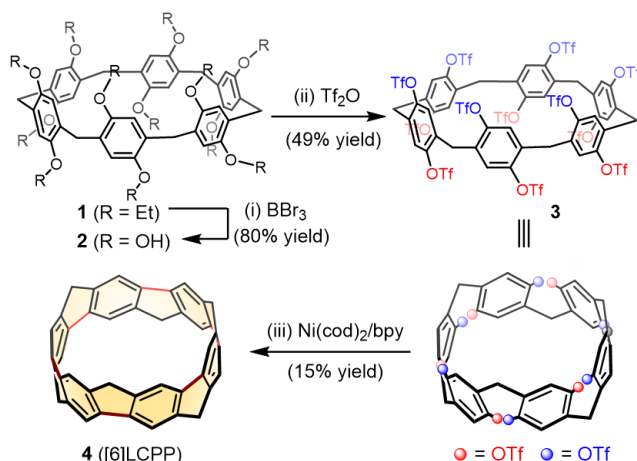
The bottom-up synthesis of an aromatic belt with a CPP skeleton has rarely been explored to date. In 2017, our group used ethynylene bridges to connect phenylene units to create a fully fused and conjugated carbon nanobelt ([6,6]CNB, Figure 1B).⁸ Subsequently, Chi, Miao, and coworkers achieved the synthesis of phenylene-bridged carbon nanobelt (see Figure S28).⁹ Very recently, Tanaka's group prepared the CH₂O-bridged [8]CPP (see Figure S28).¹⁰ Although partially fused CPPs by methylene bridges, *i.e.* cyclofluorene, have been reported,¹¹ the belt-shaped fully methylene-bridged CPPs still represent a synthetic challenge. The construction of the backbone is the key to achieving the synthesis of methylene-bridged CPPs. Inspired by Vögtle and co-workers' pioneering concept to access CPPs from pre-existing macrocycles,¹² we herein report the synthesis of methylene-bridged [6]CPP using triflate-functionalized pillar[6]arene as a macrocyclic precursor,¹³ through six-fold nickel-mediated Yamamoto coupling. The enforced coplanarity of methylene-bridged [6]CPP and shrinking diameter caused by the bridges results in relatively high strain energy (110.2 kcal·mol⁻¹). Furthermore, methylene-bridged [6]CPP represents a belt segment of a Haeckelite nanotube possessing pentagon-hexagon-heptagon ring systems, as well as a segment of fullerenes such as *I_h*-C₈₀ (Figure 1C).¹⁴

Results and Discussion

Synthesis

Pillararene is a pillar-shaped macrocyclic host synthesized in 2008 by Ogoshi and coworkers.¹⁵ Due to its methylene-bridged macrocyclic arene skeleton, we envisioned that pillar[6]arene¹⁶ could serve as a suitable macrocyclic precursor for the synthesis of methylene-bridged [6]CPP. The synthetic route to the target product is summarized in Scheme 1. Pillar[6]arene was prepared in one step from commercially available 1,4-diethoxybenzene.¹⁷ Taking advantage of the ethoxy groups of pillar[6]arene, the intramolecular aryl-aryl coupling of aryl triflates to provide the CPP backbone could be easily imagined based on our previous results.^{8a,b} With this in mind, pillar[6]arene triflate **3** was readily prepared through ether cleavage followed by triflation in 39% isolated yield over two steps.¹⁸ With **3** in hand, we investigated the key step of the aryl-aryl coupling of aryl triflate. Based on previous reports using an ArBr/Ni(cod)₂/2,2'-bipyridyl system,^{8b,19} we investigated the effect of ligands and other reaction parameters in the aryl-aryl coupling reaction using **3** as the pseudohalide component (see Table S1 for further details). We found that pillar[6]arene triflate **3** reacted successfully with 12 equivalents of Ni(cod)₂ and 2,2'-bipyridyl (bpy) at 80 °C for 2 hours to produce the fully fused target belt **4** in 15% isolated yield as a red solid. Compound **4** is soluble in dichloromethane (up to 20 mg/mL) and CS₂, and shows sufficient stability in solution to enable full characterization. This synthetic strategy offers a new and rapid approach to access a new type of aromatic belt.

Scheme 1. Synthetic Route of Methylene-bridged [6]CPP^a



^aReaction conditions: (i) **1** (1.0 equiv, 12.5 mM), BBr₃ (40 equiv), CHCl₃, room temperature (rt), 24 h. (ii) Tf₂O (16 equiv), pyridine (18 equiv), CH₂Cl₂, rt, 24 h. (iii) **3** (1.0 equiv, 3.0 mM), Ni(cod)₂ (12 equiv), 2,2'-bipyridyl (12 equiv), *N*-methyl-2-pyrrolidone (NMP), 80 °C, 2 h.

Nuclear Magnetic Resonance Analysis

In the ¹H NMR spectrum in CDCl₃ at 25 °C, compound **4** showed one singlet of aromatic hydrogen atoms at 7.86 ppm and two doublets of geminal hydrogen atoms at 4.09 and 4.29 ppm, corresponding with the *D*_{3d} symmetry of the belt structure (Figure 2). According to the calculated chemical shifts by using GIAO B3LYP/6-311+G(2d,p)//B3LYP/6-31G(d) level of theory (see Table S5), the signals appearing at 4.09 and 4.29 ppm can be assigned to the inner and the outer hydrogen atoms respectively. The ¹³C NMR analysis disclosed four sets of nonequivalent carbon atoms, again associated with the *D*_{3d} symmetry of **4**.

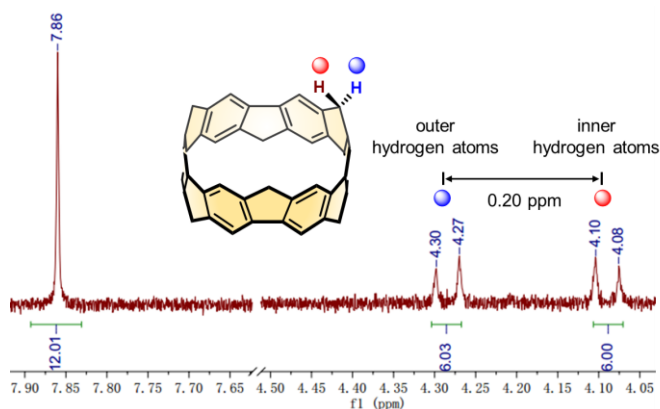


Figure 2. ¹H NMR spectrum of **4** (600 MHz, CDCl₃, 25 °C).

X-ray Crystal Structures

The belt-shaped structure of **4** was confirmed by single crystal X-ray diffraction analysis (Figure 3) and was further explored using gas-phase DFT calculations. Slow diffusion of *n*-hexane into a CH₂Cl₂ solution of **4** at room temperature resulted in the formation of red single crystals with both solvent molecules (*n*-hexane and CH₂Cl₂) as a ternary co-crystal (Figure 3A and 3C). Compound **4** exhibits a small elliptic deformation of the cylindrical shape in the crystal structure (Figure 3B). Interestingly, the phenylene units of [6]CPP linked with methylene bridges form a condensed belt structure because of the shorter length (Figure S2), resulting in a shrinking diameter (7.758 Å), considerably less than that of [6]CPP (8.072 Å)²⁰ and [6,6]CNB (8.053 Å) (Table 1). On the other hand, the dihedral angles between the adjacent phenylene units are almost zero (Figure 3B, cf. [6]CPP, 27.4°).⁷ The symmetrically independent C–C bond lengths of the six-membered rings are 1.408, 1.395, and 1.384 Å (Table S3). These approximately equivalent bond lengths imply that a benzenoid structure is still preserved in methylene-bridged [6]CPP. Moreover, the C–C single bond connecting the phenylene units in **4** (average 1.478 Å)

is shorter than that of [6]CPP (1.489 Å)²¹ and longer than the analogous bond in [6,6]CNB (1.464 Å). Furthermore, compound **4** contains phenylene units that are less bent (Table S3, averaged bent angle, 8.4°) than that of corresponding [6]CPP (12.5°). These results are in good agreement with the structure optimized by DFT calculations (see Table S3). This new belt-shaped nanocarbon structure would be of great interest as an element of supramolecular architecture.

The packing mode of **4** in the crystal is also interesting. Unlike the tubular packing structure of [6]CPP obtained at room temperature,²¹ the crystal packing of **4** results in a herringbone pattern in the [0 1̄ 1] plane with CH–π interactions between adjacent molecules (Figure 3C upper left, and Figure S1). The different complexes of compound **4** are packed in an alternating fashion between layers in the [001] (*ab*) plane (Figure 3C, bottom-left). Intriguingly, the methylene hydrogen atoms prevent efficient π–π stacking. Therefore, no clear intermolecular π–π interaction was observed. Instead, close CH–π interactions (2.821–2.862 Å) were observed (Figure 3C, right).

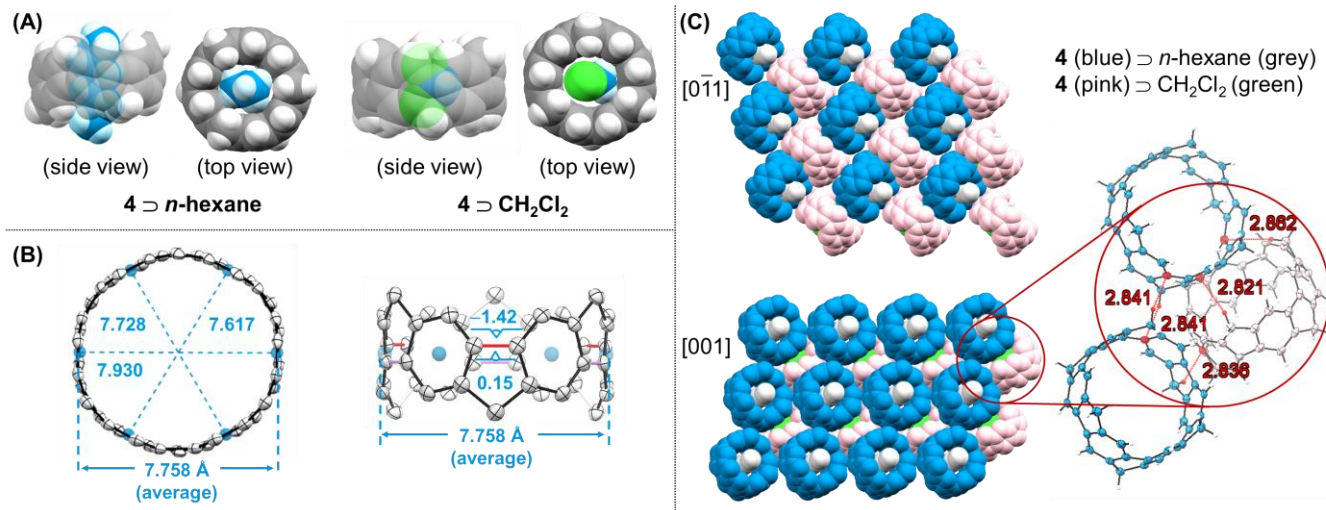
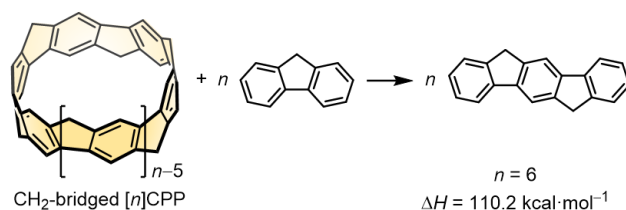


Figure 3. (A) X-ray structures of crystallographically independent molecules of **4** incorporating *n*-hexane (left) and dichloromethane (right). The solvent molecules are disordered on stereocenters (carbon: blue, hydrogen: light blue, chlorine: green). (B) ORTEP drawing of **4**·*n*-hexane with 50% thermal probability (hydrogen atoms and *n*-hexane are omitted for clarity.). The diameter was measured as the distance between the two central phenylene units located at opposite sides. The internal and external dihedral angles are 0.15° and -1.42°, respectively. (C) The packing structure of **4**. Hydrogen atoms are omitted for clarity. Inset: Distances between the hydrogen and the nearest aromatic carbon.

Strain Energy

Based on homodesmotic reaction schemes,⁶ the ring strain energies of compound **4** corresponding to the distortion caused by the formation of methylene-bridged [6]CPP were calculated to be 110.2 kcal·mol⁻¹ at the B3LYP/6-31G(d) level (Scheme 2). This value is higher than the analogous energy calculated for [6]CPP (96.9 kcal·mol⁻¹),⁶ and lower than that of [6,6]CNB (119.5 kcal·mol⁻¹).^{8a} The higher strain energy of compound **4** compared to [6]CPP is attributed largely to the condensed structure with a smaller diameter. The strain energy of even-numbered methylene-bridged [*n*]CPPs was also estimated (see Scheme S3 and Figure S26).

Scheme 2. Homodesmotic Reactions to Calculate Strain Energy of Methylene-bridged [*n*]CPP.



To gain insight into the effect of the methylene bridges on **4**, the photophysical properties of compound **4** were measured (Figure 4A and Figure S27). In comparison to [6]CPP, which exhibits a major absorption band at 339 nm and much weaker peaks at 400–500 nm, compound **4** shows one major absorption band at 347 nm with one weaker band at 370 nm in the CH₂Cl₂ solution. A much weaker absorption extending up to 600 nm is also observed, and detectable fluorescence was not observed from **4** in CH₂Cl₂ solution. This behavior is similar to that of small CPPs, such as [6]CPP, which has no detectable fluorescence.

For further understanding of the absorption spectrum, TD-DFT calculation of compound **4** was carried out at the B3LYP/6-31G(d) level of theory. Compound **4** has degenerate HOMO–1/HOMO–2 and degenerate LUMO+2/LUMO+3 (HOMO = highest occupied molecular orbital, LUMO = lowest unoccupied molecular orbital, Figure 4B). The major absorption band can be assigned to a combination of the HOMO–1 and HOMO–2 to LUMO, and the HOMO to LUMO+2 and LUMO+3 transitions (Figure 4B). This transition is different from the assignments for [6]CPP^{21a} and [6,6]CNB (see Table S6 for comparison). The weak absorption at 450–600 nm, associated with the symmetry-forbidden HOMO–LUMO transition, was also observed in [6,6]CNB reflecting their structural rigidity, whereas the corresponding band of [6]CPP is relatively high owing to its conformational flexibility. The non-emission property of **4** can also be attributed to the symmetrically forbidden $S_1 \rightarrow S_0$ transition.²² The energy levels of the calculated frontier molecular orbitals of **4** are shown in Figure 4B. The HOMO and LUMO of **4** are delocalized over the phenylene units.

Comparing **4** to [6]CPP, the LUMO and HOMO energies are raised by 0.04 eV and 0.52 eV, respectively, leading to an energy gap of 2.66 eV, 0.48 eV narrower than that of [6]CPP and 0.29 eV narrower than that of [6,6]CNB (Table 1). This is consistent with the bathochromic shift in the absorption spectra of **4**. This calculated narrow HOMO–LUMO gap of **4** is comparable to that of C₆₀ (2.77 eV),²³ which suggests that **4** would be a prominent organic material for optoelectronic devices. Furthermore, the energy gap between the S_2 and S_1 of **4** (1.1 eV) is significantly larger than that of [6,6]CNB (0.24 eV) (see Table S6 for comparison between **4** and [6,6]CNB).

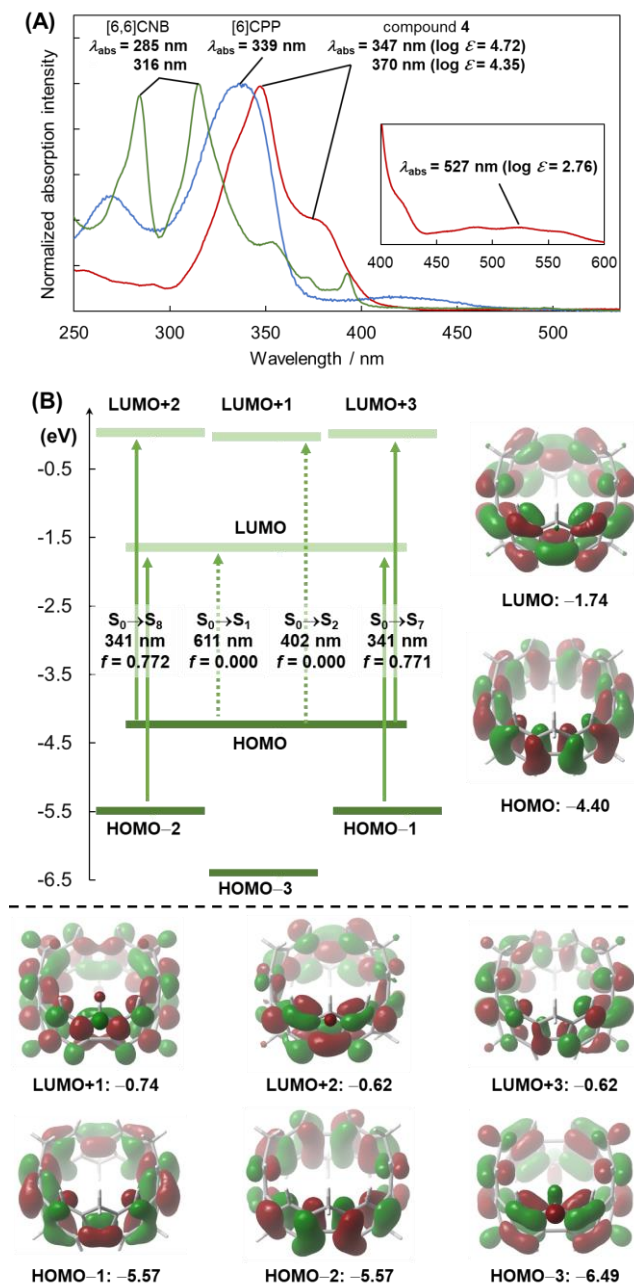


Figure 4. (A) UV/vis absorption spectra (**4**: red line; [6]CPP: blue line; [6,6]CNB: green line) in CH₂Cl₂. A weakly absorbing region (inset) was measured at high concentration. (B) Energy diagrams and frontier molecular orbitals of **4** calculated at the B3LYP/6-31G(d) level of theory (unit: eV).

Next, the energies of frontier orbitals of even-numbered [*n*]LPPs, [*n*]CPPs, and methylene-bridged [*n*]CPPs are plotted in Figure 5 (also see Figures S5–S25). Methylene-bridged [*n*]CPPs have increasing HOMO energies and decreasing LUMO energies (narrowing HOMO–LUMO gaps) with a decreased number of benzene rings (*n*). This size dependency of the HOMO/LUMO energies of methylene-bridged [*n*]CPPs is similar to those of [*n*]CPP and in direct contrast to [*n*]LPPs.²⁴ The size dependency of the LUMO level of methylene-bridged [*n*]CPPs is smaller than that of [*n*]CPPs, which is similar to the previous report on the [*n*]CPPs in which phenylene–phenylene torsion angles are restricted.⁷ Importantly, owing to the bending effect,⁷

methylene-bridged CPPs have narrower HOMO–LUMO gaps than very long $[n]$ LPPs, which possess high HOMO level compared with $[n]$ CPPs. The readily available high HOMO level and narrow HOMO–LUMO gap of methylene-bridged $[n]$ CPPs highlight their potential utility as organic semiconducting materials.

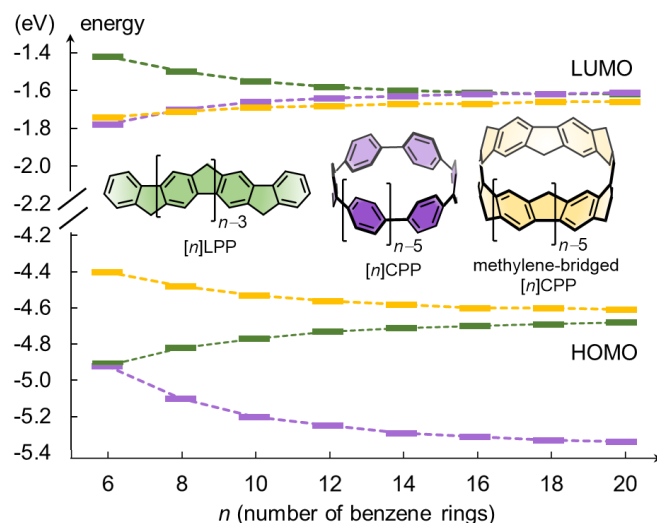


Figure 5. HOMO and LUMO energies of even-numbered $[n]$ LPPs (green dotted line), $[n]$ CPPs (purple dotted line), and methylene-bridged $[n]$ CPPs (orange dotted line) calculated at the B3LYP/6-31G(d) level of theory.

Comparison among 4, [6]CPP, and [6,6]CNB

Methylene-bridged [6]CPP (**4**) represents an exciting new addition to the family of carbon nanoring and nanobelt. Moreover, the present study allows us to better understand the structure–property relationship around these molecular entities. Representative parameters of **4**, [6]CPP, and [6,6]CNB are summarized in Table 1 (see Table S8 for the detailed comparison). Compared with [6]CPP and [6,6]CNB, methylene-bridged [6]CPP containing alternating five- and six-membered rings gives rise to the smallest diameter, highest HOMO energy, and narrowest HOMO–LUMO gap. These unique geometric features and physical properties make methylene-bridged $[n]$ CPPs a brand-new aromatic belt.

Table 1. Comparison among **4**, [6]CPP, and [6,6]CNB.

compound ^a	4	[6]CPP	[6,6]CNB
diameter (Å) ^b	7.758	8.072	8.053
C–C (Å) ^c	1.478	1.489	1.464
HOMO (eV) ^d	−4.40	−4.92	−4.92
LUMO (eV) ^d	−1.74	−1.78	−1.97
HOMO–LUMO gap (eV)	2.66	3.14	2.95
strain energy (kcal·mol ^{−1}) ^e	110.2	96.9	119.5

^aThe crystal data of [6]CPP²⁰ and [6,6]CNB^{8a} were taken from references. ^bThe averaged diameter was measured as the distance between the two central phenylene units located at opposite sides. ^cThe averaged length of C–C single

bond connecting the neighboring phenylene units. ^dFrontier molecular orbitals calculated at the B3LYP/6-31G(d) level of theory. ^eThe strain energy data of [6]CPP⁶ and [6,6]CNB^{8a} were taken from references.

Conclusions

In summary, we have established an efficient synthetic strategy to synthesize the first methylene-bridged [6]CPP through the use of pillar[6]arene as an easily accessible macrocyclic precursor. The product is synthesized through an efficient six-fold intramolecular nickel-mediated Yamamoto coupling. The belt-shaped structure was determined by single-crystal X-ray structure analysis. A particular advantage of this methylene-bridged CPPs over pristine CPPs is its enhancement of π -conjugation along the backbone by reducing the torsion angle between neighboring phenylene units, which has been proven as an efficient strategy to reduce the energy gap. Moreover, the incorporation of small molecules in the defined pocket of methylene-bridged [6]CPP also paves the way for its application in supramolecular chemistry. This work not only exhibits an efficient strategy to construct a new family of aromatic belt, but also showcases their properties, which combine the merits of CPPs and pillararenes. In a broader perspective, further oxidation of methylene-bridged [6]CPP to form the fully conjugated and lower energy gap belt is also attractive for potential future applications in nanoelectronics and photonics.²⁵ Further exploration in this area is ongoing in our laboratory.

ASSOCIATED CONTENT

Supporting Information

The Supporting Information is available free of charge on the ACS Publications website.

Synthetic procedures, characterization data, details of the photophysical measurements, and NMR spectra of new compounds (PDF)

Cartesian coordinates of optimized structures (XYZ)

X-ray crystallographic data for **4** (CIF)

AUTHOR INFORMATION

Corresponding Author

*E-mail: itami@chem.nagoya-u.ac.jp (K.I.).

ORCID

Yuanming Li: 0000-0003-3180-1305

Yasutomo Segawa: 0000-0001-6439-8546

Akiko Yagi: 0000-0003-2941-4357

Kenichiro Itami: 0000-0001-5227-7894

Notes

The authors declare no competing financial interest.

ACKNOWLEDGMENT

This work was supported by the ERATO program from JST (JPMJER1302 to K.I.), JSPS KAKENHI (grant numbers 19H05463 to K.I., JP19H02701 and JP19K22183 to Y.S., and

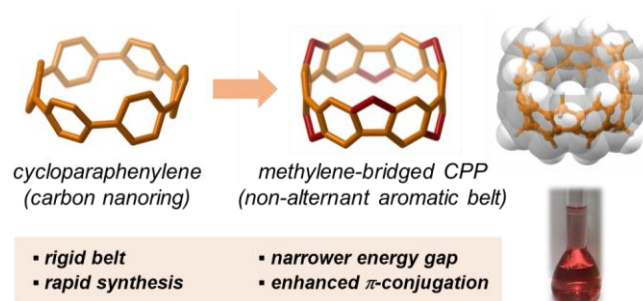
19K15537 to A.Y.) and CREST program from JST (JPMJCR19R1 to A.Y.). We thank Mr. Wataru Matsuoka for X-ray crystal structure analysis, and Dr. Iain A. Stepek, Dr. Kwan Yin Cheung, and Dr. Kenta Kato for constructive criticism of the manuscript. Y.L. is a recipient of JSPS Postdoctoral Fellowships for Research in Japan. Calculations were performed using the resources of the Research Center for Computational Science, Okazaki, Japan. ITbM is supported by the World Premier International Research Center Initiative (WPI), Japan.

REFERENCES

- (1) (a) *Fragments of Fullerenes and Carbon Nanotubes: Designed Synthesis, Unusual Reactions, and Coordination Chemistry*; Petrukhina, M. A.; Scott, L. T., Eds.; John Wiley & Sons: Hoboken, NJ, 2012. (b) Wu, Y.-T.; Siegel, J. S. Synthesis, Structures, and Physical Properties of Aromatic Molecular-Bowl Hydrocarbons. In *Polyarenes I*, Siegel, J. S.; Wu, Y.-T. Eds. Springer Berlin Heidelberg: Berlin, Heidelberg, 2014; pp 63–120. (c) Narita, A.; Wang, X.-Y.; Feng, X.; Müllen, K. New advances in nanographene chemistry. *Chem. Soc. Rev.* **2015**, *44*, 6616–6643. (d) Segawa, Y.; Ito, H.; Itami, K. Structurally uniform and atomically precise carbon nanostructures. *Nat. Rev. Mater.* **2016**, *1*, 15002. (e) Pun, S. H.; Miao, Q. Toward Negatively Curved Carbons. *Acc. Chem. Res.* **2018**, *51*, 1630–1642. (f) Bols, P. S.; Anderson, H. L. Template-Directed Synthesis of Molecular Nanorings and Cages. *Acc. Chem. Res.* **2018**, *51*, 2083–2092. (g) Segawa, Y.; Levine, D. R.; Itami, K. Topologically Unique Molecular Nanocarbons. *Acc. Chem. Res.* **2019**, *52*, 2760–2767. (h) Majewski, M. A.; Stępień, M. Bowls, Hoops, and Saddles: Synthetic Approaches to Curved Aromatic Molecules. *Angew. Chem., Int. Ed.* **2019**, *58*, 86–116. (i) Leonhardt, E. J.; Jasti, R. Emerging applications of carbon nanohoops. *Nat. Rev. Chem.* **2019**, *3*, 672–686.
- (2) (a) Iyoda, M.; Yamakawa, J.; Rahman, M. J. Conjugated Macrocycles: Concepts and Applications. *Angew. Chem., Int. Ed.* **2011**, *50*, 10522–10553. (b) Darzi, E. R.; Jasti, R. The dynamic, size-dependent properties of [5]–[12]cycloparaphenylenes. *Chem. Soc. Rev.* **2015**, *44*, 6401–6410. (c) Lewis, S. E. Cycloparaphenylenes and related nanohoops. *Chem. Soc. Rev.* **2015**, *44*, 2221–2304. (d) Yamago, S.; Kayahara, E.; Hashimoto, S. Cycloparaphenylenes and Carbon Nanorings. In *Polycyclic Arenes and Heteroarenes: Synthesis, Properties, and Applications*; Miao, Q., Ed.; John Wiley & Sons: Chichester, U.K., 2015; pp 143–162. (e) Guo, L.; Yang, X.; Cong, H. Synthesis of Macrocyclic Oligoparaphenylenes Derived from Anthracene Photodimer. *Chin. J. Chem.* **2018**, *36*, 1135–1138. (f) Lu, D.; Huang, Q.; Wang, S.; Wang, J.; Huang, P.; Du, P. The Supramolecular Chemistry of Cycloparaphenylenes and Their Analogs. *Front. Chem.* **2019**, *7*, 668.
- (3) (a) Kawase, T.; Kurata, H. Ball-, Bowl-, and Belt-Shaped Conjugated Systems and Their Complexing Abilities: Exploration of the Concave–Convex π – π Interaction. *Chem. Rev.* **2006**, *106*, 5250–5273. (b) Tahara, K.; Tobe, Y. Molecular Loops and Belts. *Chem. Rev.* **2006**, *106*, 5274–5290. (c) Gleiter, R.; Esser, B.; Kornmayer, S. C. Cyclacenes: Hoop-Shaped Systems Composed of Conjugated Rings. *Acc. Chem. Res.* **2009**, *42*, 1108–1116. (d) Eisenberg, D.; Shenhar, R.; Rabinovitz, M. Synthetic approaches to aromatic belts: building up strain in macrocyclic polyarenes. *Chem. Soc. Rev.* **2010**, *39*, 2879–2890.
- (4) (a) Grimsdale, A. C.; Müllen, K. Bridged Polyphenylenes – from Polyfluorenes to Ladder Polymers. In *Polyfluorenes*, Scherf, U.; Neher, D. Eds. Springer Berlin Heidelberg: Berlin, Heidelberg, 2008; pp 1–48. (b) Grimsdale, A. C.; Müllen, K. *Phenylene-Based Ladder Polymers*. In *Design and Synthesis of Conjugated Polymers*, Leclerc, M.; Morin, J. Eds. Wiley-VCH, Weinheim, 2010, pp. 227–245.
- (5) (a) Grimsdale, A. C.; Müllen, K. Polyphenylene-type Emissive Materials: Poly(para-phenylene)s, Polyfluorenes, and Ladder Polymers. In *Emissive Materials Nanomaterials*, Springer Berlin Heidelberg: Berlin, Heidelberg, 2006; pp 1–82. (b) Xie, L.-H.; Yin, C.-R.; Lai, W.-Y.; Fan, Q.-L.; Huang, W. Polyfluorene-based semiconductors combined with various periodic table elements for organic electronics. *Prog. Polym. Sci.* **2012**, *37*, 1192–1264.
- (6) Segawa, Y.; Omachi, H.; Itami, K. Theoretical Studies on the Structures and Strain Energies of Cycloparaphenylenes. *Org. Lett.* **2010**, *12*, 2262–2265.
- (7) Segawa, Y.; Fukazawa, A.; Matsuura, S.; Omachi, H.; Yamaguchi, S.; Irle, S.; Itami, K. Combined experimental and theoretical studies on the photophysical properties of cycloparaphenylenes. *Org. Biomol. Chem.* **2012**, *10*, 5979–5984.
- (8) (a) Povie, G.; Segawa, Y.; Nishihara, T.; Miyauchi, Y.; Itami, K. Synthesis of a carbon nanobelt. *Science* **2017**, *356*, 172–175. (b) Povie, G.; Segawa, Y.; Nishihara, T.; Miyauchi, Y.; Itami, K. Synthesis and Size-Dependent Properties of [12], [16], and [24]Carbon Nanobelts. *J. Am. Chem. Soc.* **2018**, *140*, 10054–10059. (c) Cheung, K. Y.; Watanabe, K.; Segawa, Y.; Itami, K. *Synthesis of a Zigzag Carbon Nanobelt*. *ChemRxiv* **2020**, 10.26434/chemrxiv.12324353.v1.
- (9) Cheung, K. Y.; Gui, S.; Deng, C.; Liang, H.; Xia, Z.; Liu, Z.; Chi, L.; Miao, Q. Synthesis of Armchair and Chiral Carbon Nanobelts. *Chem* **2019**, *5*, 838–847.
- (10) Nishigaki, S.; Shibata, Y.; Nakajima, A.; Okajima, H.; Masumoto, Y.; Osawa, T.; Muranaka, A.; Sugiyama, H.; Horikawa, A.; Uekusa, H.; Koshino, H.; Uchiyama, M.; Sakamoto, A.; Tanaka, K. Synthesis of Belt- and Möbius-Shaped Cycloparaphenylenes by Rhodium-Catalyzed Alkyne Cyclotrimerization. *J. Am. Chem. Soc.* **2019**, *141*, 14955–14960.
- (11) (a) Kayahara, E.; Qu, R.; Kojima, M.; Iwamoto, T.; Suzuki, T.; Yamago, S. Ligand-Controlled Synthesis of [3]- and [4]Cyclo-9,9-dimethyl-2,7-fluorenes through Triangle- and Square-Shaped Platinum Intermediates. *Chem. Eur. J.* **2015**, *21*, 18939–18943. (b) Liu, Y.-Y.; Lin, J.-Y.; Bo, Y.-F.; Xie, L.-H.; Yi, M.-D.; Zhang, X.-W.; Zhang, H.-M.; Loh, T.-P.; Huang, W. Synthesis and Crystal Structure of Highly Strained [4]Cyclofluorene: Green-Emitting Fluorophore. *Org. Lett.* **2016**, *18*, 172–175. (c) Li, S.; Aljhdli, M.; Thakellapalli, H.; Farajidizaji, B.; Zhang, Y.; Akhmedov, N. G.; Milsman, C.; Popp, B. V.; Wang, K. K. Synthesis and Structure of a Functionalized

- [9] Cycloparaphenylene Bearing Three Indeno[2,1-a]fluorene-11,12-dione-2,9-diyl Units. *Org. Lett.* **2017**, *19*, 4078–4081. (d) Sicard, L.; Jeannin, O.; Rault-Berthelot, J.; Quinton, C.; Poriel, C. [4]Cyclofluorene: Unexpected Influence of Alkyl Chain Length. *ChemPlusChem* **2018**, *83*, 874–880. (e) Poriel, C.; Sicard, L.; Quinton, C.; Rault-berthelot, J.; Jeannin, O.; Lucas, F.; Bouit, P. A. [n]-Cyclo-9,9-dibutyl-2,7-fluorene ($n = 4,5$): Nanoring size influence in carbon bridged cyclo-para-phenylenes. *Angew. Chem., Int. Ed.* 10.1002/anie.202002517.
- (12) Friederich, R.; Nieger, M.; Vögtle, F. Auf dem Weg zu makrocyclischen para-Phenylenen. *Chem. Ber.* **1993**, *126*, 1723–1732.
- (13) While this project is ongoing in our group, Wang and coworkers reported the synthesis of hydrocarbon belts using resorcin[n]arenes, which represents a breakthrough in this area. (a) Zhang, Q.; Zhang, Y.-E.; Tong, S.; Wang, M.-X. Hydrocarbon Belts with Truncated Cone Structures. *J. Am. Chem. Soc.* **2020**, *142*, 1196–1199. (b) Shi, T.-H.; Guo, Q.-H.; Tong, S.; Wang, M.-X. Toward the Synthesis of a Highly Strained Hydrocarbon Belt. *J. Am. Chem. Soc.* **2020**, *142*, 4576–4580. (c) Wang, M.-X.; Shi, T.-H.; Tong, S. Construction of Hydrocarbon Nanobelts. *Angew. Chem., Int. Ed.* 10.1002/anie.202002827.
- (14) (a) Stevenson, S.; Rice, G.; Glass, T.; Harich, K.; Cromer, F.; Jordan, M. R.; Craft, J.; Hadju, E.; Bible, R.; Olmstead, M. M.; Maitra, K.; Fisher, A. J.; Balch, A. L.; Dorn, H. C. Small-bandgap endohedral metallofullerenes in high yield and purity. *Nature* **1999**, *401*, 55–57. (b) Charlier, J. C. Defects in Carbon Nanotubes. *Acc. Chem. Res.* **2002**, *35*, 1063–1069. (c) Segawa, Y.; Yagi, A.; Matsui, K.; Itami, K. Design and Synthesis of Carbon Nanotube Segments. *Angew. Chem., Int. Ed.* **2016**, *55*, 5136–5158. (d) Hitosugi, S.; Sato, S.; Matsuno, T.; Koretsune, T.; Arita, R.; Isobe, H. Pentagon-Embedded Cycloarylenes with Cylindrical Shapes. *Angew. Chem., Int. Ed.* **2017**, *56*, 9106–9110.
- (15) Ogoshi, T.; Kanai, S.; Fujinami, S.; Yamagishi, T.-a.; Nakamoto, Y. para-Bridged Symmetrical Pillar[5]arenes: Their Lewis Acid Catalyzed Synthesis and Host–Guest Property. *J. Am. Chem. Soc.* **2008**, *130*, 5022–5023.
- (16) Cao, D.; Kou, Y.; Liang, J.; Chen, Z.; Wang, L.; Meier, H. A Facile and Efficient Preparation of Pillararenes and a Pillarquinone. *Angew. Chem., Int. Ed.* **2009**, *48*, 9721–9723.
- (17) Hu, X.-B.; Chen, Z.; Chen, L.; Zhang, L.; Hou, J.-L.; Li, Z.-T. Pillar[n]arenes ($n = 8–10$) with two cavities: synthesis, structures and complexing properties. *Chem. Commun.* **2012**, *48*, 10999–11001.
- (18) (a) Ogoshi, T.; Umeda, K.; Yamagishi, T.-a.; Nakamoto, Y. Through-space π -delocalized Pillar[5]arene. *Chem. Commun.* **2009**, 4874–4876. (b) Ma, Y.; Chi, X.; Yan, X.; Liu, J.; Yao, Y.; Chen, W.; Huang, F.; Hou, J.-L. per-Hydroxylated Pillar[6]arene: Synthesis, X-ray Crystal Structure, and Host–Guest Complexation. *Org. Lett.* **2012**, *14*, 1532–1535.
- (19) Myśliwiec, D.; Kondratowicz, M.; Lis, T.; Chmielewski, P. J.; Stępień, M. Highly Strained Nonclassical Nanotube End-caps. A Single-Step Solution Synthesis from Strain-Free, Non-Macrocyclic Precursors. *J. Am. Chem. Soc.* **2015**, *137*, 1643–1649.
- (20) Spisak, S. N.; Wei, Z.; Darzi, E.; Jasti, R.; Petrukhina, M. A. Highly strained [6]cycloparaphenylene: crystallization of an unsolvated polymorph and the first mono- and dianions. *Chem. Commun.* **2018**, *54*, 7818–7821.
- (21) (a) Xia, J.; Jasti, R. Synthesis, Characterization, and Crystal Structure of [6]Cycloparaphenylene. *Angew. Chem., Int. Ed.* **2012**, *51*, 2474–2476. (b) Fukushima, T.; Sakamoto, H.; Tanaka, K.; Hijikata, Y.; Irle, S.; Itami, K. Polymorphism of [6]Cycloparaphenylene for Packing Structure-dependent Host–Guest Interaction. *Chem. Lett.* **2017**, *46*, 855–857.
- (22) Adamska, L.; Nayyar, I.; Chen, H.; Swan, A. K.; Oldani, N.; Fernandez-Alberti, S.; Golder, M. R.; Jasti, R.; Doorn, S. K.; Tretiak, S. Self-Trapping of Excitons, Violation of Condon Approximation, and Efficient Fluorescence in Conjugated Cycloparaphenylenes. *Nano Lett.* **2014**, *14*, 6539–6546.
- (23) Shukla, M. K.; Leszczynski, J. A density functional theory study on the effect of shape and size on the ionization potential and electron affinity of different carbon nanostructures. *Chem. Phys. Lett.* **2006**, *428*, 317–320.
- (24) Iwamoto, T.; Watanabe, Y.; Sakamoto, Y.; Suzuki, T.; Yamago, S. Selective and Random Syntheses of [n]Cycloparaphenylenes ($n = 8–13$) and Size Dependence of Their Electronic Properties. *J. Am. Chem. Soc.* **2011**, *133*, 8354–8361.
- (25) (a) Tobe, Y. Non-Alternant Non-Benzenoid Aromatic Compounds: Past, Present, and Future. *Chem. Rec.* **2015**, *15*, 86–96. (b) Esser, B. Theoretical analysis of [5.5.6]cyclacenes: electronic properties, strain energies and substituent effects. *Phys. Chem. Chem. Phys.* **2015**, *17*, 7366–7372. (c) Hu, P.; Lee, S.; Herng, T. S.; Aratani, N.; Gonçalves, T. P.; Qi, Q.; Shi, X.; Yamada, H.; Huang, K.-W.; Ding, J.; Kim, D.; Wu, J. Toward Tetraradicaloid: The Effect of Fusion Mode on Radical Character and Chemical Reactivity. *J. Am. Chem. Soc.* **2016**, *138*, 1065–1077. (d) Maekawa, T.; Ueno, H.; Segawa, Y.; Haley, M. M.; Itami, K. Synthesis of open-shell ladder π -systems by catalytic C–H annulation of diarylacetylenes. *Chem. Sci.* **2016**, *7*, 650–654. (e) Frederickson, C. K.; Rose, B. D.; Haley, M. M. Explorations of the Indenofluorenes and Expanded Quinoidal Analogues. *Acc. Chem. Res.* **2017**, *50*, 977–987.

Table of Contents (TOC)



NonAlternantBelt_20200603.pdf (1.17 MiB)

[view on ChemRxiv](#) • [download file](#)

Supporting Information

A Non-alternant Aromatic Belt: Methylene-bridged [6]Cycloparaphenylene Synthesized from Pillar[6]arene

Yuanming Li,[†] Yasutomo Segawa,^{‡, #, §, \$} Akiko Yagi,[‡] and Kenichiro Itami^{*, †, ‡, #}

[†]Institute of Transformative Bio-Molecules (WPI-ITbM), Nagoya University, Chikusa, Nagoya 464-8602, Japan

[‡]Graduate School of Science, Nagoya University, Chikusa, Nagoya 464-8602, Japan

[#]JST-ERATO, Itami Molecular Nanocarbon Project, Nagoya University, Chikusa, Nagoya 464-8602, Japan

[§]Institute for Molecular Science, Myodaiji, Okazaki, 444-8787, Japan

^{\$}Department of Structural Molecular Science, SOKENDAI (The Graduate University for Advanced Studies), Myodaiji, Okazaki, 444-8787, Japan.

****E-mail: itami@chem.nagoya-u.ac.jp (K.I.).***

Table of Contents

1. General.....	S3
2. The synthesis of methylene-bridged [6]CPP	S4
2.1 The synthesis of pillar[6]arene.....	S4
2.2 The synthesis of hydroxylated pillar[6]arene	S5
2.3 The synthesis of triflate-functionalized pillar[6]arene.....	S6
2.4 The synthesis of methylene-bridged [6]CPP	S7
2.5 The optimization of intramolecular nickel-mediated Yamamoto coupling	S8
3. The X-ray crystal structure	S9
3.1 The comparison of X-ray crystal structure and DFT calculated result	S10
3.2 The CH– π distances between methylene-bridged [6]CPPs	S11
3.3 The reduction of length of LPP	S12
4. Computational study	S14
4.1 HOMO and LUMO energies of [n]CPP, CH ₂ -bridged [n]CPP, and [n]LPP.....	S14
4.2 Optimized structures and frontier molecular orbitals	S16
4.3 The calculation of strain energy.....	S36
4.4 Simulated NMR chemical shifts (ppm)	S38
4.5 TD-DFT vertical one-electron excitations	S39
4.6 Uncorrected and thermal-corrected energies of stationary points	S41
4.7 Cartesian coordinates of optimized structures	S42
5. Photophysical properties and stability test.....	S42
6. Representative aromatic belts having CPP skeleton.....	S43
7. Comparison among 4 , [6]CPP, [6,6]CNB, and pillar[6]arene	S44
8. NMR spectra of new compounds.....	S45
9. References.....	S51

1. General

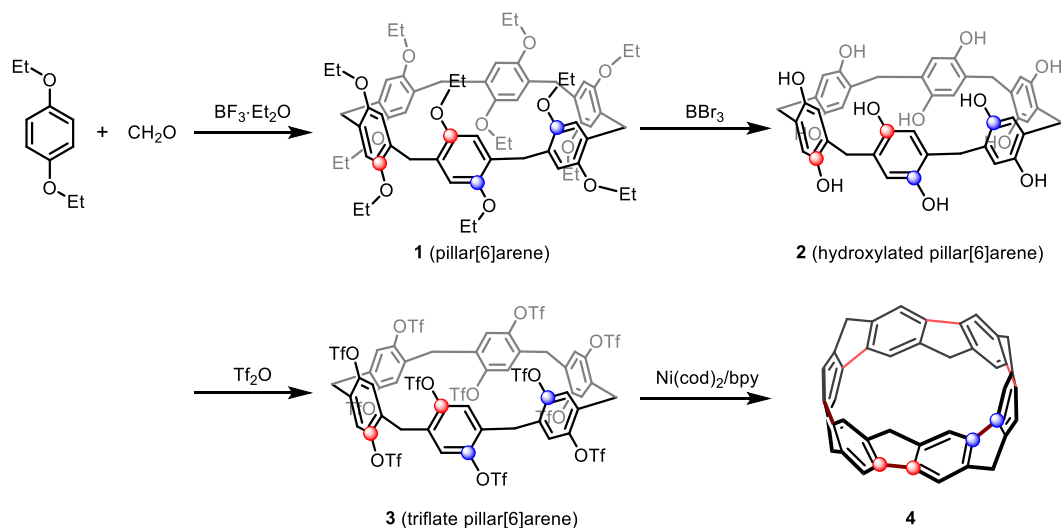
Unless otherwise noted, all reactants or reagents including dry solvents were obtained from commercial suppliers and used as received. Unless otherwise noted, all reactions were performed with dry solvents under an atmosphere of argon in dried glassware using standard vacuum-line techniques. All work-up and purification procedures were carried out with reagent-grade solvents in air.

Analytical thin-layer chromatography (TLC) was performed using E. Merck silica gel 60 F254 precoated plates (0.25 mm); detection with UV light or by dipping into a solution of KMnO_4 (1.5 g in 400 mL H_2O , 5 g NaHCO_3), followed by heating. Flash column chromatography was performed with E. Merck silica gel 60 (230-400 mesh). The developed chromatogram was analyzed by a UV lamp (254 nm). Medium pressure liquid chromatography (MPLC) was performed using Yamazen W-prep 2XY. Preparative thin-layer chromatography (PTLC) was performed using Wakogel B5-F silica-coated plates (0.75 mm) prepared in our laboratory. Preparative gel permeation chromatography (GPC) was performed with a JAI LC-9204 instrument equipped with JAIGEL-1H/JAIGEL-2H columns using chloroform as an eluent. Gas chromatography (GC) analysis was conducted on a Shimadzu GC-2010 instrument equipped with a HP-5 column (30 m \cdot 0.25 mm, Hewlett-Packard) with dodecane as an internal standard.

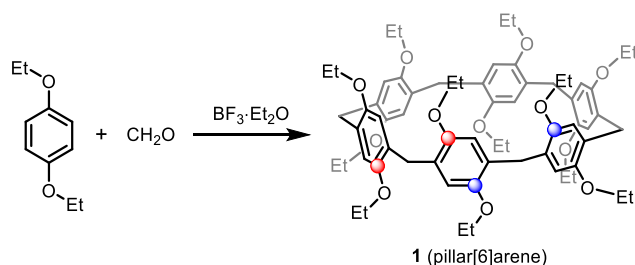
The high-resolution mass spectra (HRMS) were conducted on Thermo Fisher Scientific Exactive. Infrared spectra were recorded on a JASCO FTIR-6100 spectrometer. Nuclear magnetic resonance (NMR) spectra were recorded on a JEOLJNM-ECA-600 (^1H 600 MHz, ^{13}C 150 MHz) spectrometer and a JEOL JNM-ECA-400 (^1H 400 MHz, ^{13}C 100 MHz) spectrometer. Chemical shifts for ^1H NMR are expressed in parts per million (ppm) relative to tetramethylsilane (δ 0.00 ppm) or residual peak of CDCl_3 (δ 7.26 ppm). Chemical shifts for ^{13}C NMR are expressed in ppm relative to CDCl_3 (δ 77.16 ppm) or acetone- d_6 (δ 29.84 ppm). Chemical shifts for ^{19}F NMR are expressed in ppm relative to C_6F_6 (δ -164.9 ppm). Data are reported as follows: chemical shift, multiplicity (s = singlet, d = doublet, dd = doublet of doublets, t = triplet, m = multiplet, brs = broad singlet), coupling constant (Hz), and integration.

2. The synthesis of methylene-bridged [6]CPP

Scheme S1. The synthetic route leading to methylene-bridged [6]CPP.

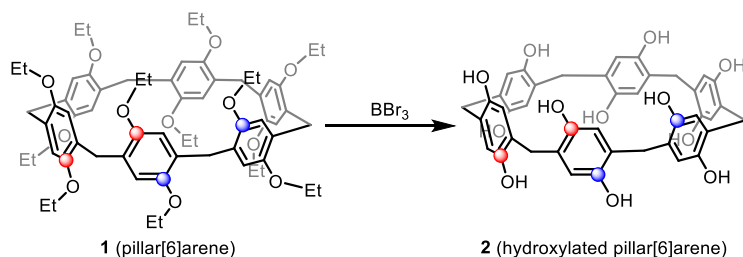


2.1 The synthesis of pillar[6]arene



In 2009, pillar[6]arene was first synthesized by Cao and coworker.¹ Although many high-yield synthetic methods were reported recently, the synthesis of pillar[6]arene from 1,4-diethoxybenzene and paraformaldehyde using $\text{BF}_3 \cdot \text{Et}_2\text{O}$ as a catalyst is still attractive,² due to the easily accessible starting materials and applicable to large-scale synthesis. The mixture of 1,4-diethoxybenzene (6.15 g, 37.0 mmol, 1.0 equiv) and paraformaldehyde (1.33 g, 44.4 mmol, 1.2 equiv) in anhydrous CHCl_3 (300 mL) was stirred at 30 °C under nitrogen for 0.5 h, followed by dropwise addition of $\text{BF}_3 \cdot \text{Et}_2\text{O}$ (5.9 mL, 48.1 mmol, 1.2 equiv). (Temperature is crucial for the reaction). After being stirred for 1 h at 30 °C, a dark green solution was obtained. And the reaction solution was washed with brine (100 mL). The organic layers were dried over anhydrous Na_2SO_4 , filtered and concentrated by rotary evaporation. The residue was then purified by silica gel column chromatography with gradient elution of *n*-hexane/EtOAc/ CH_2Cl_2 (25:1:1→5:1:1) to give **1** (pillar[6]arene) (470 mg, 0.44 mmol, 7.0%, white solid) and pillar[5]arene (1.9 g, 2.1 mmol, white solid). R_f (EtOAc/hexane = 1:10): 0.4 (pillar[5]arene) and 0.2 (pillar[6]arene); ^1H and ^{13}C NMR spectra are consistent with the previous report.² ^1H NMR (CDCl_3 , 400 MHz): δ 6.69 (s, 12H), 3.83 (q, J = 6.4 Hz, 24H), 3.79 (s, 12H), 1.28 (t, J = 6.4 Hz, 36H).

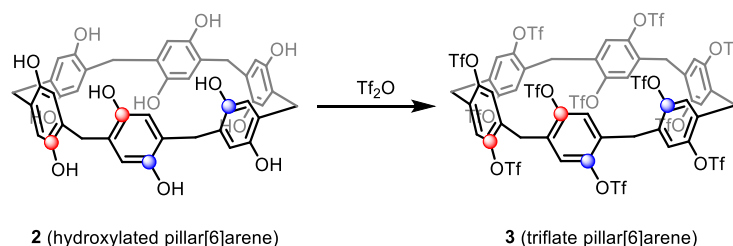
2.2 The synthesis of hydroxylated pillar[6]arene³



To a solution of pillar[6]arene (600 mg, 561 μmol , 1.0 equiv) in dry CHCl_3 (22 mL) was added BBr_3 (22.4 mL, 22.4 mmol, 40 equiv, 1 M in dichloromethane) dropwise at 0 $^\circ\text{C}$. After the addition, the mixture was warmed slowly to room temperature and stirred for 24 h. After the reaction, MeOH (1 mL) was added very slowly at 0 $^\circ\text{C}$ and followed by ice water (10 mL). (The quenching of BBr_3 fumes violently!) And the precipitate was collected by filtration and washed with copious amounts of 0.5 M aqueous hydrochloric acid, water, and chloroform.

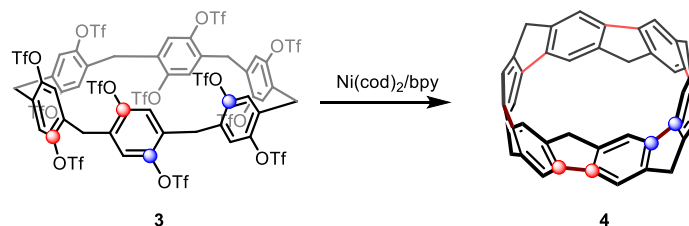
Subsequently, the precipitate was dissolved in acetone, dried over Na_2SO_4 , and filtered. CHCl_3 (50 mL) was added to the resulting acetone solution. The mixture was concentrated until about 10 mL of the solution remained, 100 mL CHCl_3 was further added slowly. The resulting precipitate was collected and dried under high vacuum to give **2** (330 mg, 0.45 mmol, 80%) as a light pink solid without further purification (keep the compound in a fridge). R_f ($\text{CH}_2\text{Cl}_2/\text{MeOH} = 10:1$): 0.3; ^1H and ^{13}C NMR spectra are consistent with the previous report.³ ^1H NMR (acetone- d_6 , 400 MHz): δ 6.55 (s, 12H), 3.65 (s, 12H).

2.3 The synthesis of triflate-functionalized pillar[6]arene⁴



To a solution of hydroxylated pillar[6]arene (352 mg, 480 μmol , 1.0 equiv) in CH_2Cl_2 (65 mL), pyridine (0.69 mL, 8.6 mmol, 18 equiv) and trifluoromethanesulfonic anhydride (1.3 mL, 7.7 mmol, 16 equiv) were added at 0 $^\circ\text{C}$ under N_2 atmosphere. After addition, a large amount of precipitate was formed. The mixture was warmed slowly to room temperature and stirred for 22 hours. After the reaction, water (10 mL) was added at 0 $^\circ\text{C}$ slowly. The reaction mixture was concentrated until about 20 mL amount of CH_2Cl_2 remained. And the precipitate was collected by filtration, washed with copious amounts of water, and 10 mL solution of *n*-hexane/ CH_2Cl_2 (1:1), followed by drying under high vacuum. Subsequently, the solid was dissolved with acetone and purified by a short column of silica with gradient elution of acetone/hexane (2:1 \rightarrow 1:0). The solution was concentrated until about 10 mL of the solution remained, 50 mL *n*-hexane was further added slowly. The resulting precipitate was collected to give triflate-functionalized pillar[6]arene **3** (550 mg, 237 μmol , 49%) as a white solid. R_f (*n*-hexane/acetone = 5:1): 0.5; ^1H NMR (600 MHz, acetone- d_6) δ 7.51 (s, 12H), 4.47 (s, 12H). ^{19}F NMR (369 MHz, acetone- d_6) δ -74.88. ^{13}C NMR (150 MHz, acetone- d_6) δ 147.5, 133.5, 126.2, 119.3 (q, J_{FC} = 320 Hz), 30.9. HRMS (ESI): Exact mass calculated for $\text{C}_{54}\text{H}_{24}\text{F}_{36}\text{NaO}_{36}\text{S}_{12}$ ($[\text{M}+\text{Na}]^+$): 2338.6013, mass found: 2338.6089.

2.4 The synthesis of methylene-bridged [6]CPP

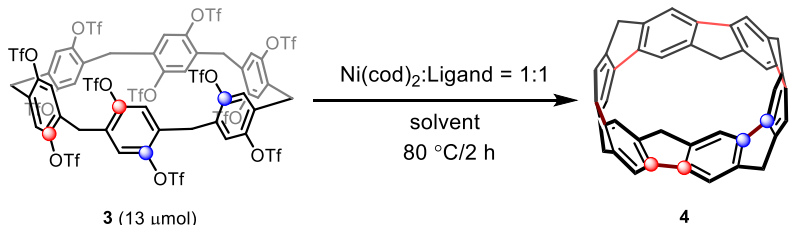
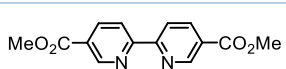
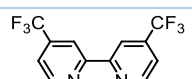
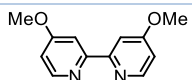
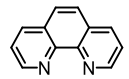
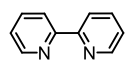
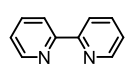
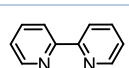
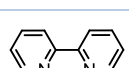
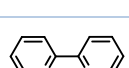
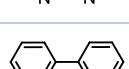
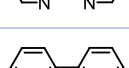


To a dry Schlenk tube charged with 2,2'-bipyridyl (84.3 mg, 540 μ mol, 12 equiv), was added Ni(cod)₂ (148 mg, 540 μ mol, 12 equiv) under argon (this operation in the glovebox), followed by *N*-methyl-2-pyrrolidone (NMP) (6.0 mL). The mixture was stirred for 40 mins at room temperature and a dark purple solution of the complex was obtained quickly (about 3 mins later). The mixture was set in an oil bath at 80 °C and stir for 5 mins to reach thermal equilibrium and complete the formation of the nickel complex. The solution of pillar[6]arene triflate **3** (104 mg, 45.0 μ mol, 1.0 equiv) in NMP (9.0 mL) was then added in one portion. After 2 hours of stirring at 80 °C, the reaction mixture was allowed to cool down to rt, then diluted with CH₂Cl₂ (50 mL) and sat. aq. NH₄Cl (50 mL).

The dark purple heterogeneous mixture was vigorously stirred for 10 mins. The organic layer was separated and then washed once with sat. aq. NH₄Cl (50 mL), two-time with water (2×50 mL) and one-time with brine (50 mL). Subsequently, the organic layer was dried over Na₂SO₄, filtered and concentrated to give 1 mL solution by rotary evaporation. The remaining NMP was further removed by high vacuum at 55 °C. The residual solid was dissolved by CH₂Cl₂/CS₂ and then purified by a short (2 cm long) silica gel column chromatography quickly with CH₂Cl₂/*n*-hexane/CS₂ (25:25:2) as eluent. (Before purification by column, the silica gel column should be washed with CH₂Cl₂/*n*-hexane/CS₂ (25:25:2).) The solvent was removed under rotary evaporation and dried under high vacuum. Subsequently, *n*-hexane/CHCl₃ (3:1, 10 mL) was added in the flask and then decanted. The red solid on the flask wall was dried to give the target compound **4** (crude NMR yield 27%, purity: \geq 90%). The solid was further purified by recycling preparative gel-permeation chromatography (GPC), affording red solid which was dried under high vacuum for 30 mins. The red solid was washed with CHCl₃ (5 mL) until the solution of CHCl₃ become colorless. The red solid was dried under high vacuum to give a red solid (3.6 mg, 6.8 μ mol, purity \geq 95%). (After purification by GPC, the solid is practically insoluble in CHCl₃, less than 1 mg/10 mL.) *R_f* (*n*-hexane/CH₂Cl₂/CS₂ = 20:10:1): 0.4 (Without CS₂, the product could not be observed on TLC.). ¹H NMR (600 MHz, CDCl₃, **4**) δ 7.86 (s, 12H), 4.29 (d, *J* = 17.0 Hz, 6H), 4.09 (d, *J* = 17.0 Hz, 6H). ¹H NMR (600 MHz, CDCl₃/CS₂) δ 7.84 (s, 12H), 4.30 (s, 6H), 4.02 (d, *J* = 16.5 Hz, 6H). ¹³C NMR (150 MHz, CDCl₃/CS₂) δ 148.0, 137.1, 121.8, 40.9. HRMS (ESI): Exact mass calculated for C₄₂H₂₅ ([M+H]⁺): 529.1951, mass found: 529.1902. (See Figure S27 for the photostability data.)

2.5 The optimization of intramolecular nickel-mediated Yamamoto coupling

Table S1. The optimization of intramolecular nickel-mediated aryl-aryl coupling.^a

 <p style="text-align: center;">3 (13 μmol) 4</p>			
entry	ligand	solvent (mM) ^b	4 (%) ^c
1		DMA (4.3)	3.0
2		DMA (4.3)	6.9
3		DMA (4.3)	3.8
4		DMA (4.3)	1.3
5		DMA (4.3)	13
6^d		DMA (4.3)	n.d.
7		DMA/toluene = 2:1 (4.3)	9.4
8		NMP (4.3)	19 (15)
9		NMP (1.5)	18
10		NMP (3.0)	20 (15)
11		NMP (6.0)	17

^a**3** (13 μ mol), Ni(cod)₂ (12 equiv), ligand (12 equiv), 80 °C, 2 h. ^bThe concentration of **3** in the solvent. ^c¹H NMR yield using CH₂Br₂ as the internal standard. Isolated yields are shown in parentheses. ^dNo preformation of the Ni(cod)₂/2,2'-bipyridyl complex.

3. The X-ray crystal structure

Details of the crystal data and a summary of the intensity data collection parameters are listed in Table S2. A suitable crystal was mounted with mineral oil on a MiTeGen MicroMounts and transferred to the goniometer of the kappa goniometer of a RIGAKU XtaLAB Synergy-S system with 1.2 kW MicroMax-007HF microfocus rotating anode (Graphite-monochromated Mo K α radiation ($\lambda = 0.71073$ Å)) and PILATUS200K hybrid photon-counting detector. Cell parameters were determined and refined, and raw frame data were integrated using CrysAlisPro (Agilent Technologies, 2010). The structures were solved by direct methods with SHELXT⁵ and refined by full-matrix least-squares techniques against F^2 (SHELXL-2018/3 or SHELXL-2014/4)⁶ by using Olex2 software package.⁷ The intensities were corrected for Lorentz and polarization effects. The non-hydrogen atoms were refined anisotropically. Hydrogen atoms were placed using AFIX instructions. CCDC 2007092 contains the supplementary crystallographic data for this paper. These data can be obtained free of charge from The Cambridge Crystallographic Data Centre via www.ccdc.cam.ac.uk/data_request/cif.

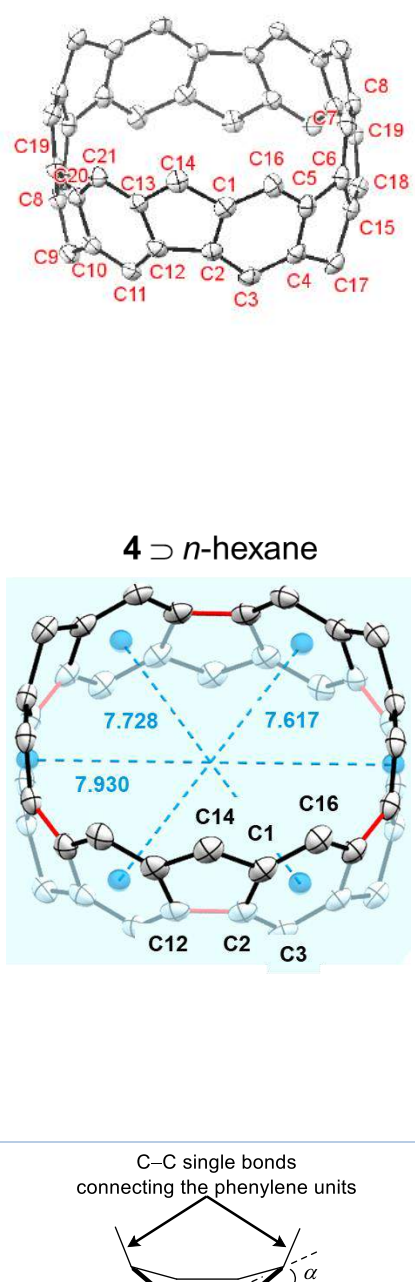
Table S2. Crystallographic data and structure refinement details for **4**.

	4		
formula	C _{45.5} H ₃₂ Cl	V (Å ³)	1530.71(6)
fw	614.16	Z	2
T (K)	123(2)	D_{calc} (g/cm ³)	1.333
λ (Å)	0.71073	μ (mm ⁻¹)	0.160
cryst syst	Triclinic	$F(000)$	644.0
space group	$P-1$	cryst size (mm)	0.15 \times 0.10 \times 0.10
a (Å)	11.4850(3)	2θ range (deg)	3.53 to 55.768
b (Å)	11.7900(3)	reflns collected	18175
c (Å)	12.1794(3)	indep reflns/ R_{int}	6100/0.0444
α (deg)	107.588(2)	params	460
β (deg)	92.5269(19)	GOF on F^2	1.056
γ (deg)	101.5278(19)	R_1, wR_2 [$I > 2\sigma(I)$]	0.0582, 0.1543
		R_1, wR_2 (all data)	0.0903, 0.1702

3.1 The comparison of X-ray crystal structure and DFT calculated result

The optimization of the structure of compound **4** was carried out by DFT calculations at the B3LYP/6-31G(d) level of theory, and the calculated optimized structure reproduced the experimentally observed structure well.

Table S3. The comparison of the X-ray crystal structure and DFT calculated result.

Bond length (Å) (4 \supset <i>n</i> -hexane)				
	Bond	Observed	Averaged	Calculated
	C1–C2	1.408(3)	1.408	1.416
	C12–C13	1.405(3)		
	C20–C10	1.409(3)		
	C19–C8	1.412(3)		
	C15–C6	1.410(3)		
	C4–C5	1.406(3)		
	C1–C14	1.512(3)	1.518	1.521
	C13–C14	1.519(3)		
	C9–C10	1.521(3)		
	C8–C9	1.518(3)		
	C4–C17	1.519(3)		
	C17–C15	1.520(3)		
	C2–C12	1.475(3)	1.478	1.478
	C19–C20	1.474(3)		
	C6–C5	1.485(3)		
	C11–C12	1.393(3)	1.395	1.404
	C20–C21	1.395(3)		
	C2–C3	1.403(3)		
	C16–C5	1.389(3)		
	C6–C7	1.397(3)		
	C18–C19	1.395(3)		
	C21–C13	1.384(3)	1.384	1.391
	C10–C11	1.380(3)		
	C1–C16	1.390(3)		
	C3–C4	1.383(3)		
	C15–C18	1.383(3)		
	C7–C8	1.383(3)		
	Diameter		7.758	7.759
	Bent angle α	9.08, 9.51 8.54, 8.60 7.79, 7.04	8.43	—

3.2 The CH- π^{centroid} distances between methylene-bridged [6]CPPs

There is no clear intermolecular π - π interaction was observed. Instead, close CH- π^{centroid} interactions were observed.

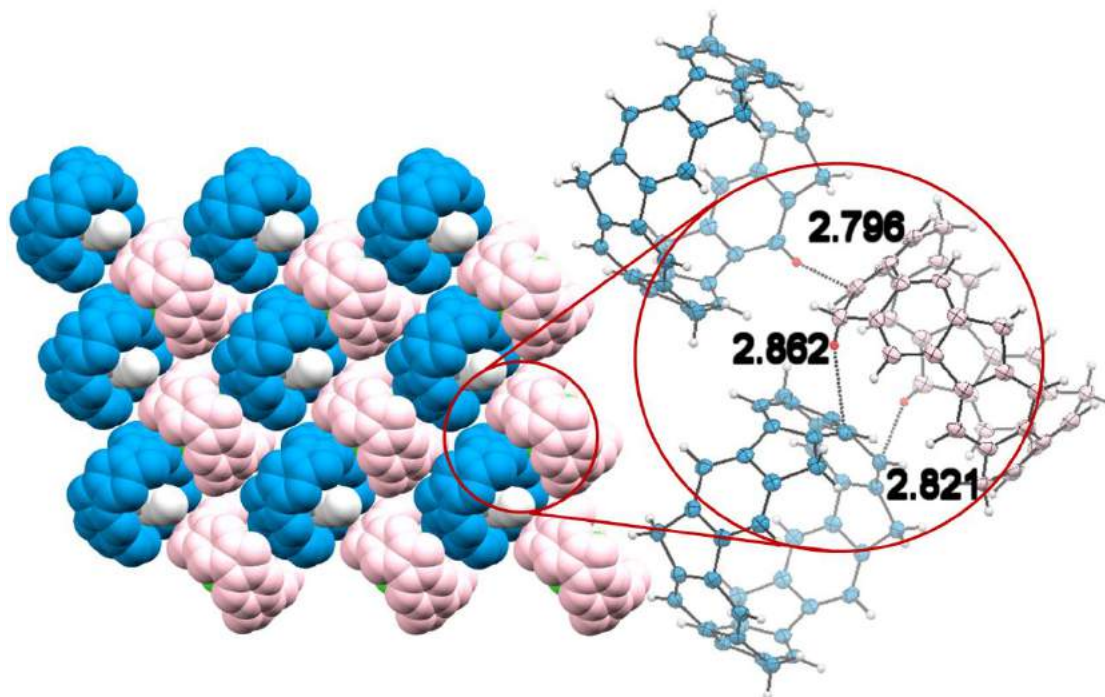
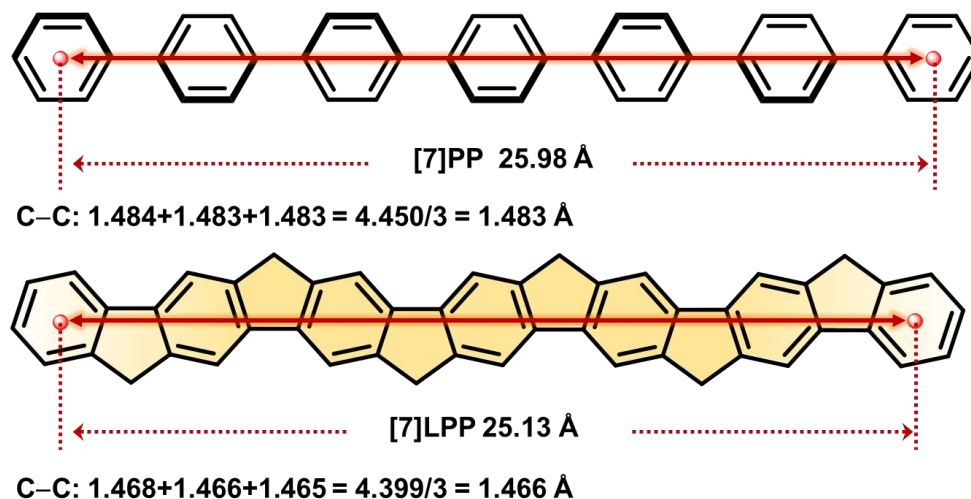


Figure S1: Packing structure of **4** (the $[0\bar{1}1]$ plane) (**4** (blue) \supset *n*-hexane (grey); **4** (pink) \supset CH_2Cl_2 (green)). View of the X-ray crystal structures and the CH- π distances.

3.3 The reduction of length of LPP

The phenylene units of linear paraphenylenes linked with methylene bridges forms the condensed ladder-type paraphenylenes (LPPs) with shorter length (25.98 Å vs 25.13 Å). This result is consistent with the reduction of the diameter of **4** compared to the diameter of [6]CPP.



$25.98 - 25.13 = 0.86 \text{ \AA}$ (This length difference come from two reasons.)

(1) The shortness of six C–C single bonds: $1.483 - 1.466 = 0.017 \times 6 = 0.10 \text{ \AA}$

(2) The major reason is the different alignment of phenylene units: $0.86 - 0.10 = 0.76 \text{ \AA}$

Figure S2. The optimized structures of [7]PP and [7]LPP were calculated at the B3LYP/6-31G(d) level of theory.

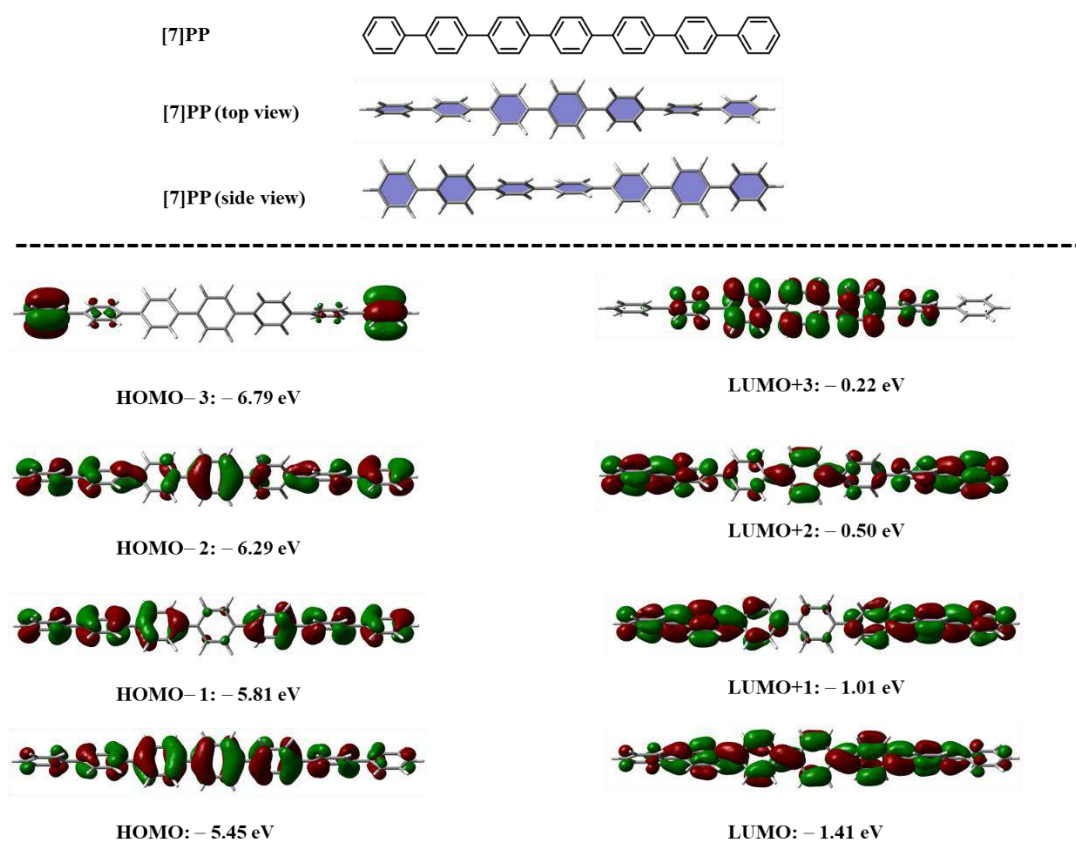


Figure S3. The frontier orbital energies of [7]PP calculated by B3LYP/6-31G(d).

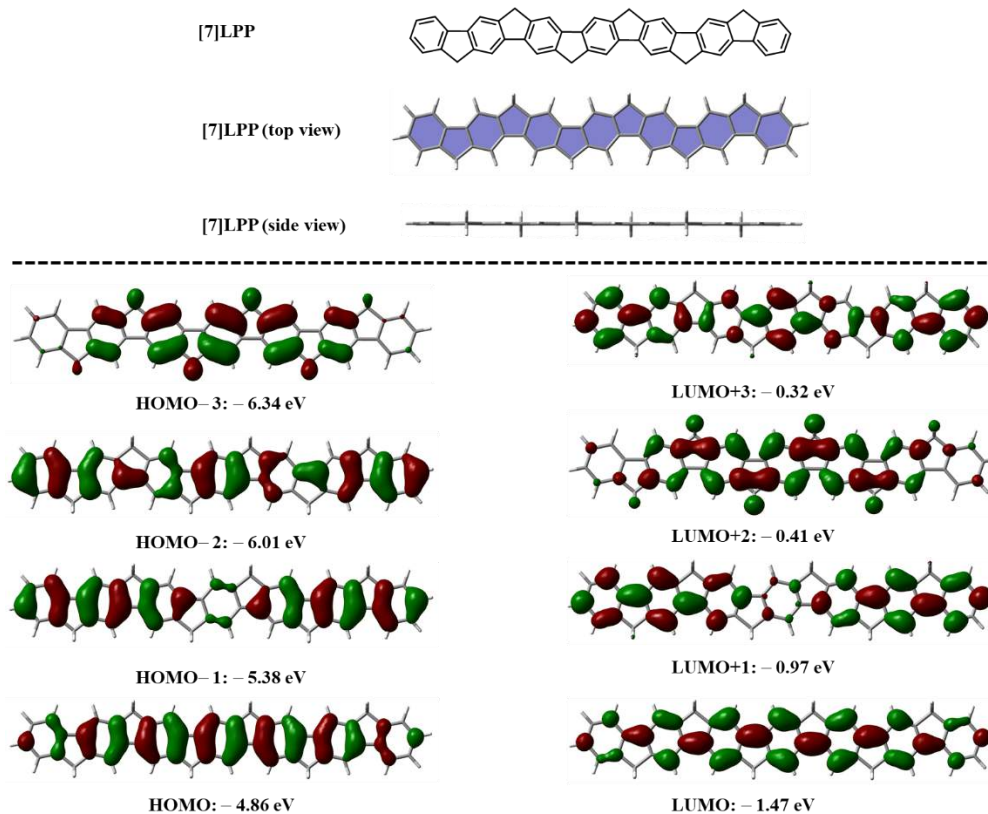


Figure S4. The frontier orbital energies of [7]LPP calculated by B3LYP/6-31G(d).

4. Computational study

The Gaussian 16 program⁸ running on the NEC LX system was used for optimization (B3LYP/6-31G(d)).⁹ Structures were optimized without any symmetry assumptions. Zero-point energy, enthalpy, and Gibbs free energy at 298.15 K and 1 atm were estimated from the gas-phase studies. Harmonic vibration frequency calculation at the same level was performed to verify all stationary points as local minima (with no imaginary frequency) or transition states (with one imaginary frequency). IRC calculations were also performed to check transition states. Visualization of the results was performed by the use of GaussView 5.0.9 software.

4.1 HOMO and LUMO energies of [n]CPP, methylene-bridged [n]CPP, and [n]LPP

Table S4. The frontier orbital energies of [n]CPP, methylene-bridged [n]CPP and [n]LPP series calculated by B3LYP/6-31G(d) level of theory with Gaussian 16 program (unit: eV).

	[n]CPP		[n]LPP		CH ₂ -bridged [n]CPP	
<i>n</i>	HOMO	LUMO	HOMO	LUMO	HOMO	LUMO
6	−4.92	−1.78	−4.92	−1.42	−4.40	−1.74
8	−5.10	−1.70	−4.82	−1.50	−4.48	−1.71
10	−5.20	−1.66	−4.77	−1.55	−4.53	−1.69
12	−5.25	−1.64	−4.73	−1.58	−4.56	−1.68
14	−5.29	−1.63	−4.71	−1.60	−4.58	−1.67
16	−5.31	−1.62	−4.70	−1.61	−4.60	−1.67
18	−5.33	−1.62	−4.69	−1.62	−4.60	−1.66
20	−5.34	−1.61	−4.68	−1.62	−4.61	−1.66

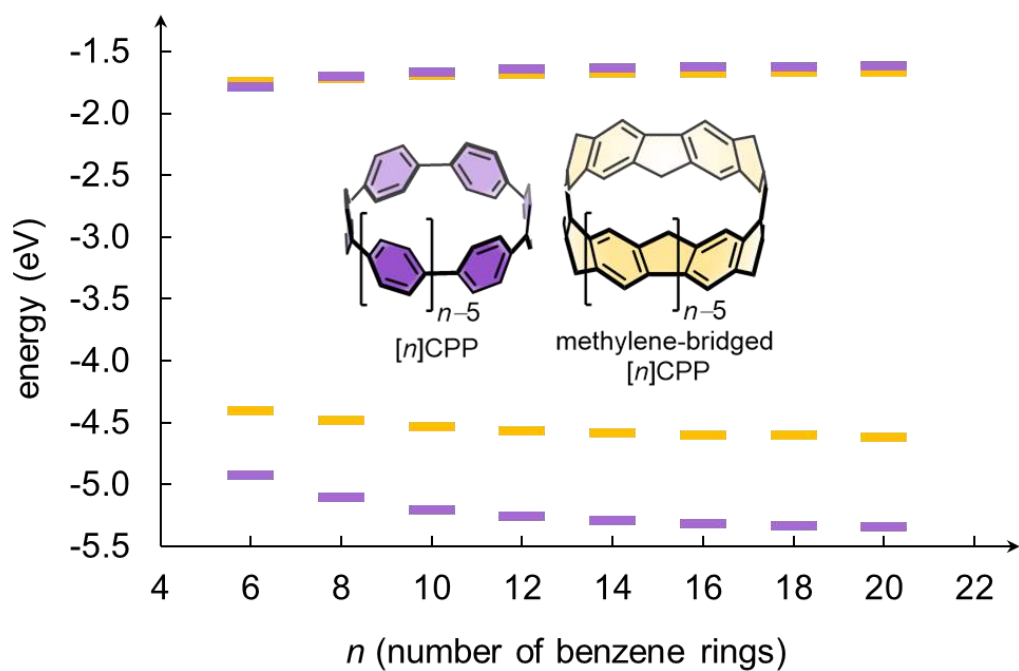


Figure S5. HOMO and LUMO energies of $[n]$ CPP (purple) and methylene-bridged $[n]$ CPP (orange) calculated at the B3LYP/6-31G(d) level of theory.

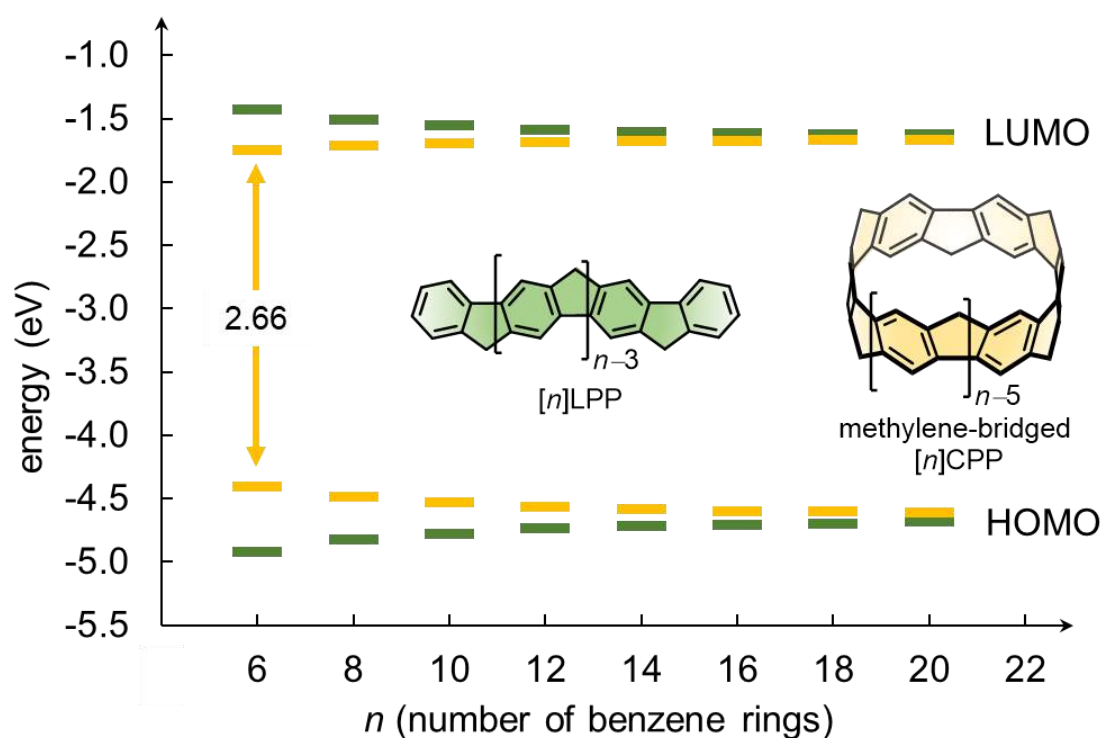
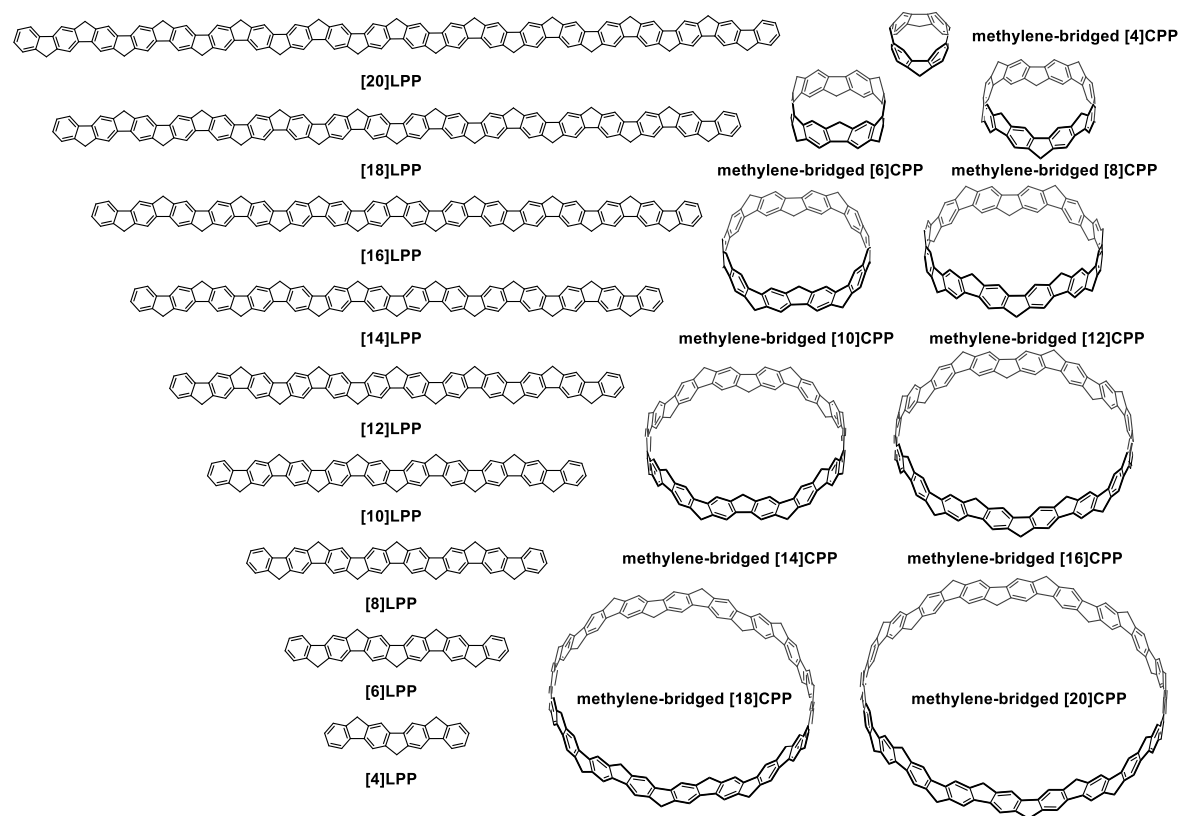


Figure S6. HOMO and LUMO energies of $[n]$ LPP (green) and methylene-bridged $[n]$ CPP (orange) calculated at the B3LYP/6-31G(d) level of theory.

4.2 Optimized structures and frontier molecular orbitals

Scheme S2. The optimized structures and frontier orbital energies of $[n]$ CPP, methylene-bridged $[n]$ CPP and $[n]$ LPP series calculated by B3LYP/6-31G(d).



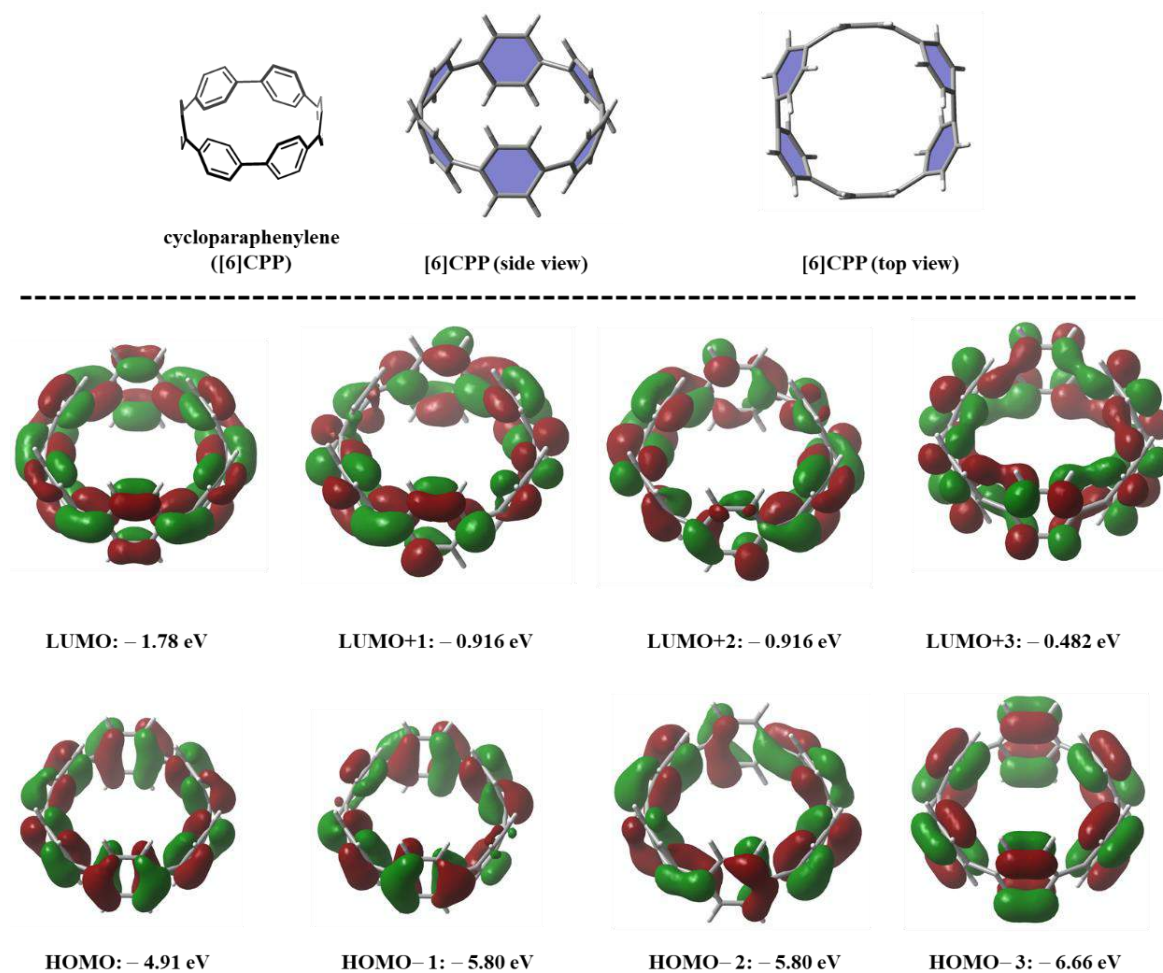


Figure S7. The optimized structures and frontier orbital energies of [6]CPP calculated by B3LYP/6-31G(d) level of theory.

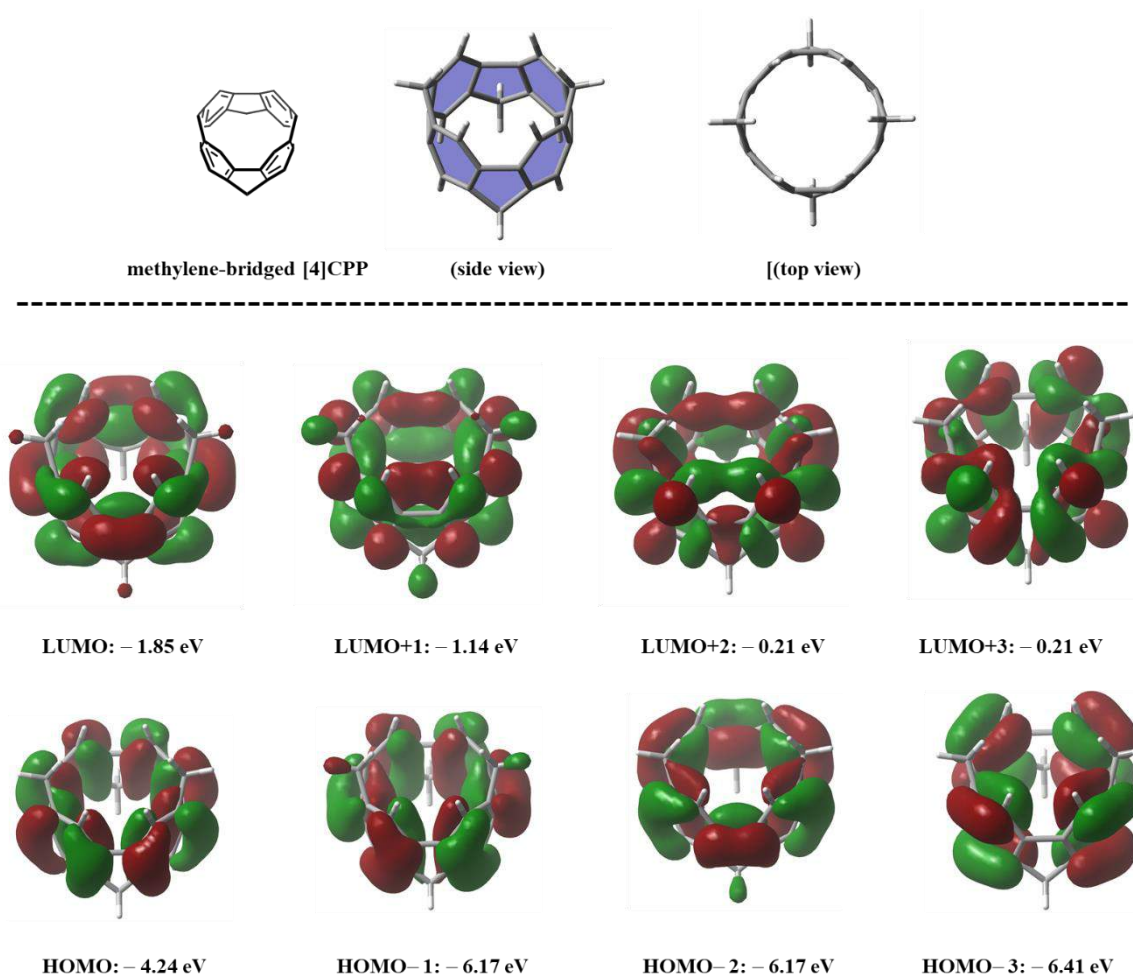


Figure S8. The optimized structures and frontier orbital energies of methylene-bridged [4]CPP calculated by B3LYP/6-31G(d) level of theory.

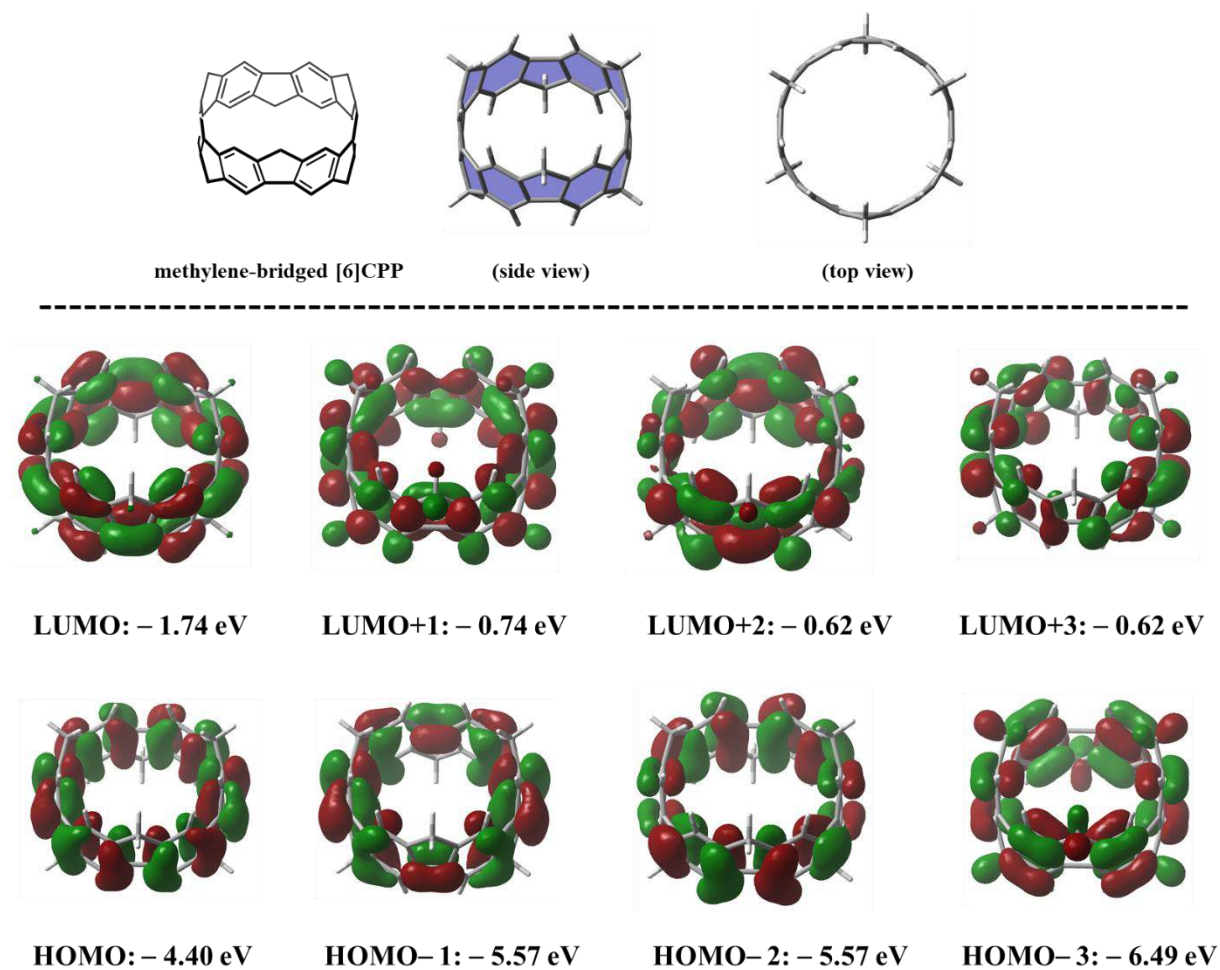


Figure S9. The optimized structures and frontier orbital energies of methylene-bridged [6]CPP calculated by B3LYP/6-31G(d) level of theory.

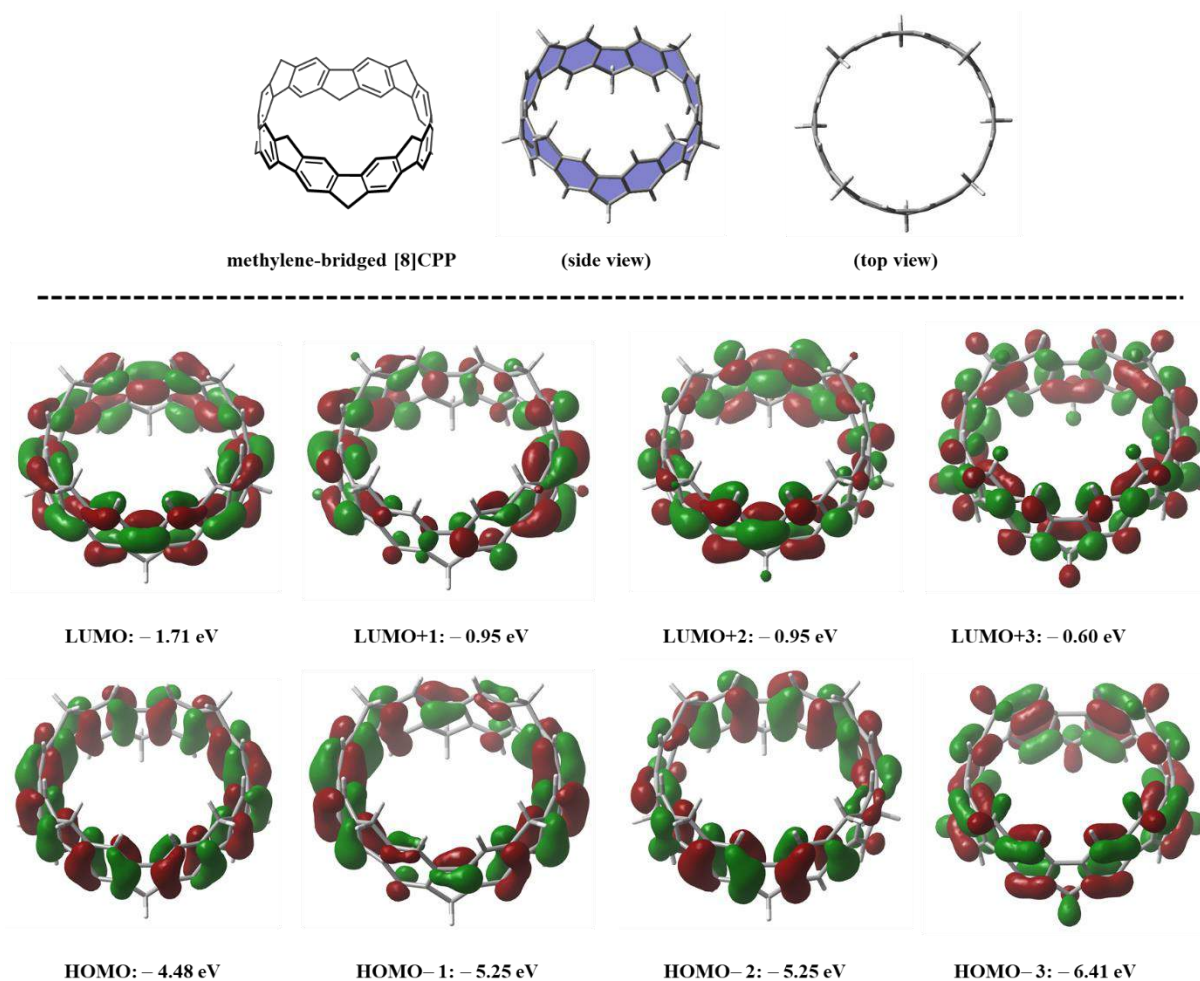


Figure S10. The optimized structures and frontier orbital energies of methylene-bridged [8]CPP calculated by B3LYP/6-31G(d) level of theory.

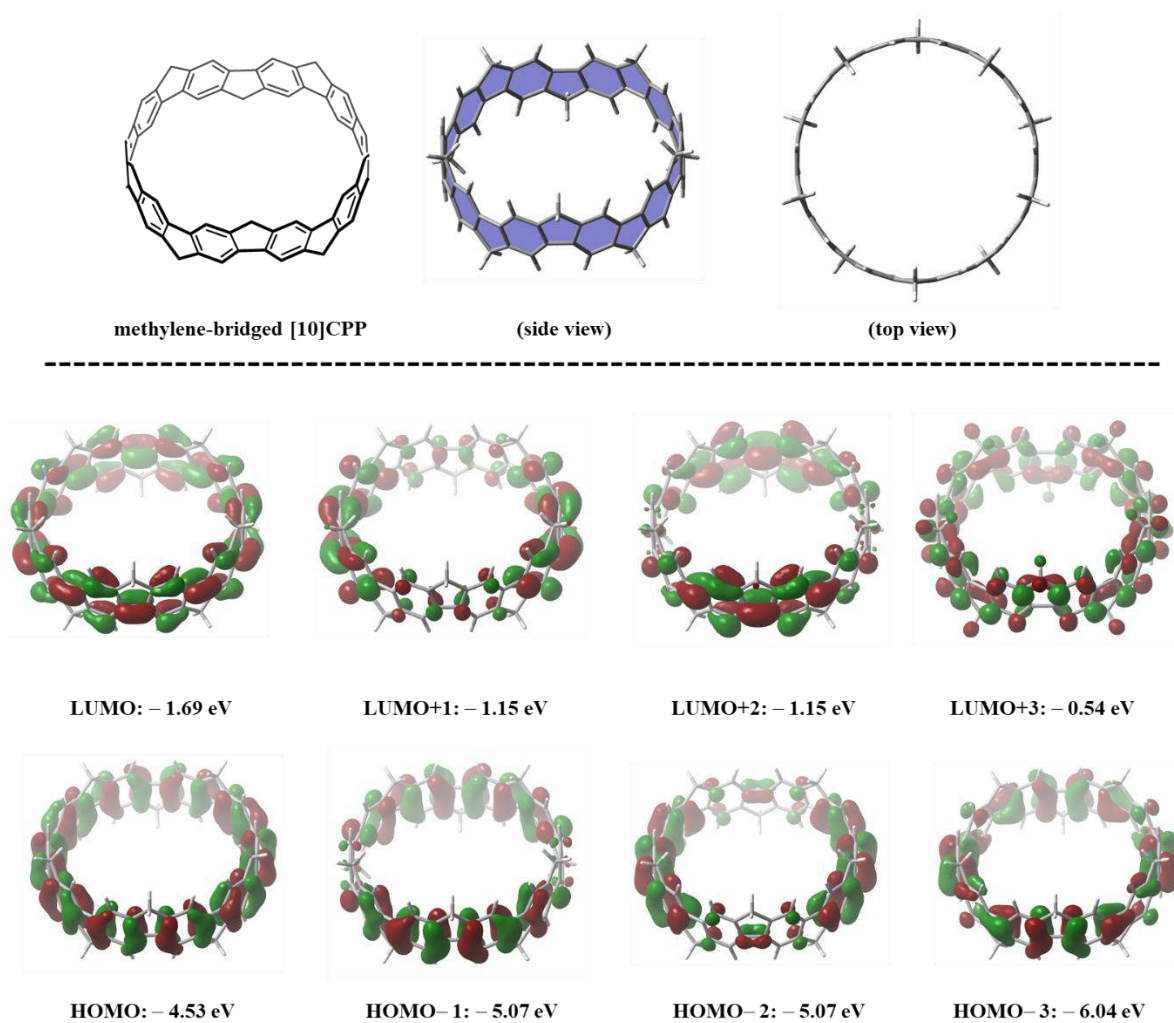


Figure S11. The optimized structures and frontier orbital energies of methylene-bridged [10]CPP calculated by B3LYP/6-31G(d) level of theory.

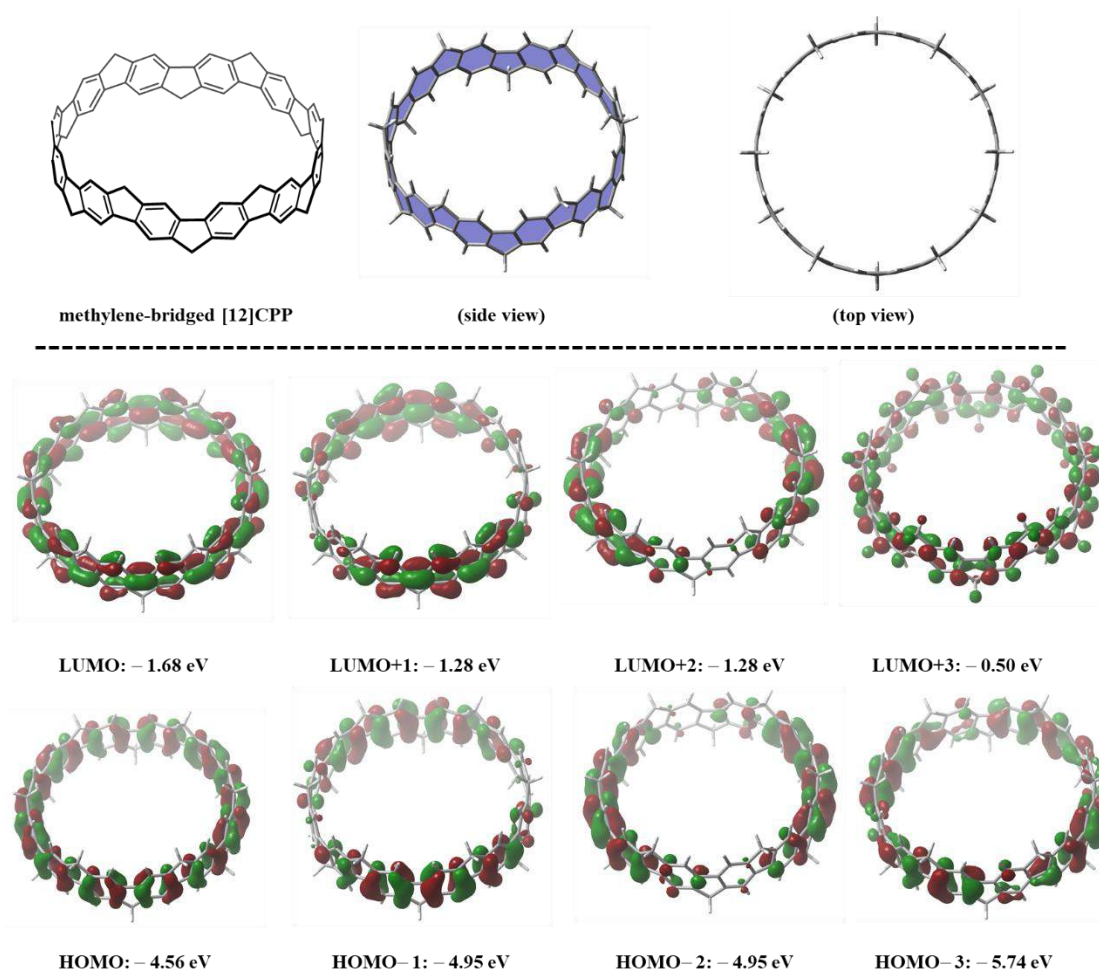


Figure S12. The optimized structures and frontier orbital energies of methylene-bridged [12]CPP calculated by B3LYP/6-31G(d) level of theory.

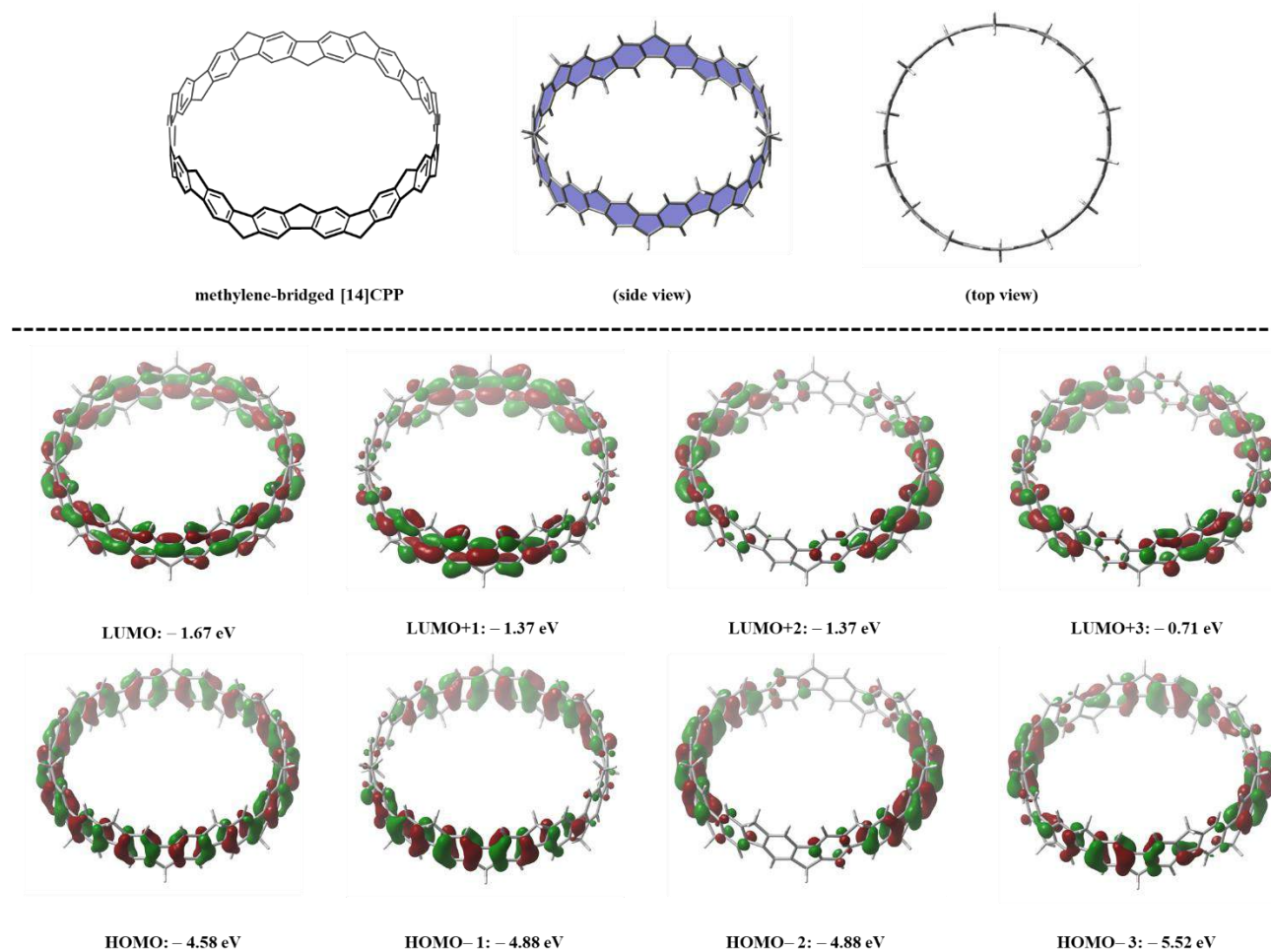


Figure S13. The optimized structures and frontier orbital energies of methylene-bridged [14]CPP calculated by B3LYP/6-31G(d) level of theory.

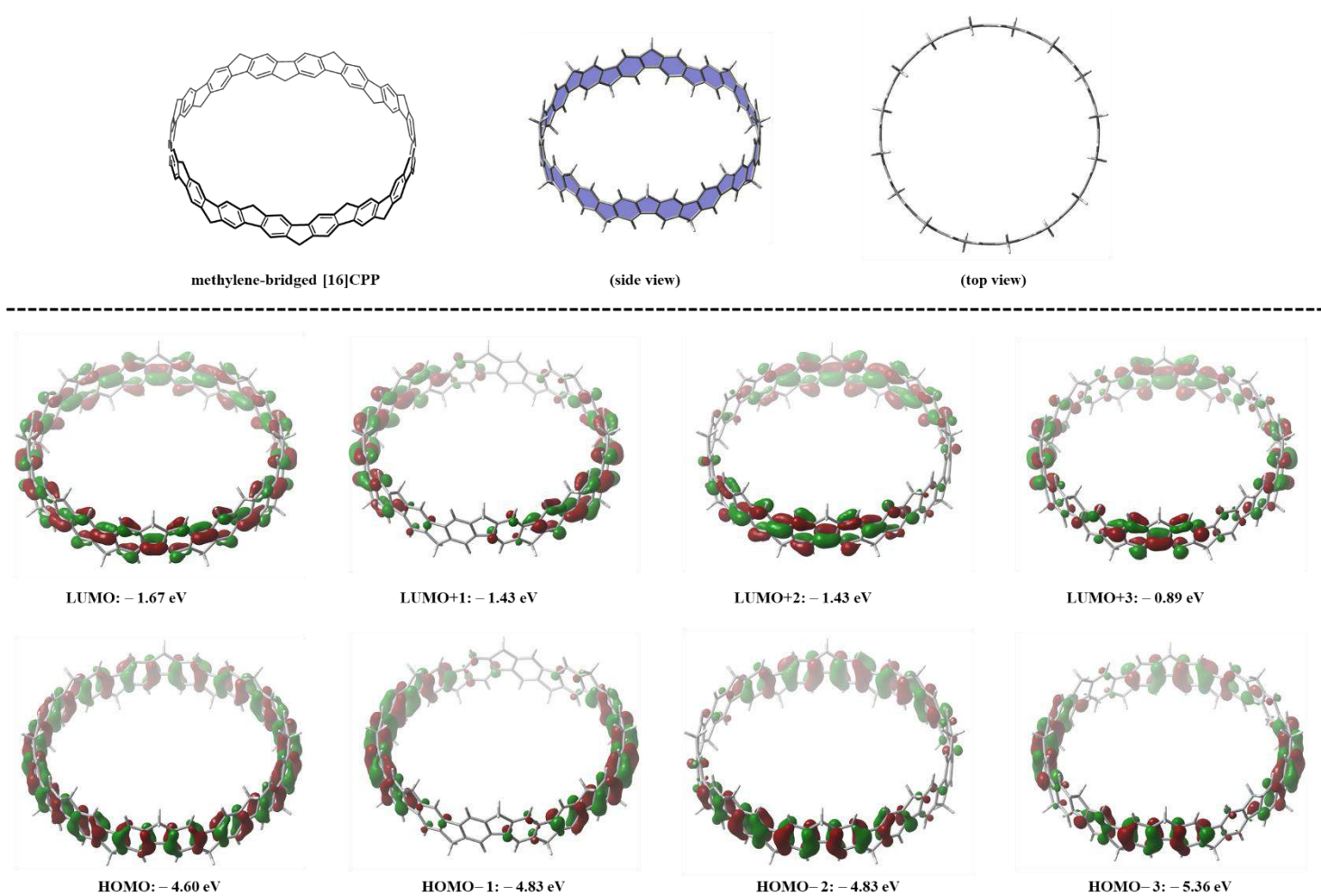


Figure S14. The optimized structures and frontier orbital energies of methylene-bridged [16]CPP calculated by B3LYP/6-31G(d) level of theory.

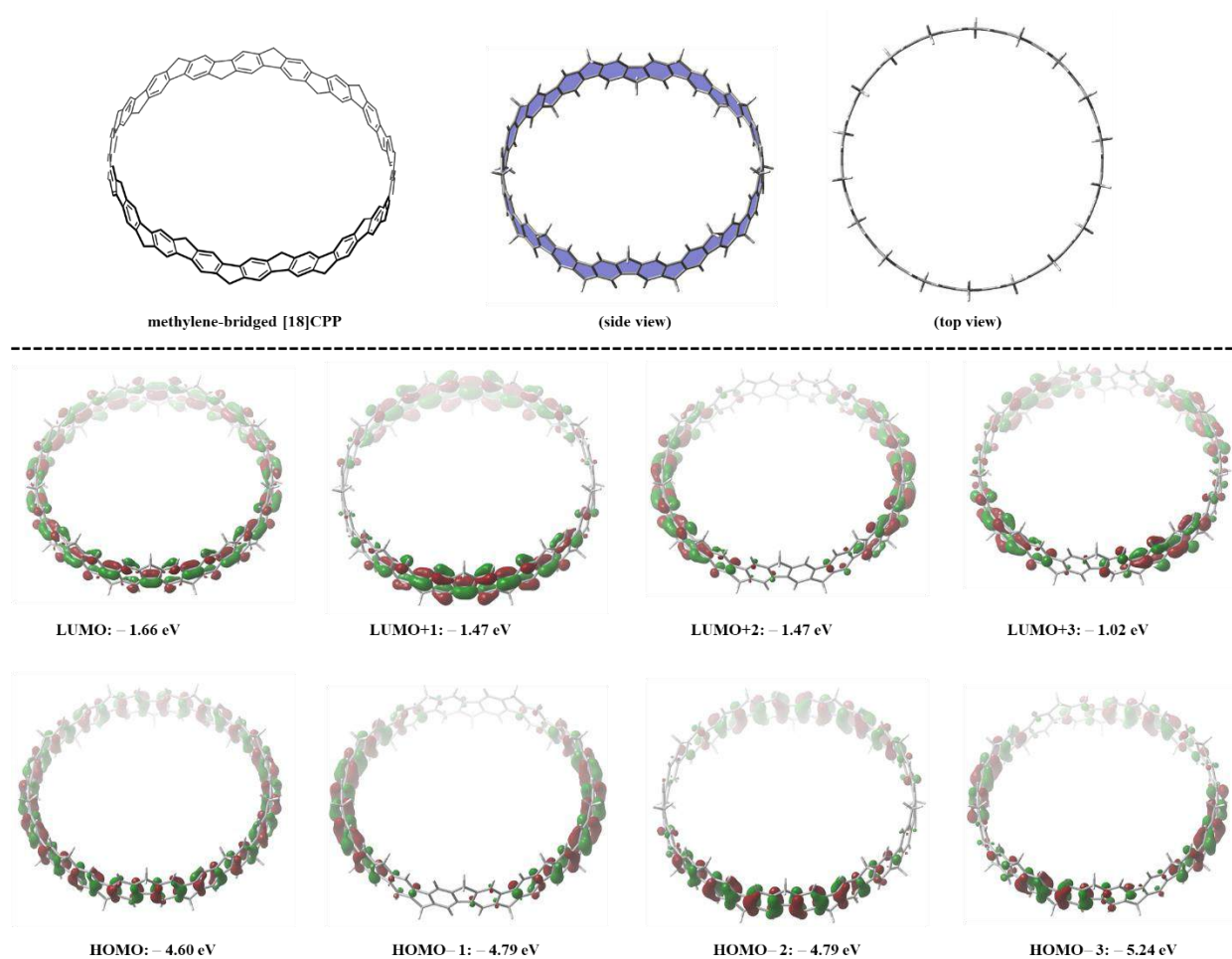


Figure S15. The optimized structures and frontier orbital energies of methylene-bridged [18]CPP calculated by B3LYP/6-31G(d) level of theory.

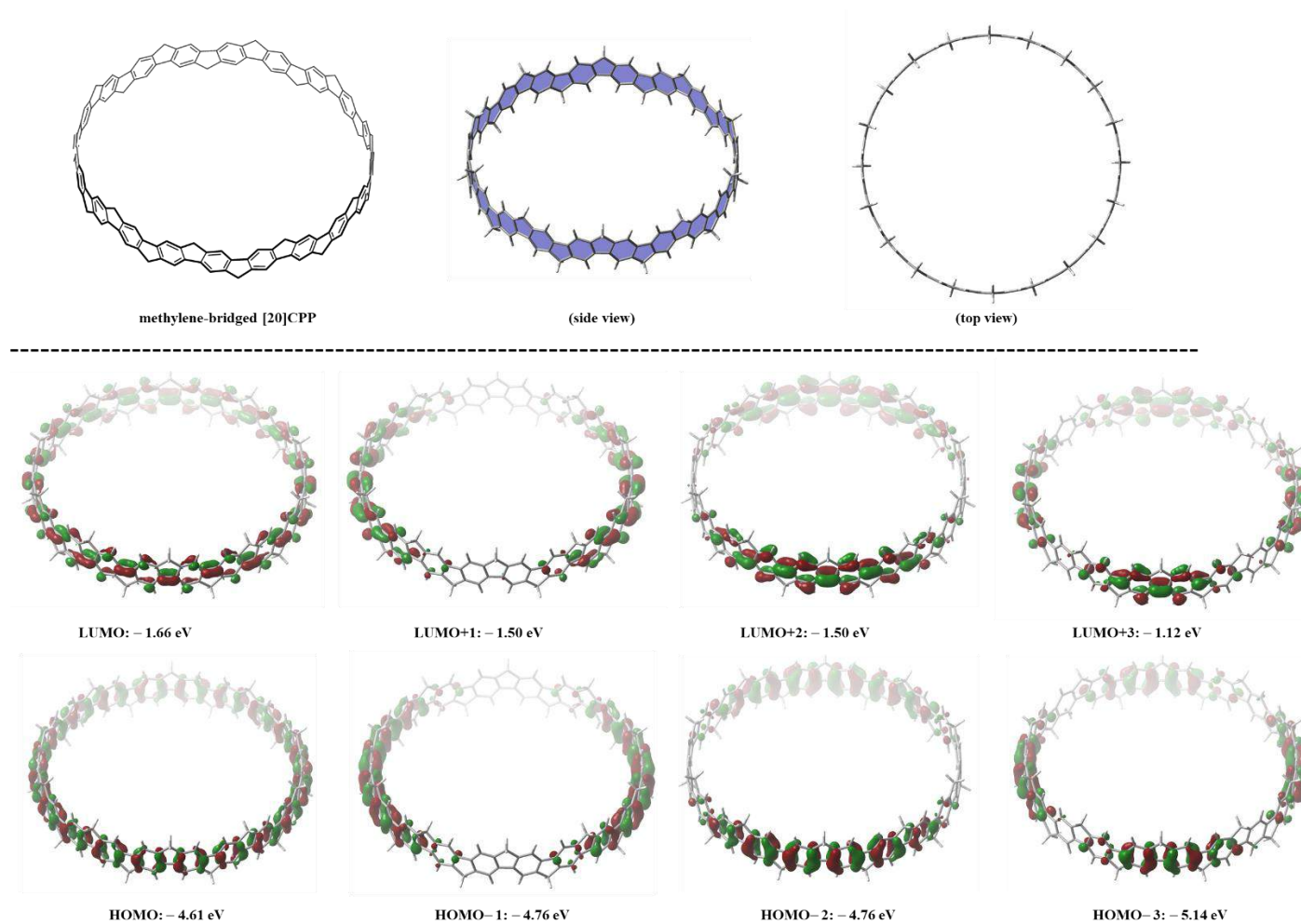


Figure S16. The optimized structures and frontier orbital energies of methylene-bridged [20]CPP calculated by B3LYP/6-31G(d) level of theory.

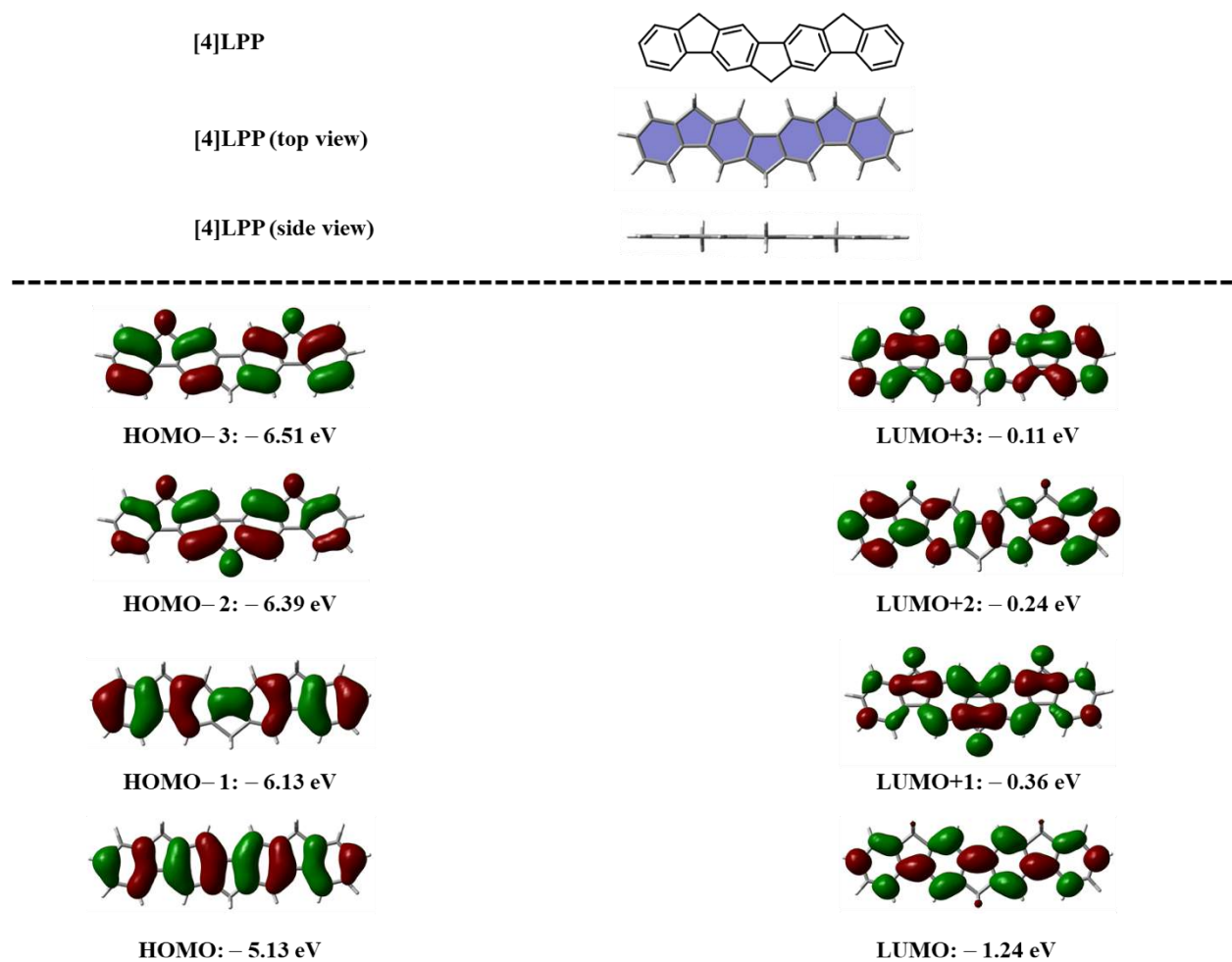


Figure S17. The optimized structures and frontier orbital energies of [4]LPP calculated by B3LYP/6-31G(d) level of theory.

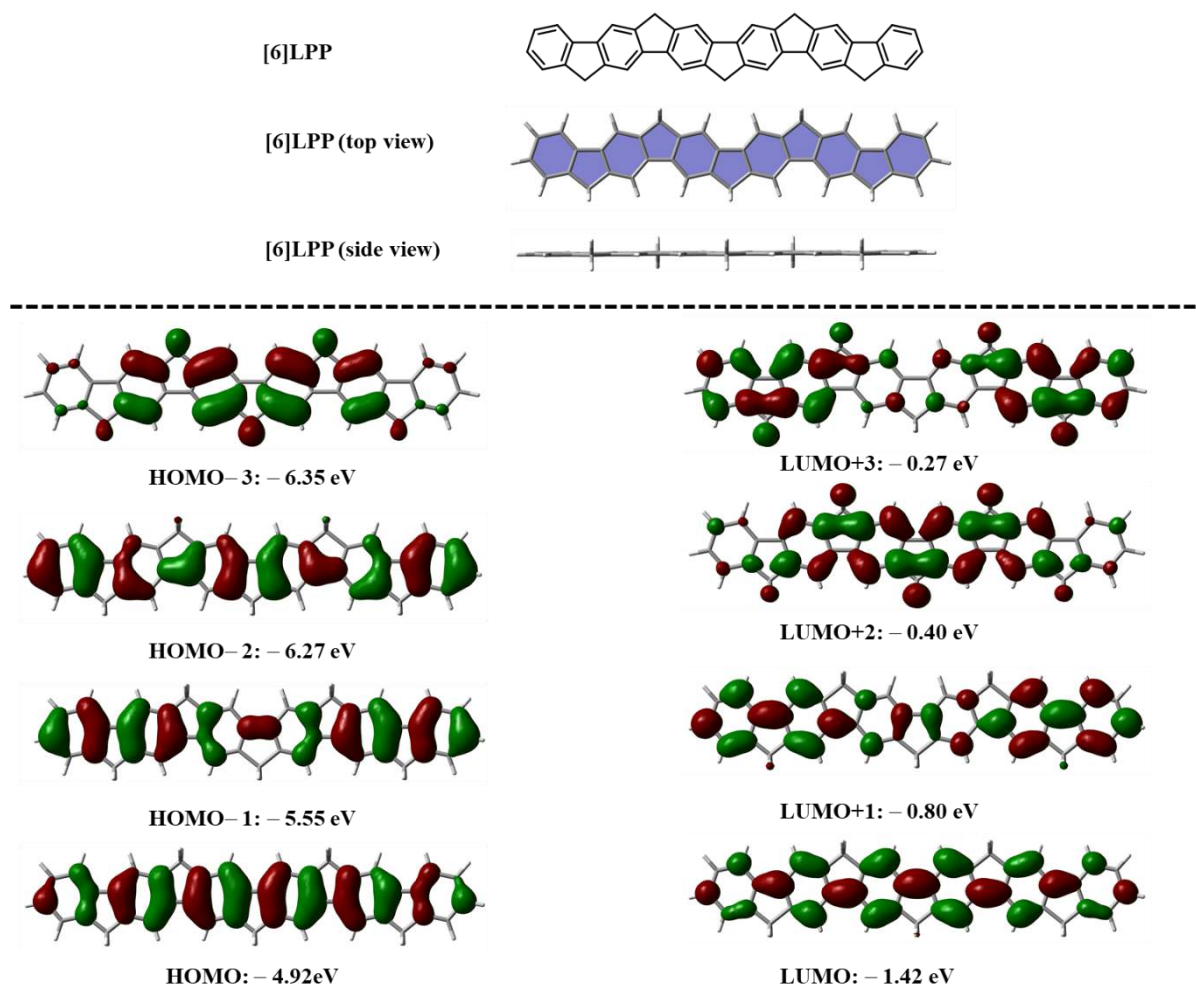


Figure S18. The optimized structures and frontier orbital energies of [6]LPP calculated by B3LYP/6-31G(d) level of theory.

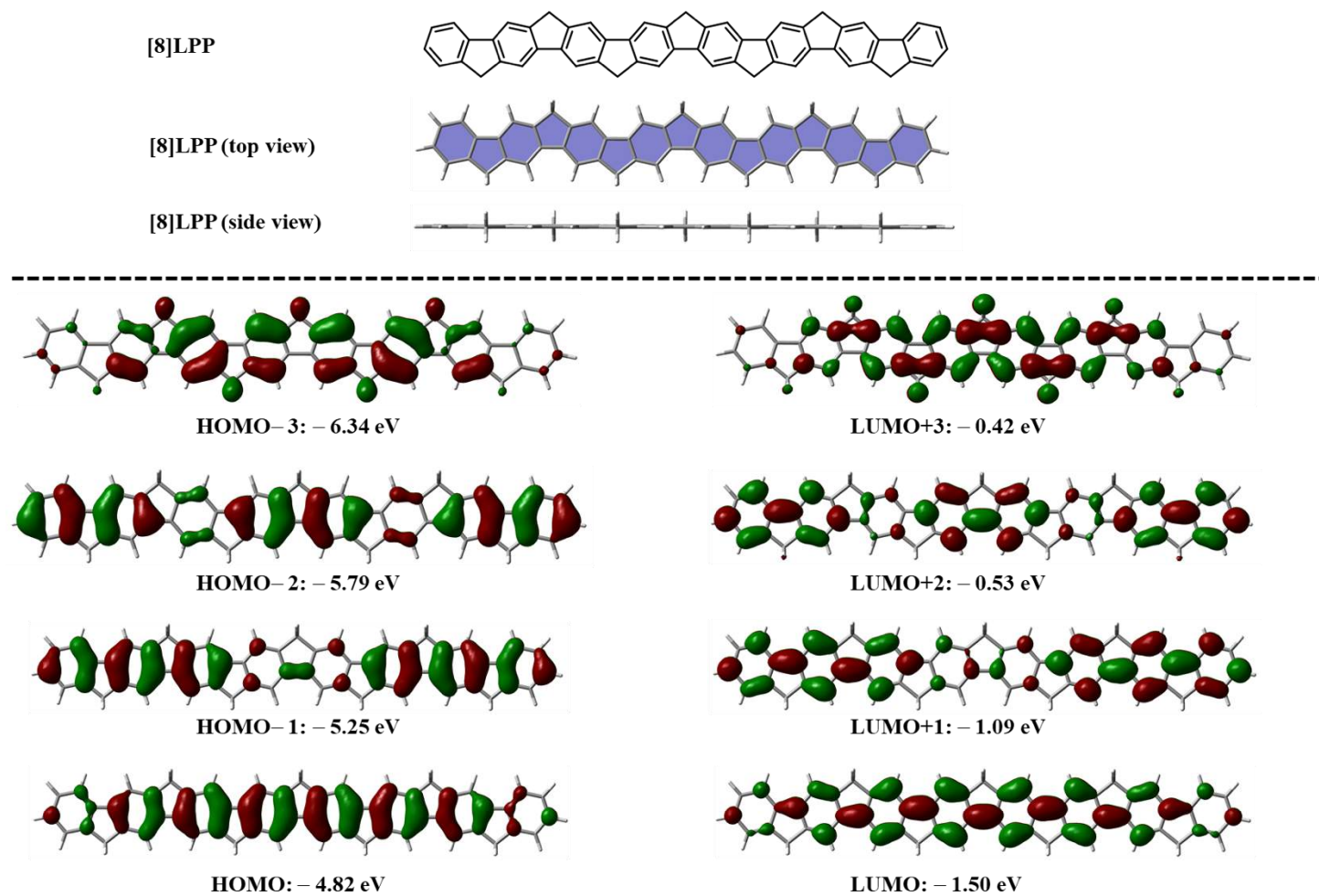


Figure S19. The optimized structures and frontier orbital energies of [8]LPP calculated by B3LYP/6-31G(d) level of theory.

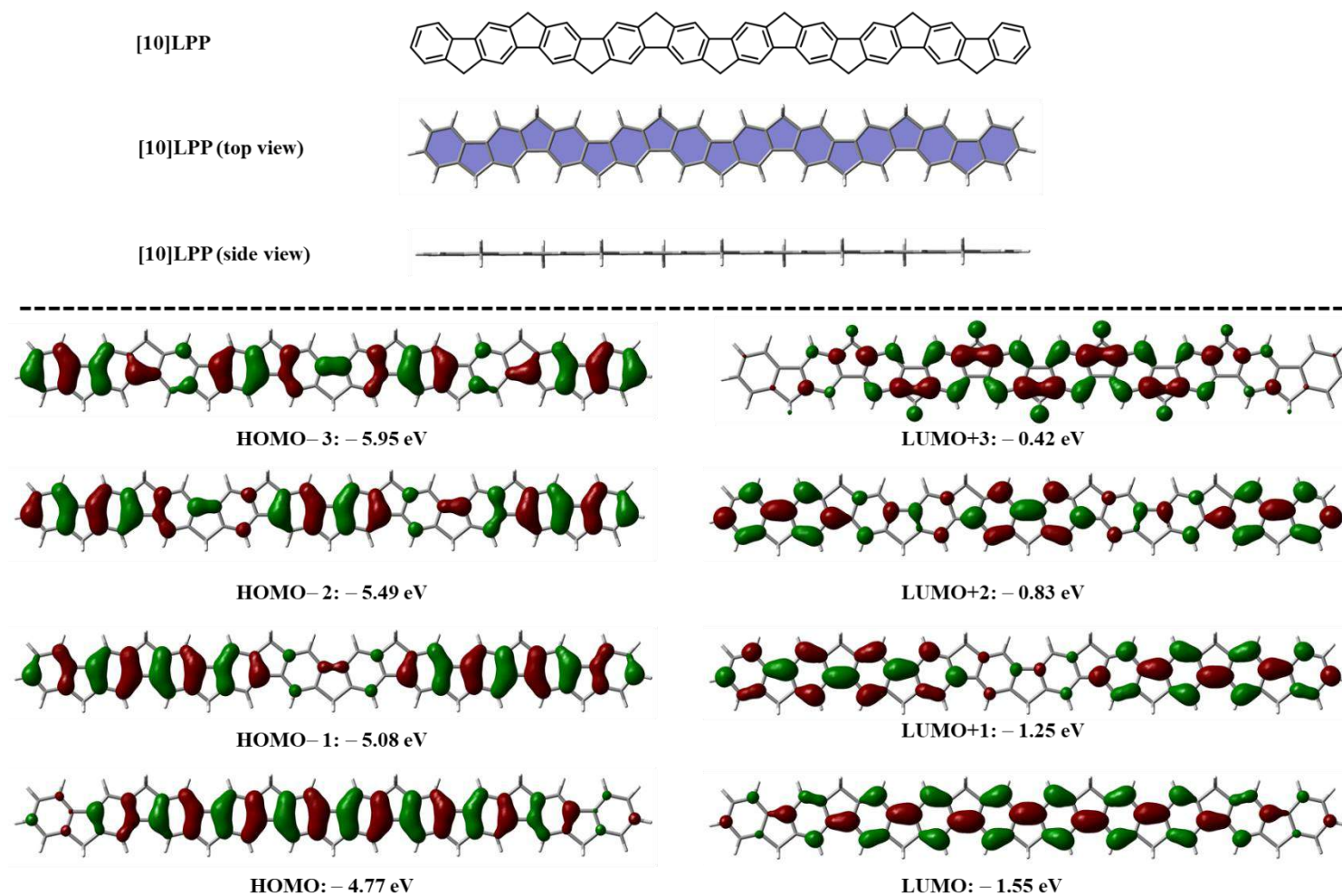


Figure S20. The optimized structures and frontier orbital energies of [10]LPP calculated by B3LYP/6-31G(d) level of theory.

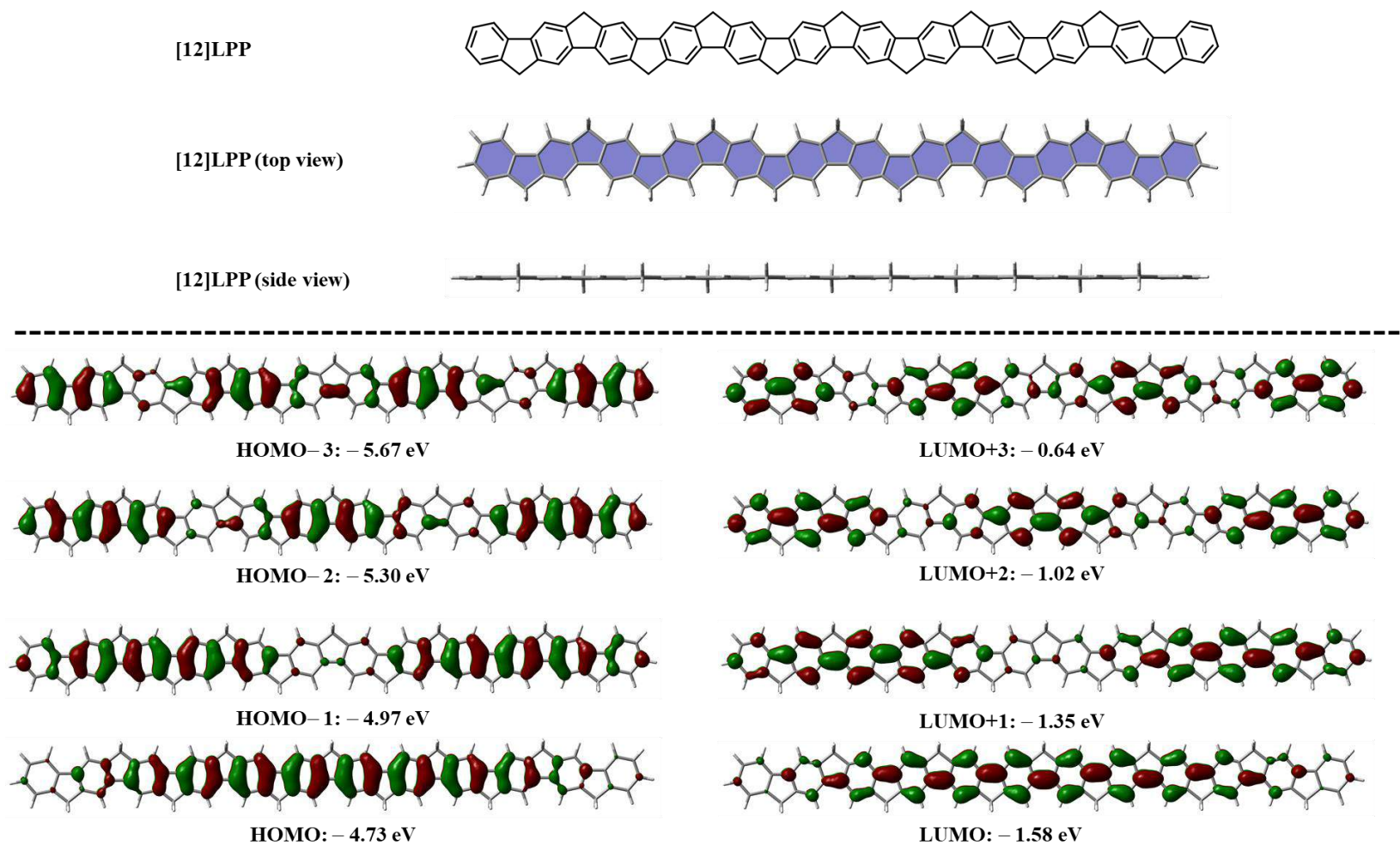


Figure S21. The optimized structures and frontier orbital energies of [12]LPP calculated by B3LYP/6-31G(d) level of theory.

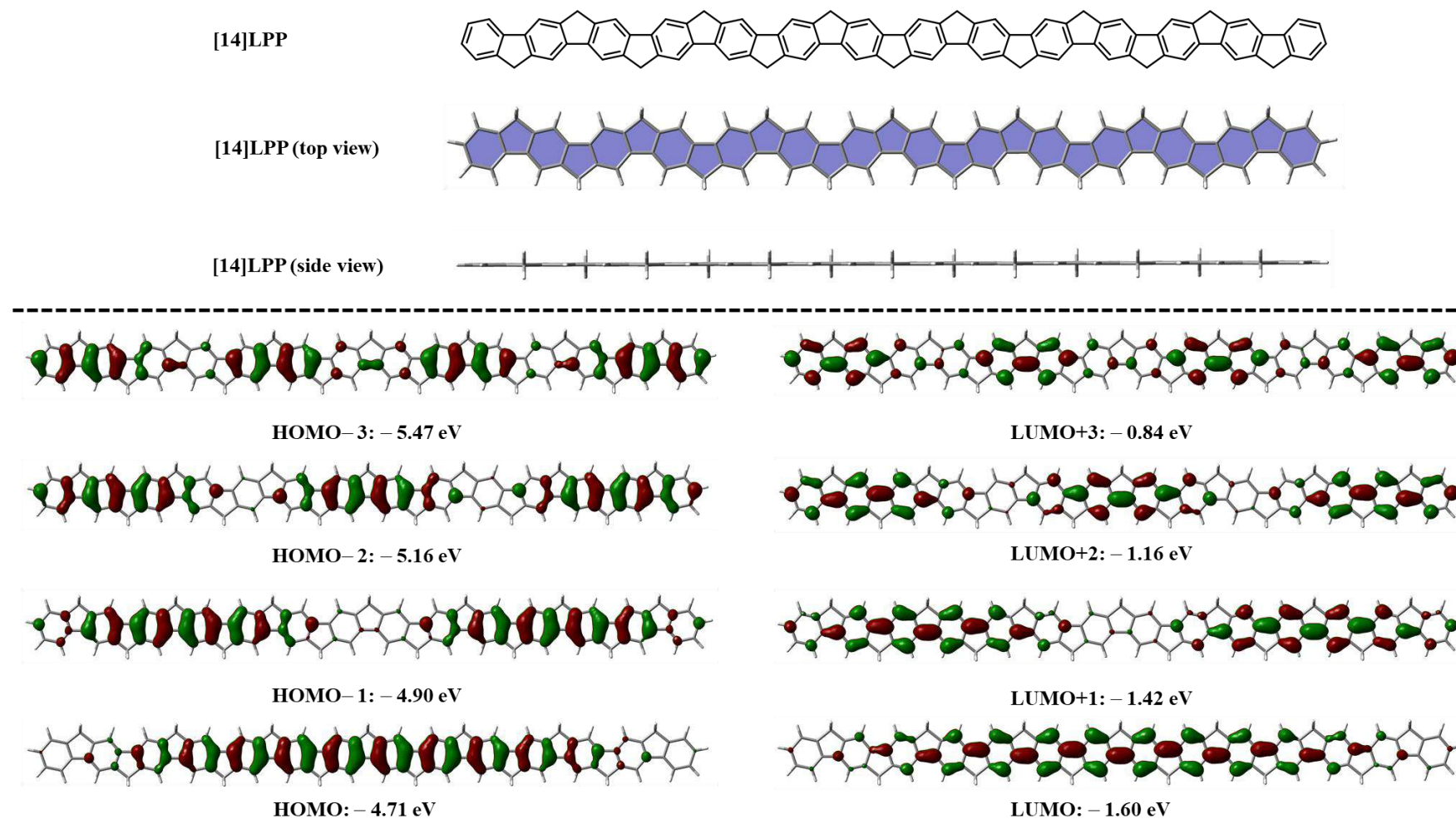


Figure S22. The optimized structures and frontier orbital energies of [14]LPP calculated by B3LYP/6-31G(d) level of theory.

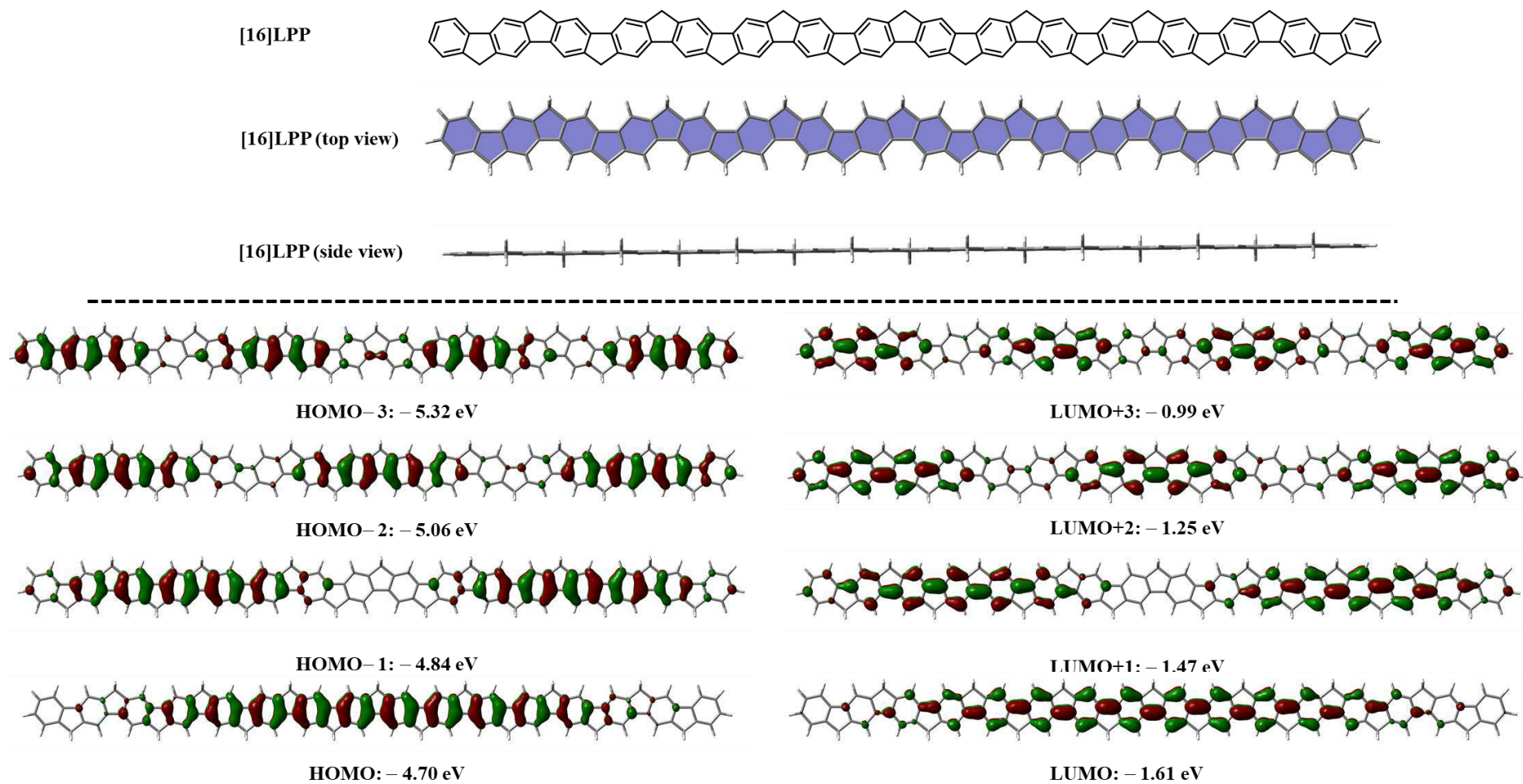


Figure S23. The optimized structures and frontier orbital energies of [16]LPP calculated by B3LYP/6-31G(d) level of theory.

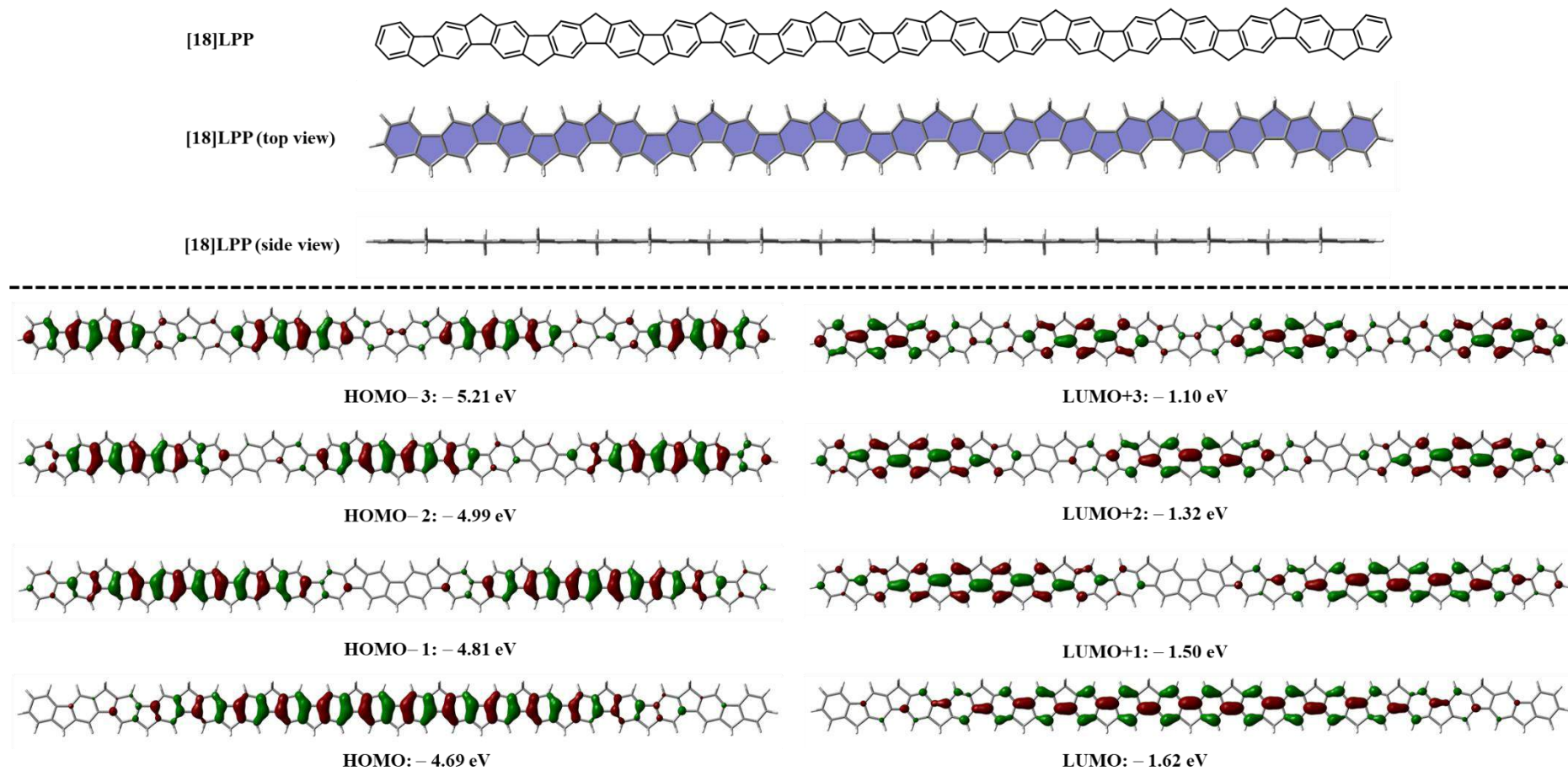


Figure S24. The optimized structures and frontier orbital energies of [18]LPP calculated by B3LYP/6-31G(d) level of theory.

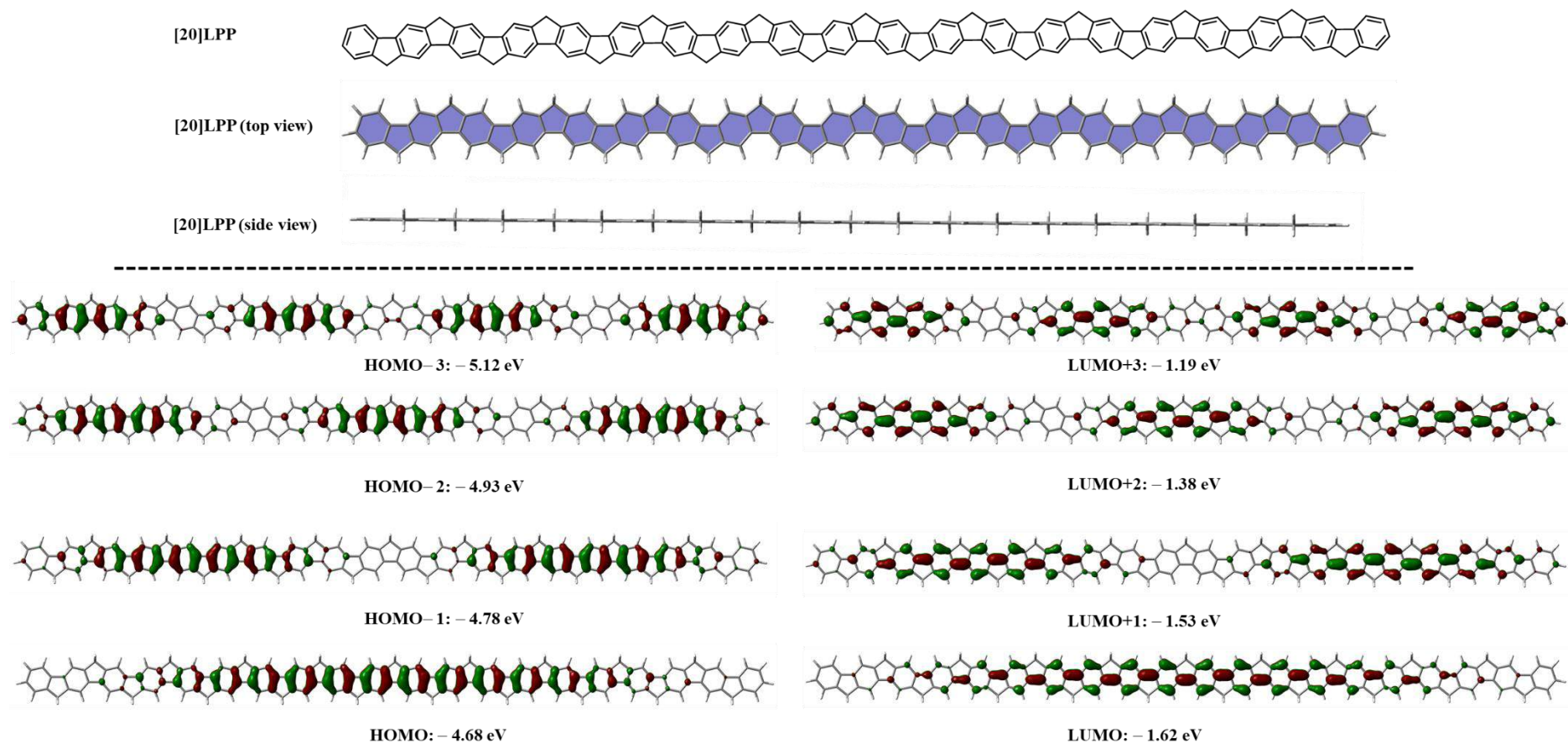
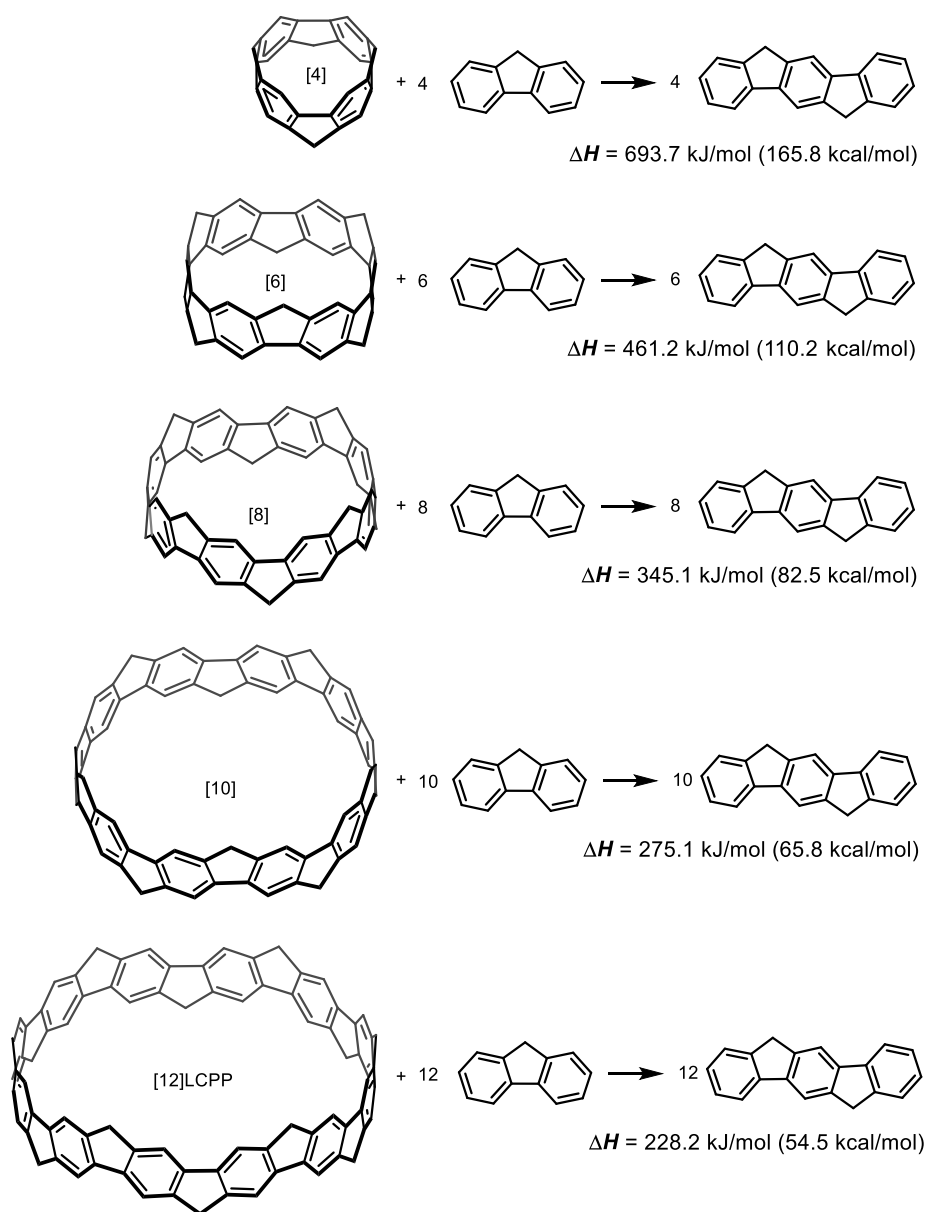


Figure S25. The optimized structures and frontier orbital energies of [20]LPP calculated by B3LYP/6-31G(d) level of theory..

4.3 The calculation of strain energy¹⁰

Scheme S3. Homodesmotic reactions for the calculation of strain energies for methylene-bridged $[n]$ CPP calculated by B3LYP/6-31G(d) level of theory respectively.



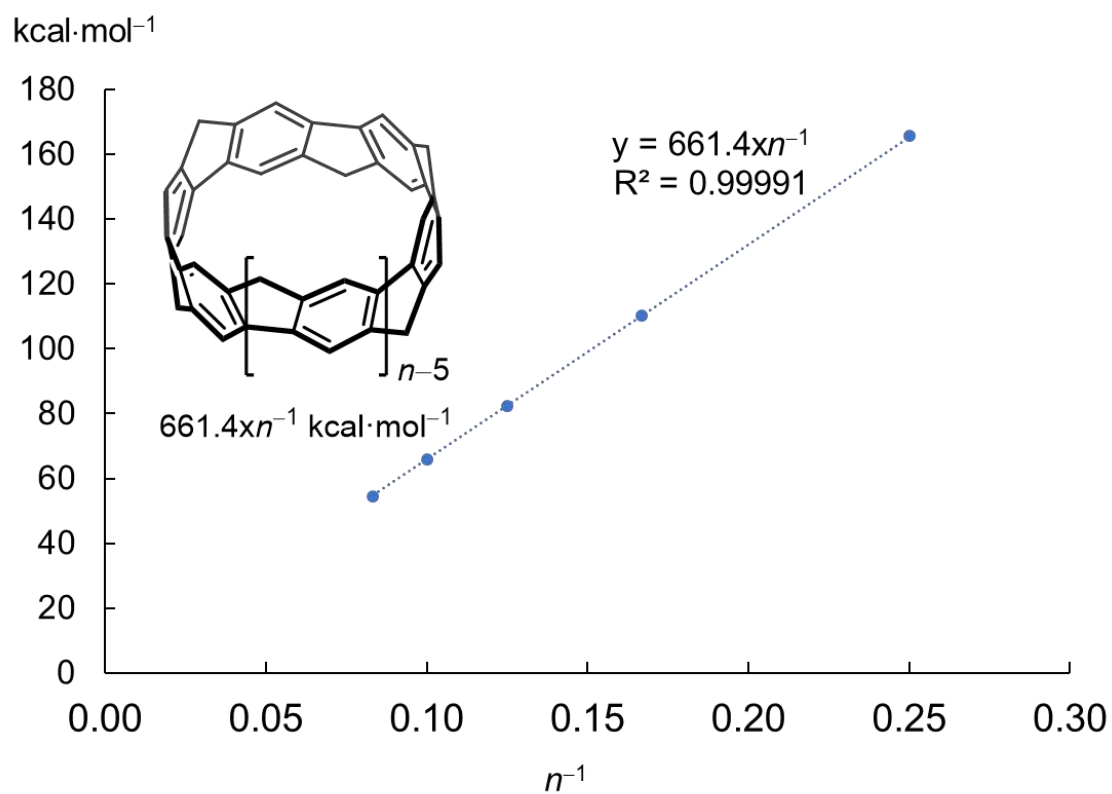
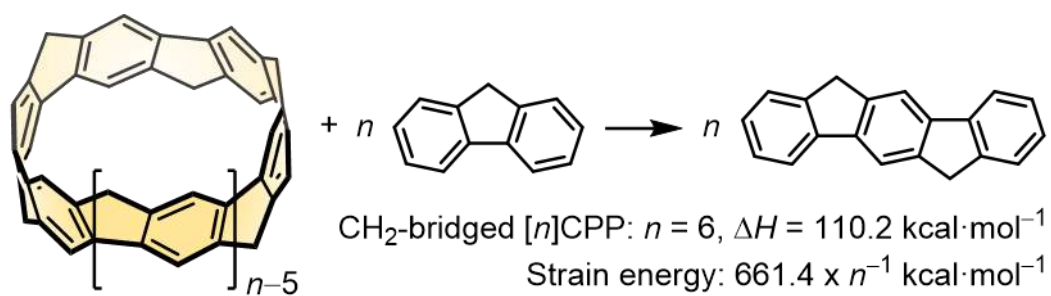
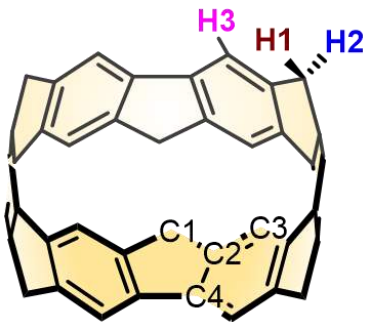


Figure S26. Plot of the strain energy with linear regression line.

4.4 Simulated NMR chemical shifts (ppm)

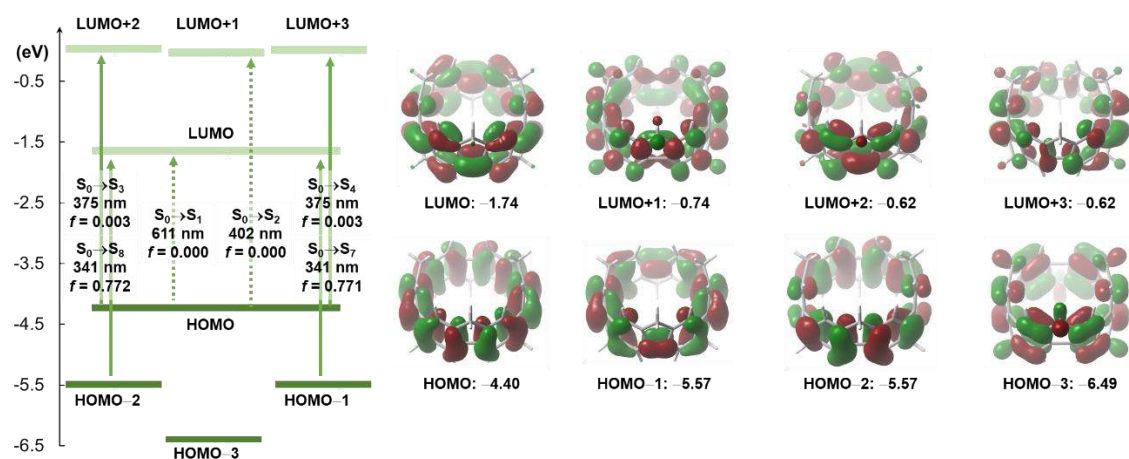
Table S5. Simulated NMR chemical shifts (ppm) calculated by B3LYP/6-311+G(2d,p) level of theory. Geometry optimization of **4** was calculated by B3LYP/6-31G(d).

		simulated	observed
	H3	8.31	7.86
	H2	4.47 (outer)	4.29
	H1	4.32 (inner)	4.09
	C2	156.1	148.0
	C4	142.5	137.1
	C3	125.3	121.8
	C1	45.3	40.9

4.5 TD-DFT vertical one-electron excitations

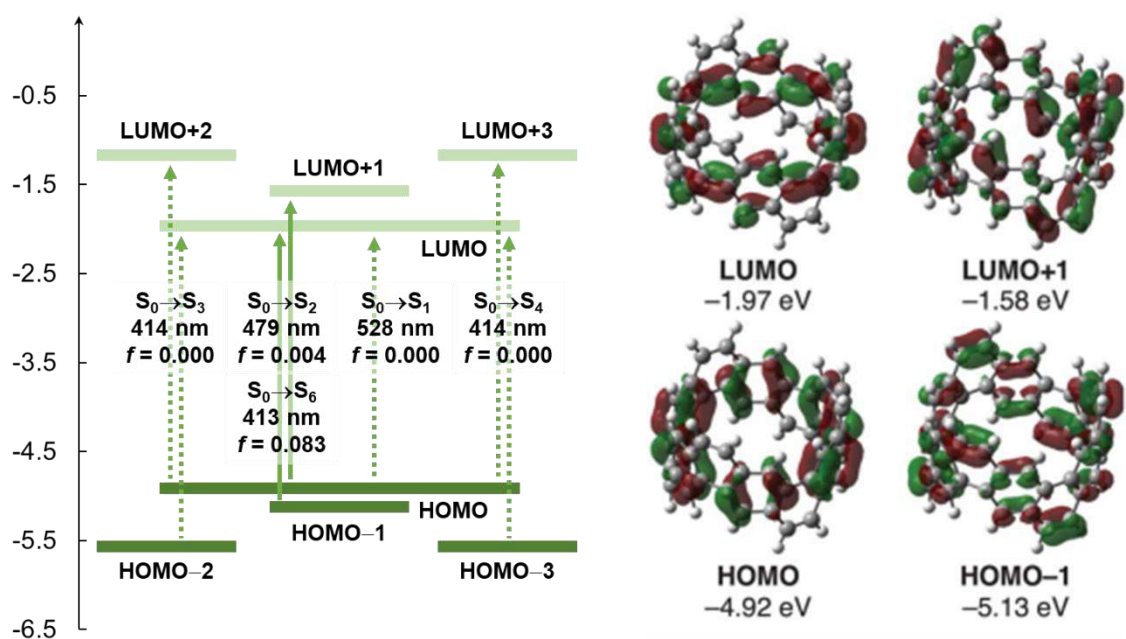
Table S6. Major electronic transitions for **4** by TD-DFT method using B3LYP/6-31G(d).

	energy (eV)	Excitation [nm]	Oscillator strength (f)	Description
S1	2.0296	610.89	0.0000	H→L (0.70517)
S2	3.0826	402.21	0.0000	H→L+1 (0.69621)
S3	3.3037	375.29	0.0027	H-2→L (-0.45228); H→L+2 (0.51103); H→L+3 (-0.15142)
S4	3.3037	375.29	0.0027	H-1→L (0.45235); H→L+3 (0.51093); H→L+2 (0.15140)
S5	3.4303	361.44	0.0003	H→L+4 (0.67860)
S6	3.4303	361.43	0.0003	H→L+5 (0.67864)
S7	3.6309	341.47	0.7714	H-1→L (0.52617); H→L+3 (-0.44484)
S8	3.6309	341.47	0.7715	H-2→L (0.52630); H→L+2 (0.44472)
S11	4.1792	296.67	0.0252	H-3→L (0.63741); H→L (0.24758)
S19	4.4372	279.42	0.0439	H-6→L (0.60029); H-1→L+1 (-0.32050)



Major electronic transitions for [6,6]CNB by TD-DFT method using B3LYP/6-31G(d).

	energy (eV)	Excitation [nm]	Oscillator strength (f)	Description
S1	2.3475	528.16	0.0000	H→L (0.70267)
S2	2.5870	479.25	0.0038	H-1→L (0.59483); H→L+1 (0.36630)
S3	2.9975	413.62	0.0000	H-2→L (0.57315); H→L+2 (0.37325)
S4	2.9980	413.56	0.0000	H-3→L (0.57328); H→L+3 (0.37325)
S5	3.0017	413.04	0.0000	H-1→L+1 (0.69572)
S6	3.0046	412.64	0.0828	H-1→L (0.37159); H→L+1 (0.59477)
S18	3.8386	323.00	0.7244	H-4→L (0.39610); H-2→L+1 (-0.30692); H→L+4 (0.29796);



4.6 Uncorrected and thermal-corrected energies of stationary points

Table S7. Uncorrected and thermal-corrected (298 K) energies of stationary points (Hartree) ([*n*]CPP, methylene-bridged [*n*]CPP and [*n*]LPP, B3LYP/6-31G(d)).

Compound	<i>E</i> + <i>ZPE</i>	<i>E</i>	<i>H</i>	<i>G</i>
[4]CPP	−923.676125	−923.660701	−923.659756	−923.716499
[6]CPP	−1385.705155	−1385.679890	−1385.678946	−1385.757072
[8]CPP	−1847.696459	−1847.661820	−1847.660876	−1847.759410
[10]CPP	−2309.672941	−2309.628859	−2309.627915	−2309.748712
[12]CPP	−2771.641932	−2771.588385	−2771.587441	−2771.729449
[14]CPP	−3233.606496	−3233.543473	−3233.542529	−3233.709158
[16]CPP	−3695.568316	−3695.495816	−3695.494872	−3695.682502
[18]CPP	−4157.528327	−4157.446342	−4157.445397	−4157.656202
[20]CPP	−4619.487021	−4619.395550	−4619.394606	−4619.628631
CH ₂ -[4]CPP	−1076.084241	−1076.067693	−1076.066748	−1076.125470
CH ₂ -[6]CPP	−1614.347805	−1614.321728	−1614.320783	−1614.399318
CH ₂ -[8]CPP	−2152.567254	−2152.531404	−2152.530460	−2152.629646
CH ₂ -[10]CPP	−2690.769225	−2690.723542	−2690.722598	−2690.840623
CH ₂ -[12]CPP	−3228.962423	−3228.906884	−3228.905939	−3229.047419
CH ₂ -[14]CPP	−3767.150612	−3767.085217	−3767.084273	−3767.246486
CH ₂ -[16]CPP	−4305.335683	−4305.260414	−4305.259470	−4305.443962
CH ₂ -[18]CPP	−4843.518610	−4843.433489	−4843.432545	−4843.638616
CH ₂ -[20]CPP	−5381.700082	−5381.605105	−5381.604160	−5381.831886
[4]LPP	−1039.410002	−1039.391385	−1039.390441	−1039.456694
[6]LPP	−1577.585436	−1577.557009	−1577.556064	−1577.644634
[8]LPP	−2115.760889	−2115.722635	−2115.721691	−2115.832590
[10]LPP	−2653.936345	−2653.888256	−2653.887312	−2654.020537
[12]LPP	−3192.111806	−3192.053883	−3192.052938	−3192.208486
[14]LPP	−3730.287268	−3730.219509	−3730.218565	−3730.395803
[16]LPP	−4268.462732	−4268.385134	−4268.384190	−4268.584395
[18]LPP	−4806.638196	−4806.550758	−4806.549814	−4806.772359
[20]LPP	−5344.813660	−5344.716384	−5344.715440	−5344.960322

[a] *E*: electronic energy; *ZPE*: zero-point energy; *H* ($= E + ZPE + E_{\text{vib}} + E_{\text{rot}} + E_{\text{trans}} + RT$): sum of electronic and thermal enthalpies; *G* ($= H - TS$): sum of electronic and thermal free energies.

4.7 Cartesian coordinates of optimized structures

Cartesian coordinates of optimized structures calculated by B3LYP/6-31G(d) level of theory ($[n]$ CPP, methylene-bridged $[n]$ CPP, and $[n]$ LPP). See attached file (Cartesian_coordinates.xyz).

5. Photophysical properties and stability test

UV/vis absorption spectra were recorded on a Shimadzu UV-3510 spectrometer with a resolution of 0.5 nm. Emission spectra were measured with an FP-6600 Hitachi spectrometer with a resolution of 0.2 nm. Absolute fluorescence quantum yields were determined with a Hamamatsu C9920-02 calibrated integrating sphere system.

Light and solvent precautions. Compound **4** was unchanged for several days in the CHCl_3 solution shielded from light using aluminum foil (Figure S27A), but slowly decomposed under light (Figure S27B). The decomposition rate was accelerated under the diluted solution (1×10^{-5} M, Figure S27C). When exposed to ambient light, the CHCl_3 solution of the product tended to turn yellowish, indicating undesirable decomposition processes. The strong fluorescence spectrum in CHCl_3 solution is from its decomposed products. Although decomposition seems relatively slow at high concentration, manipulations involving the product was performed shielding the glassware with aluminum foil as much as possible. Furthermore, the product decomposes more slowly in CH_2Cl_2 solution. Heat precautions. Compound **4** was slowly decomposed at 100°C in the $\text{CHCl}_2\text{CHCl}_2$ solution shielded from light using aluminum foil in the dark (5×10^{-3} M, Figure S27D).

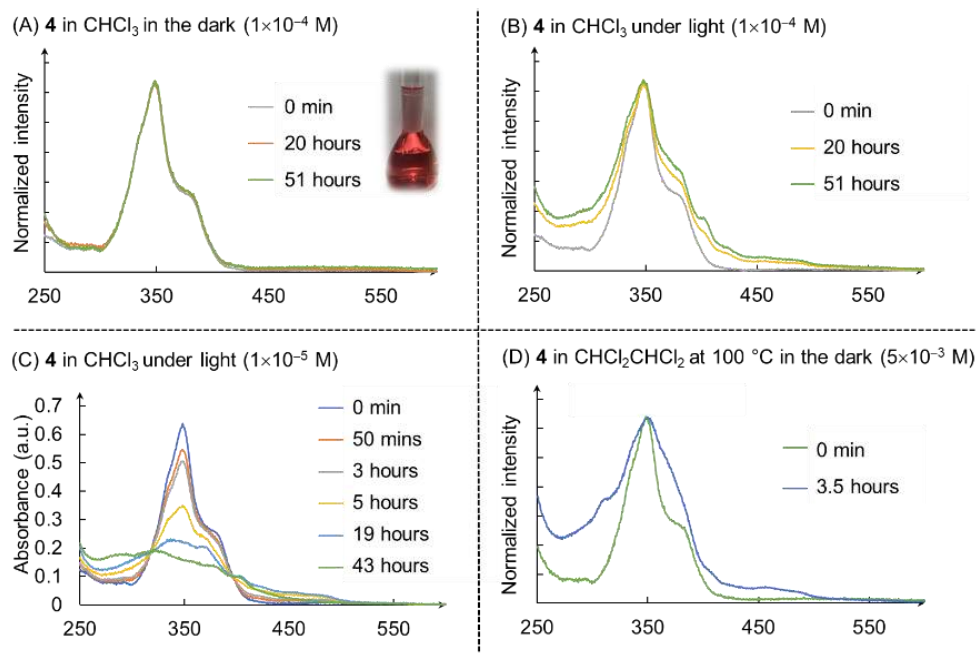


Figure S27. (A) UV/vis absorption spectra of **4** in CHCl_3 in the dark. Inset: the photo of **4** in CH_2Cl_2 ; concentration: 4.7×10^{-4} M (2.5 mg **4** in 10.0 mL CH_2Cl_2). (B–D) UV/vis absorption spectra of **4** in CHCl_3 .

6. Representative aromatic belts having CPP skeleton

The bottom-up synthesis of aromatic belt with CPP as a backbone has rarely been explored to date. In 2017, our group successfully used ethenylene bridges to connect phenylene units to give a fully fused and conjugated carbon nanobelt.¹¹ Subsequently, Chi, Miao, and coworkers achieved the synthesis of phenylene-bridged carbon nanobelt.¹² Very recently, Tanaka's group prepared the CH₂O-bridged [8]CPP.¹³

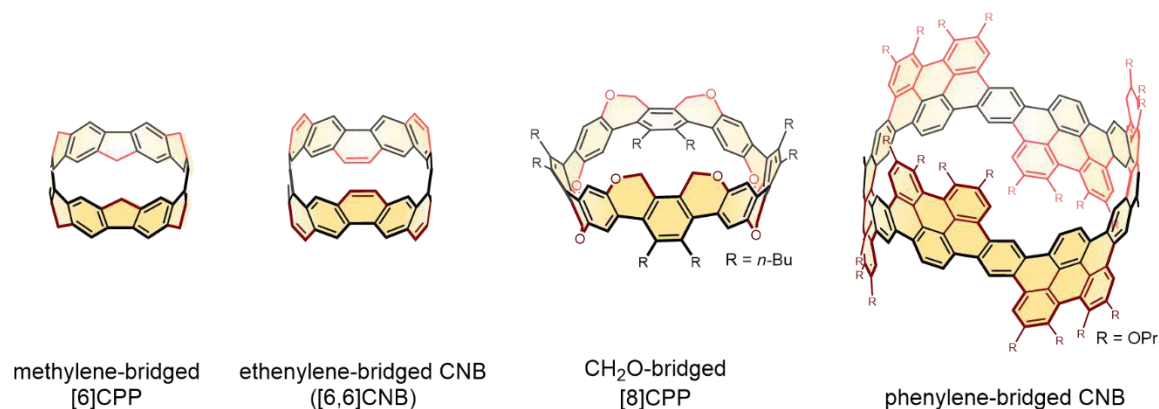

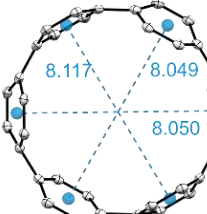
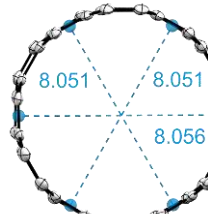
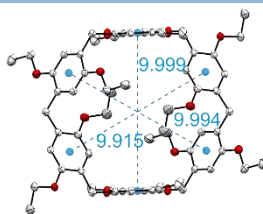
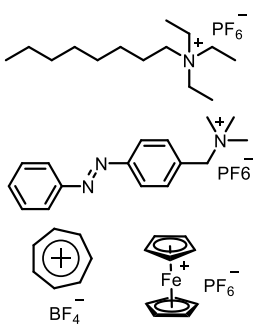
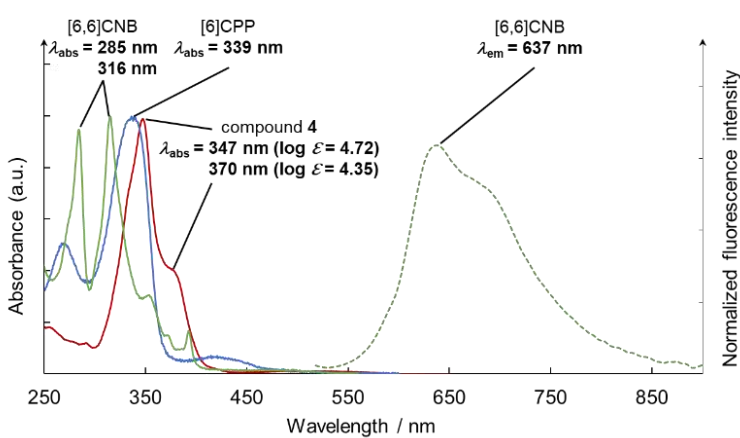


Figure S28. Aromatic belts having CPP skeleton.

7. Comparison among 4, [6]CPP, [6,6]CNB, and pillar[6]arene

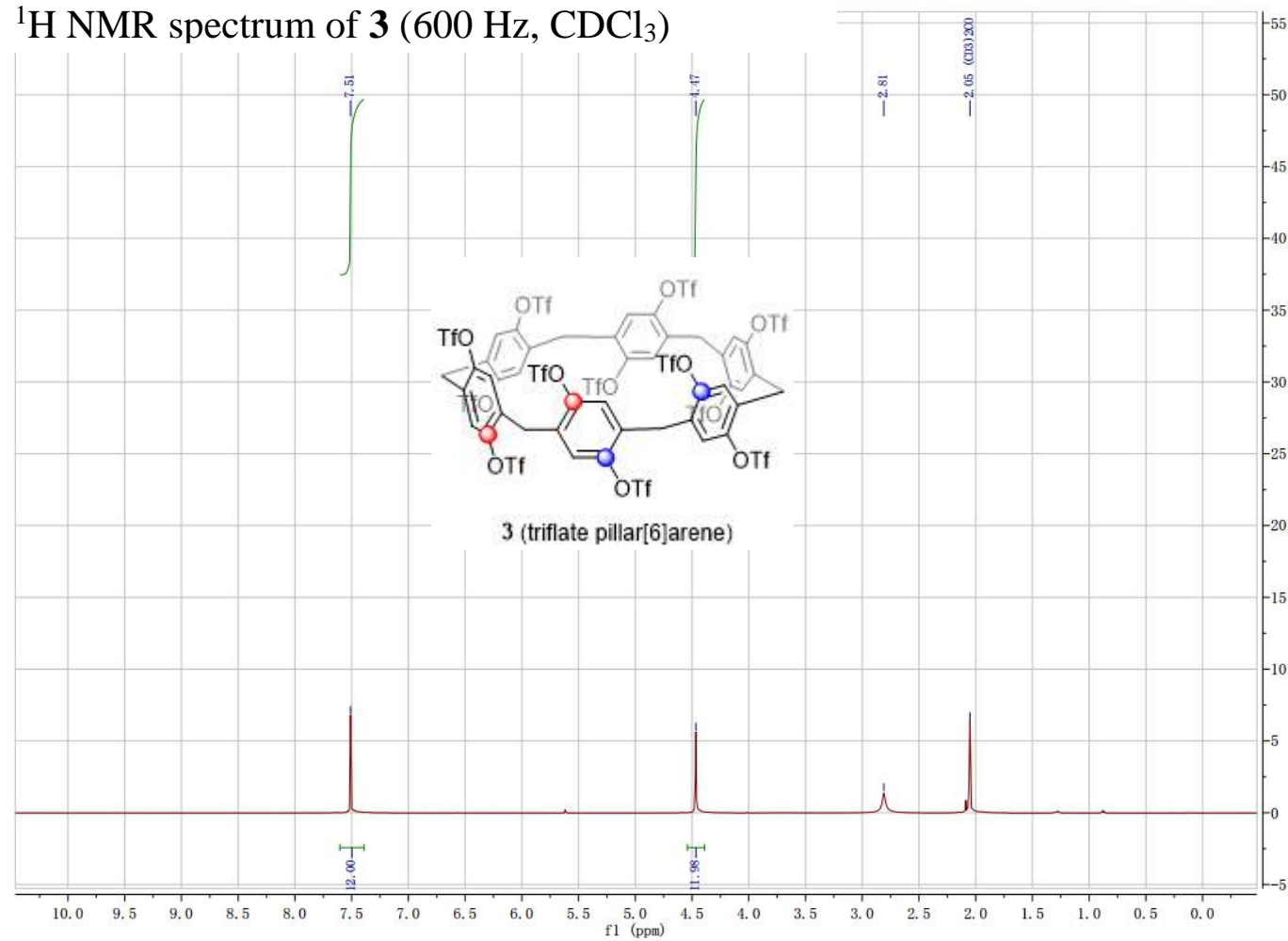
Table S8: Comparison among 4, [6]CPP, [6,6]CNB, and pillar[6]arene.

compound ^g	4	[6]CPP	[6,6]CNB	pillar[6]arene
structure				
diameter (Å) ^a	7.758	8.072	8.053	~10.0 ^b
guest	<i>n</i> -hexane CH ₂ Cl ₂	CHCl ₃ ^c	CHCl ₃ ^c THF ^c	
C–C (Å) ^d	1.478	1.489	1.464	
HOMO (eV) ^e	–4.40	–4.91	–4.92	
LUMO (eV) ^e	–1.74	–1.78	–1.97	
energy gap (eV)	2.66	3.13	2.95	
strain energy ^f (kcal/mol)	110.2	96.9	119.5	
fluorescence quantum yield ^h	–	–	3%	(see more in ref) ¹⁴
UV/Fl				

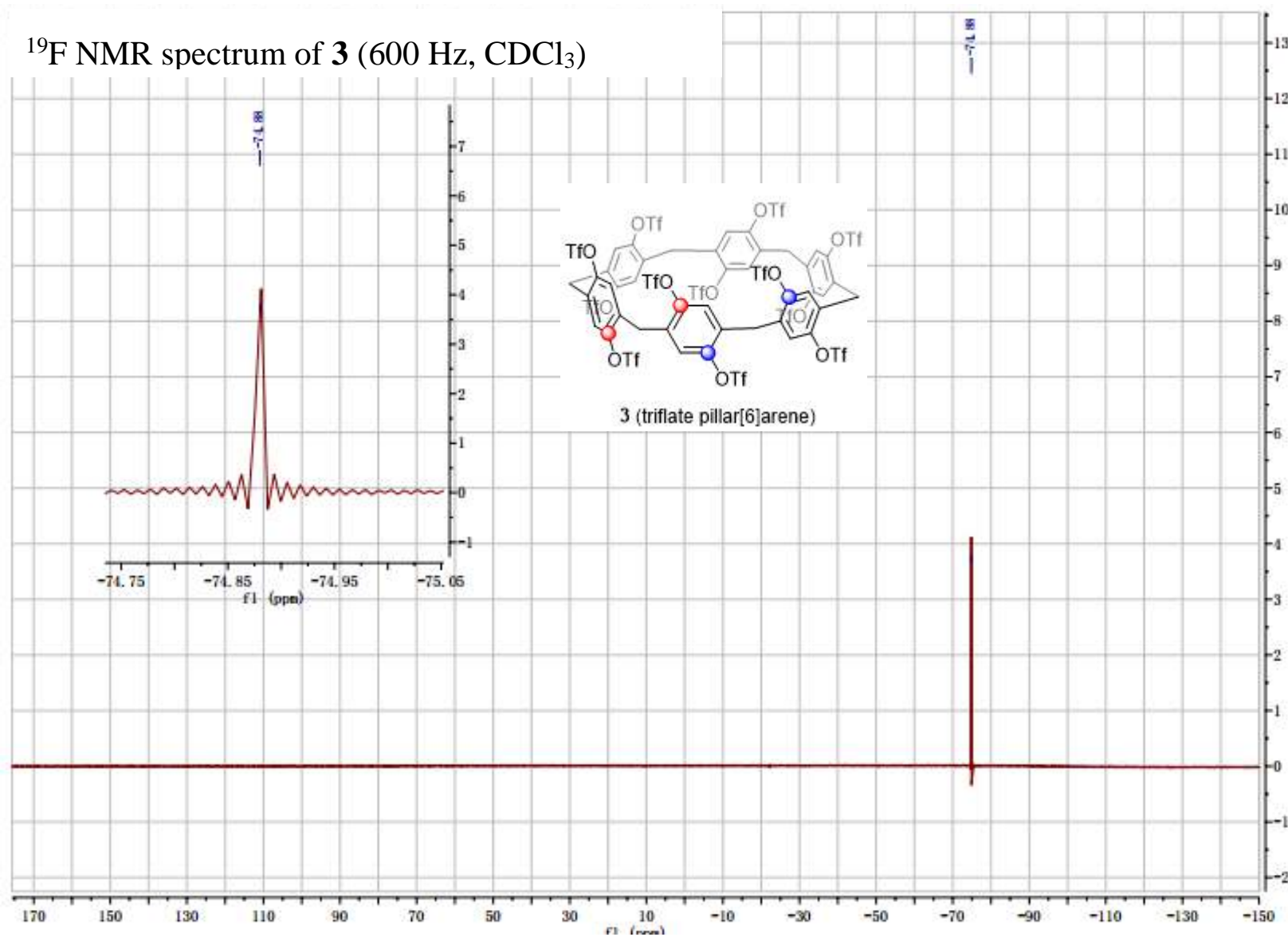
^aThe averaged diameter was measured as the distance between the two central phenylene units located at opposite sides. ^bThe structure shape of pillar[6]arene is hexagon, the diameter of the circle in the hexagon is ~10.0 Å. ^cThe guest molecule was partially incorporated. ^dThe C–C single bond connecting the neighboring phenylene units (the averaged length). ^eFrontier molecular orbitals calculated at the B3LYP/6-31G(d) level of theory. ^fThe strain energy data of [6]CPP^{10b} and [6,6]CNB^{11a} were taken from references (calculated at the B3LYP/6-31G(d) level). ^gThe crystal data of [6]CPP,¹⁵ [6,6]CNB,^{11a} and pillar[6]arene^{14b} were taken from references. ^hThe quantum yield data of [6]CPP¹⁶ and [6,6]CNB^{11a} was taken from references.

8. NMR spectra of new compounds

^1H NMR spectrum of **3** (600 Hz, CDCl_3)



^{19}F NMR spectrum of **3** (600 Hz, CDCl_3)



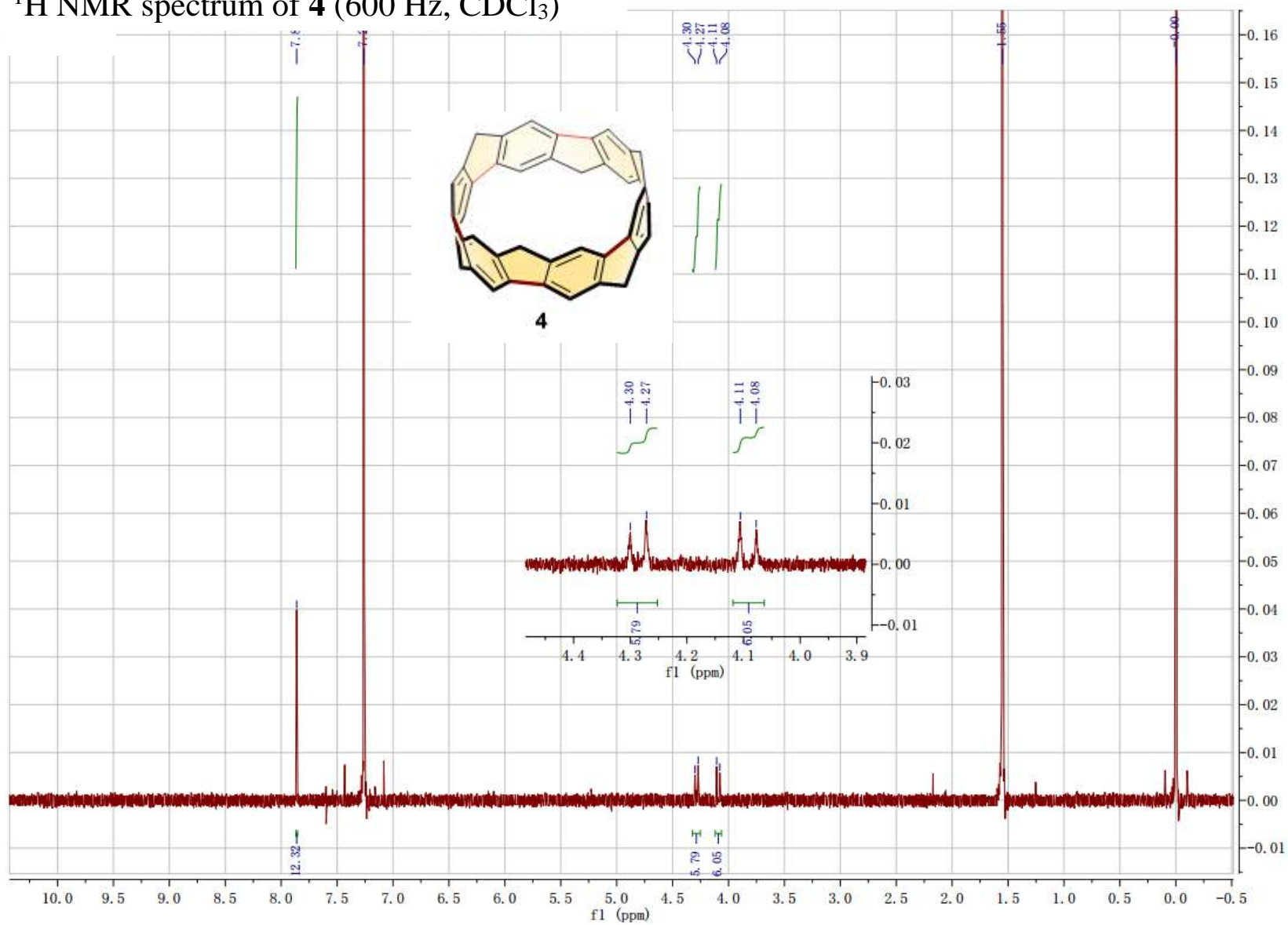
^{13}C NMR spectrum of **3** (600 Hz, CDCl_3)

Chemical structure of **3** (triflate pillar[6]arene) is shown as an inset. The structure features a central pillar[6]arene core with triflate (OTf) groups attached to the phenyl rings.

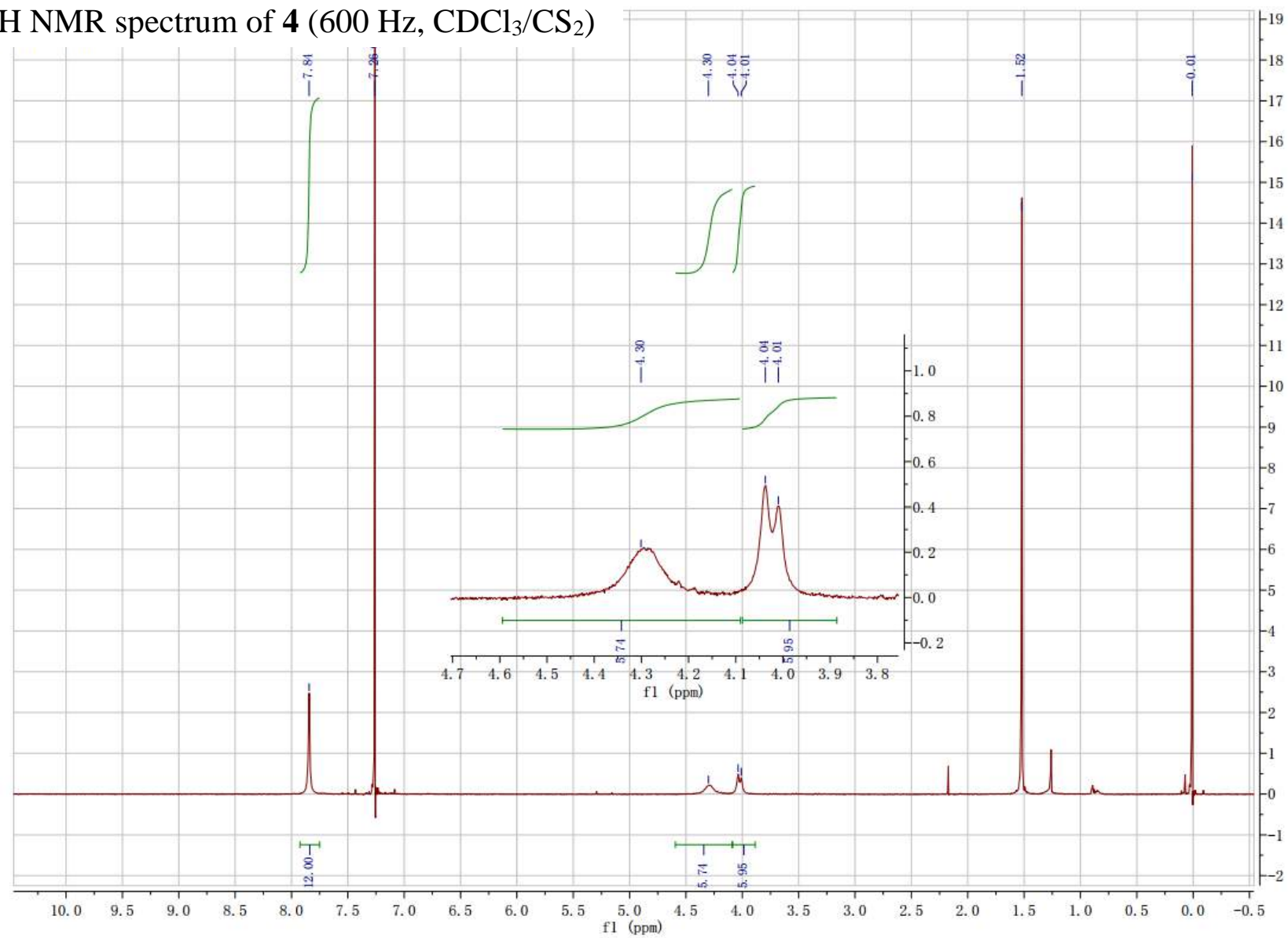
Peak list (ppm):

- 206.16
- 147.53
- 133.51
- 126.19
- 122.45
- 120.33
- 118.22
- 116.10
- 30.93
- 29.91

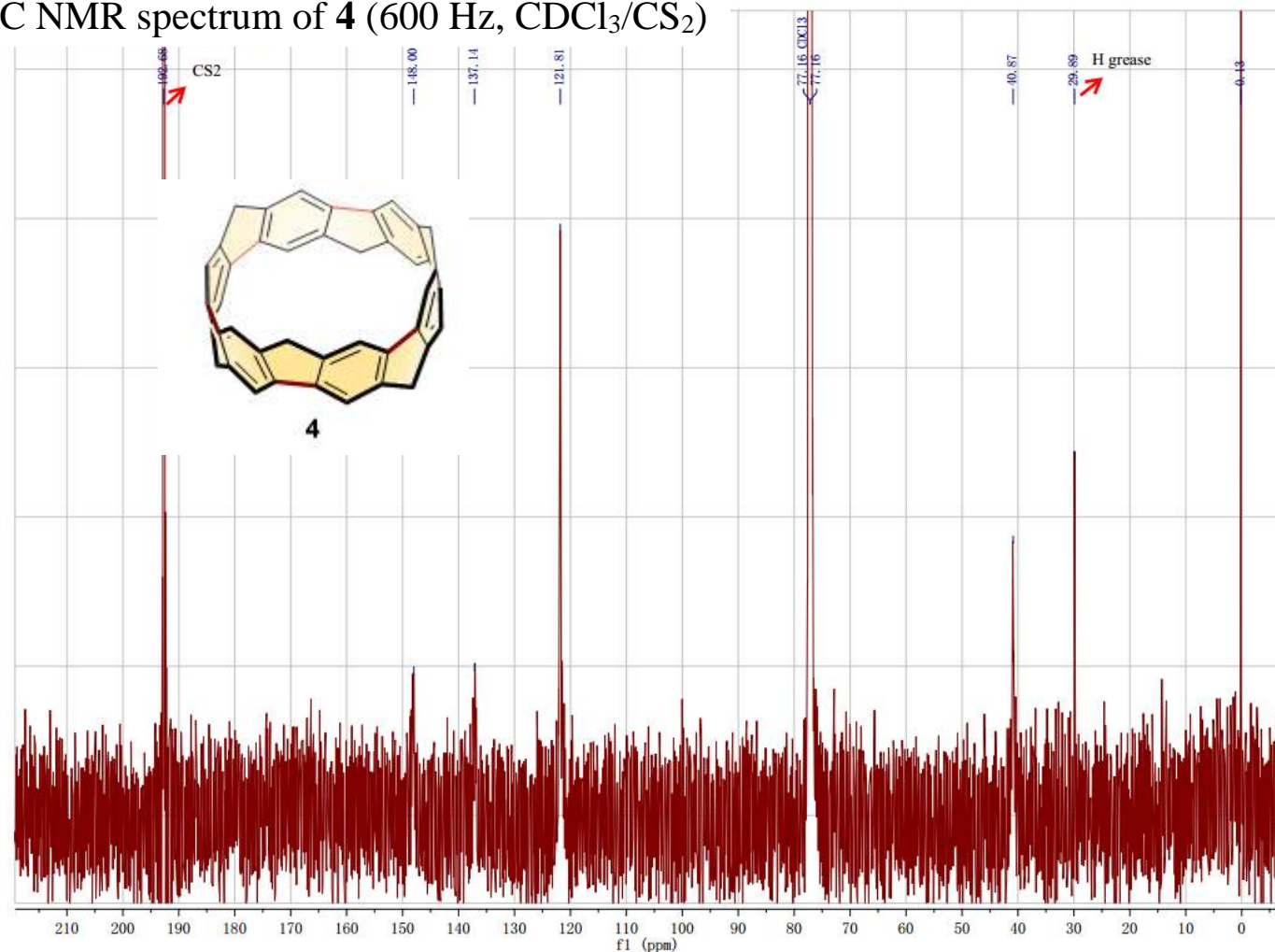
^1H NMR spectrum of **4** (600 Hz, CDCl_3)



^1H NMR spectrum of **4** (600 Hz, $\text{CDCl}_3/\text{CS}_2$)



^{13}C NMR spectrum of **4** (600 Hz, $\text{CDCl}_3/\text{CS}_2$)



Compound **4** in CDCl_3 and CS_2 :

CS_2 was added to enhance the solubility of **4**. The higher concentration of CS_2 leads to the upshift and broadening of NMR signals of **4**. It is difficult to get high quality ^{13}C NMR spectrum. However, this spectrum is consistent with the calculated results (Table S5). Its structure was confirmed by HR MS and X-ray crystallographic analysis as well. When we used $\text{CDCl}_3/\text{CH}_2\text{Cl}_2$, CD_2Cl_2 , or $\text{CDCl}_2\text{CDCl}_2$, broaden signals were observed as well. The solubility of **4** in CDCl_3 , $\text{CDCl}_3/\text{C}_6\text{F}_6$, or $\text{THF-}d_8$ was insufficient for ^{13}C NMR measurement.

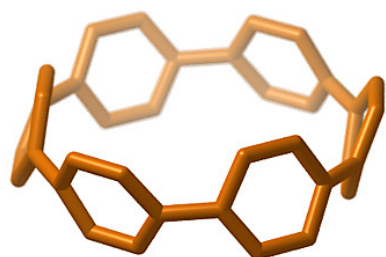
9. References

- (1) Cao, D.; Kou, Y.; Liang, J.; Chen, Z.; Wang, L.; Meier, H. A Facile and Efficient Preparation of Pillararenes and a Pillarquinone. *Angew. Chem., Int. Ed.* **2009**, *48*, 9721–9723.
- (2) Hu, X.-B.; Chen, Z.; Chen, L.; Zhang, L.; Hou, J.-L.; Li, Z.-T. Pillar[n]arenes (n = 8–10) with two cavities: synthesis, structures and complexing properties. *Chem. Commun.* **2012**, *48*, 10999–11001.
- (3) Ma, Y.; Chi, X.; Yan, X.; Liu, J.; Yao, Y.; Chen, W.; Huang, F.; Hou, J.-L. per-Hydroxylated Pillar[6]arene: Synthesis, X-ray Crystal Structure, and Host–Guest Complexation. *Org. Lett.* **2012**, *14*, 1532–1535.
- (4) Wang, G.; Qiang, H.; Guo, Y.-Z.; Yang, J.; Wen, K.; Hu, W.-B. Systematic rim cyano-functionalization of pillar[5]arene and corresponding host–guest property varieties. *Org. Biomol. Chem.* **2019**, *17*, 4600–4604.
- (5) Sheldrick, G. SHELXT - Integrated space-group and crystal-structure determination. *Acta Crystallogr. A* **2015**, *A71*, 3–8.
- (6) Sheldrick, G. Crystal structure refinement with SHELXL. *Acta Crystallogr.* **2015**, *C71*, 3–8.
- (7) Dolomanov, O. V.; Bourhis, L. J.; Gildea, R. J.; Howard, J. A. K.; Puschmann, H. OLEX2: a complete structure solution, refinement and analysis program. *J. Appl. Crystallogr.* **2009**, *42*, 339–341.
- (8) Frisch, M. J.; Trucks, G. W.; Schlegel, H. B.; Scuseria, G. E.; Robb, M. A.; Cheeseman, J. R.; Scalmani, G.; Barone, V.; Petersson, G. A.; Nakatsuji, H.; Li, X.; Caricato, M.; Marenich, A. V.; Bloino, J.; Janesko, B. G.; Gomperts, R.; Mennucci, B.; Hratchian, H. P.; Ortiz, J. V.; Izmaylov, A. F.; Sonnenberg, J. L.; Williams; Ding, F.; Lipparini, F.; Egidi, F.; Goings, J.; Peng, B.; Petrone, A.; Henderson, T.; Ranasinghe, D.; Zakrzewski, V. G.; Gao, J.; Rega, N.; Zheng, G.; Liang, W.; Hada, M.; Ehara, M.; Toyota, K.; Fukuda, R.; Hasegawa, J.; Ishida, M.; Nakajima, T.; Honda, Y.; Kitao, O.; Nakai, H.; Vreven, T.; Throssell, K.; Montgomery Jr., J. A.; Peralta, J. E.; Ogliaro, F.; Bearpark, M. J.; Heyd, J. J.; Brothers, E. N.; Kudin, K. N.; Staroverov, V. N.; Keith, T. A.; Kobayashi, R.; Normand, J.; Raghavachari, K.; Rendell, A. P.; Burant, J. C.; Iyengar, S. S.; Tomasi, J.; Cossi, M.; Millam, J. M.; Klene, M.; Adamo, C.; Cammi, R.; Ochterski, J. W.; Martin, R. L.; Morokuma, K.; Farkas, O.; Foresman, J. B.; Fox, D. J. *Gaussian 16 Rev. C.01*, Wallingford, CT, 2016.
- (9) (a) Becke, A. D. Density - functional thermochemistry. III. The role of exact exchange. *J. Chem. Phys.* **1993**, *98*, 5648 – 5652. (b) Lee, C.; Yang, W.; Parr, R. G. Development of the Colle-Salvetti correlation-energy formula into a functional of the electron density. *Phys. Rev. B* **1988**, *37*, 785–789.
- (10) (a) Segawa, Y.; Yagi, A.; Ito, H.; Itami, K. A Theoretical Study on the Strain Energy of Carbon Nanobelts. *Org. Lett.* **2016**, *18*, 1430–1433. (b) Segawa, Y.; Omachi, H.; Itami, K. Theoretical Studies on the Structures and Strain Energies of Cycloparaphenylenes. *Org. Lett.* **2010**, *12*, 2262–2265.
- (11) (a) Povie, G.; Segawa, Y.; Nishihara, T.; Miyauchi, Y.; Itami, K. Synthesis of a

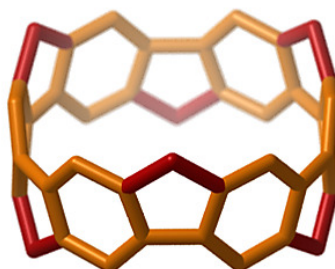
- carbon nanobelt. *Science* **2017**, *356*, 172–175. (b) Povie, G.; Segawa, Y.; Nishihara, T.; Miyauchi, Y.; Itami, K. Synthesis and Size-Dependent Properties of [12], [16], and [24]Carbon Nanobelts. *J. Am. Chem. Soc.* **2018**, *140*, 10054–10059.
- (12) Cheung, K. Y.; Gui, S.; Deng, C.; Liang, H.; Xia, Z.; Liu, Z.; Chi, L.; Miao, Q. Synthesis of Armchair and Chiral Carbon Nanobelts. *Chem* **2019**, *5*, 838–847.
- (13) Nishigaki, S.; Shibata, Y.; Nakajima, A.; Okajima, H.; Masumoto, Y.; Osawa, T.; Muranaka, A.; Sugiyama, H.; Horikawa, A.; Uekusa, H.; Koshino, H.; Uchiyama, M.; Sakamoto, A.; Tanaka, K. Synthesis of Belt- and Möbius-Shaped Cycloparaphenylenes by Rhodium-Catalyzed Alkyne Cyclotrimerization. *J. Am. Chem. Soc.* **2019**, *141*, 14955–14960.
- (14) (a) Ogoshi, T.; Yamagishi, T. Pillar[5]- and pillar[6]arene-based supramolecular assemblies built by using their cavity-size-dependent host–guest interactions. *Chem. Commun.* **2014**, *50*, 4776–4787. (b) Yuan, M.-S.; Chen, H.; Du, X.; Li, J.; Wang, J.; Jia, X.; Li, C. Host–guest complexation of pillar[6]arenes towards neutral nitrile guests. *Chem. Commun.* **2015**, *51*, 16361–16364.
- (15) Spisak, S. N.; Wei, Z.; Darzi, E.; Jasti, R.; Petrukhina, M. A. Highly strained [6]cycloparaphenylene: crystallization of an unsolvated polymorph and the first mono- and dianions. *Chem. Commun.* **2018**, *54*, 7818–7821.
- (16) Xia, J.; Jasti, R. Synthesis, Characterization, and Crystal Structure of [6]Cycloparaphenylene. *Angew. Chem., Int. Ed.* **2012**, *51*, 2474–2476.

SI_NonAlternantBelt_20200603.pdf (5.93 MiB)

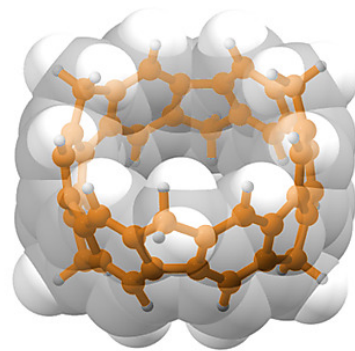
[view on ChemRxiv](#) • [download file](#)



cycloparaphenylene
(carbon nanoring)



methylene-bridged CPP
(non-alternant aromatic belt)



- *rigid belt*
- *rapid synthesis*

- *narrower energy gap*
- *enhanced π -conjugation*



Other files

4.cif (622.82 KiB)

[view on ChemRxiv](#) • [download file](#)
